2016

Differential Reactivity of Microglia in Two Mouse Models of Multiple Sclerosis

Rebecca K. Hartley
Virginia Commonwealth University, hartleyr@mymail.vcu.edu

Differential Reactivity of Microglia in Two Mouse Models of Multiple Sclerosis

A thesis submitted in partial fulfillment of the requirements for the degree of Master of Science

at Virginia Commonwealth University

By:

Rebecca Kathleen Hartley
Bachelor of Science, Indiana University of Pennsylvania, 2013

Advisor: Jeffrey L. Dupree, Ph.D.
Associate Professor of Anatomy & Neurobiology

Virginia Commonwealth University
Richmond, Virginia
May 2016

Acknowledgements

I want to thank my advisor, Dr. Jeff Dupree, for providing me with knowledge and advice over the past two years, and for helping me learn what it means to be a researcher. He always urged me to learn more and move forward with a clear hypothesis in mind. His guidance was instrumental in completing my project and I cannot thank him enough for everything he has done for me.

I would like to thank my other lab members for all their assistance and encouragement. I especially want to thank Kareem Clark and Savannah Benusa for providing me with their expertise and teaching me, and for their encouragement when obstacles arose. Their guidance was invaluable and I could not have completed this project without their help. I want to thank Nick George, my fellow master's student, for providing support as we persevered through our research together. I also want to thank Brooke Sword, our laboratory technician, for helping me with my mice and our undergraduate students for their assistance in various aspects of this project.

I would like to thank my committee members; Dr. Unsung Oh, Dr. Babette Fuss, and Dr. George DeVries for serving on my committee and helping to guide my research as my project incorporated new ideas and techniques. I would also like to thank my program director, Dr. Gail Christie, for her advice as I proceeded through the MBG program and Dr. Henderson and the VCU core microscopy facility for their training and guidance.

Finally, I want to thank my family and friends for all of their support and encouragement. They have always encouraged me to pursue my dreams and become the best person that I could be. I want to thank them for listening to me explain my research, even when it was incomprehensible to them, and for providing moral support when I became frustrated or disheartened. They have truly motivated me to be the scientist I am today.

Table of Contents

List of Figures

List of Tables

List of Abbreviations

AIS……..Axon Initial Segment

AnkG……..AnkyrinG

ANOVA……..Analysis of Variance

Arg1……Arginase 1

BBB……Blood Brain Barrier

BSA……..Bovine Serum Albumin

C1q……..Complement Component 1, q subunit

C1r…….Complement Component 1, r subunit

C1s……..Complement Component 1, s subunit

C2……Complement Component 2

C3……Complement Component 3

C3b……..Complement Component 3, b subunit

C4……..Complement Component 4

C6……Complement Component 6

Carboxy……Carboxymethycellulose

Caspr…… Contactin-Associated Protein

Caspr2……..Contactin Associated Protein 2

CD……..Cluster of Differentiation

Cfb……..Complement Factor B

Cfd……..Complement Factor D

CGT……Galactose-Ceramide Galactosyltransferase

CNP……2’,3’-Cyclic Nucleotide 3’-Phopshodiesterase

CNS……Central Nervous System

CSF1……Colony Stimulating Factor 1

Cup……Cuprizone

EAE……Experimental Autoimmune Encephalomyelitis

FOV……Field of View

GAPDH…… Glyceraldehyde-3-phosphate Dehydrogenase

HBSS……HanK's Buffered Saline Solution

HLA……Human Leukocyte Antigen

HRP……Horseradish Peroxidase

IBA-1……Ionized Calcium Binding Adaptor Molecule 1

iC3b……inactive Complement Component 3, b subunit

IFNγ……Interferon gamma

IgG……Immunoglobulin G

IL……Interleukin

IP……Intraperitoneal

kD……kilodalton

Maff……v-maf Avian Musculoaponeurotic Fibrosarcoma Oncogene Homolog F

MAG……Myelin-Associated Glycoprotein

MASP1……Mannose-Associated Serine Protease 1

MBP……Myelin Basic Protein

MHC……Major Histocompatibility Complex

MOG……Myelin Oligodendrocyte Glycoprotein

MS……Multiple Sclerosis

Na_v……Voltage-gated Sodium Channel

NAWM……Normal Appearing White Matter

NeuN……Neuronal Nuclei

NOS……Nitric Oxide Synthase

NrCAM……Neural related Cell Adhesion Molecule

PBS……Phosphate Buffered Saline

PBST……Phosphate Buffered Saline with Tween

PDZ……Post synaptic density 95, Disc large, Zona occludens-1

PLP……Proteolipid Protein

PNS……Peripheral Nervous System

PSD……Post Synaptic Density

Ptger3……Prostaglandin E Receptor 3

qRT-PCR……quantitative Reverse Transcriptase Polymerase Chain Reaction

Retnla…… Resistin-like alpha

RNA……Ribonucleic Acid

ROS……Reactive Oxygen Species

TAG-1…… transient axonal glycoprotein -1

Tlr……Toll-like Receptor

TNFα……Tumor Necrosis Factor alpha

Abstract

Multiple sclerosis (MS) is a neurodegenerative disorder characterized by CNS inflammation and axonal demyelination. In addition, axonal pathology has also been reported in MS and may be responsible for the functional deficits associated with this disease. Based on preliminary data from our laboratory, we propose that a specific domain of the neuron, known as the axon initial segment (AIS), is targeted in MS. Consistent with our work from the human tissue, we have also observed disruption of AIS integrity in a murine CNS inflammatory model and observations strongly implicate reactive microglia as mediators of AIS disruption. In contrast, a murine model of demyelination did not exhibit AIS pathology but reactive microglia were prevalent. Since we propose that reactive microglia drive AIS disruption in our inflammatory CNS model but observe no AIS pathology following demyelination even in the presence of reactive microglia, we propose that reactive microglia in these models exhibit different interactions and molecular profiles. To test this hypothesis, we employed immunofluorescence labeling combined with confocal microscopy to quantify microglia reactivity and microglia-AIS interaction. Additionally, we conducted a microarray using RNA isolated from microglia from both the inflammatory and demyelinating models. Our findings show that microglia are reactive prior to pathology in both models and that the extent of AIS-microglial contact is similar between the models but significantly increased as compared to naïve mice. Microarray data reveal a substantial difference in gene expression indicating functional differences between the reactive microglia in the inflammatory and demyelinating models. Finally, following functional enrichment analysis of microarray data, the complement pathway emerged as a potential contributor to the AIS pathology observed in EAE.

Introduction

Multiple sclerosis (MS) is a neurodegenerative disorder characterized by demyelinating plaques and neurological symptoms such as physical disability and cognitive impairment (Files et al., 2015). Inflammation is also a key characteristic of MS, seen by infiltration of T-cells and macrophages into the central nervous system (CNS) and involvement of the resident CNS immune cells, microglia, and other immune cells (Hemmer et al., 2015). Multiples sclerosis is estimated to affect 2.3 million people worldwide and 400,000 people in the United States (Browne et al., 2014). The formation of demyelinating plaques is often considered the cause of axonal pathologies and neurological damage (Files et al., 2015; Rudick et al., 2006; Haines et al., 2011). However, more recent data indicates that axonal pathology may be a primary event in MS, independent of demyelination (Haines et al., 2011; Popescu et al., 2013). This distinction is important in order to understand the overall pathology of MS and develop future treatment options. The goal of this project was to examine this contrast between demyelination-driven pathology and demyelination independent pathology with specific attention to an axonal domain known as the axon initial segment (AIS).

The Neuron

Neurons are one of the specialized cell types of the peripheral and central nervous system, and interact with the glial cells of the CNS and PNS (Kandel et al., 2013). Neurons are polarized cells that communicate electrical and chemical signals to other cells within the nervous system and to other target organs. The neuron is composed of four distinct elements: the dendrites, cell body, axon, and synaptic terminals (Figure 1). The dendrites are short, branched processes responsible for receiving inputs from other cells. The cell body (*soma*) contains the nucleus, which stores the cell's DNA. The axon is composed of distinct domains and serves to conduct electrical action potentials down its length, communicating signals to adjacent cells. In addition to the specialized regions of the axon that function

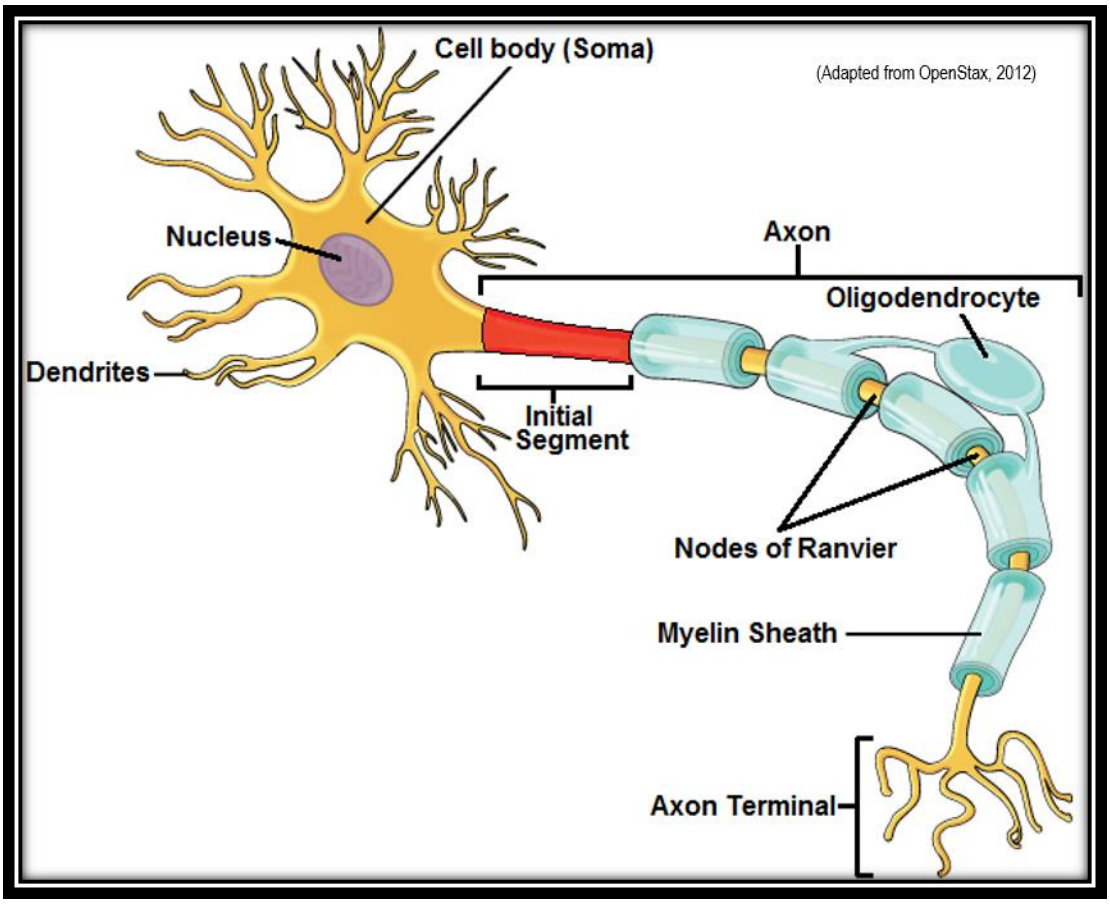

Figure 1. Schematic representation of a neuron. The dendrites, cell body, axon, and axon terminal are shown. The nucleus, axon initial segment, nodes of Ranvier, and myelin sheath are also labeled. (Adapted from openstar 2012).

to ensure efficient and rapid communication along the axon, many axons are also covered by the membranous insulator known as myelin. Myelin wraps the axon of many neurons and facilitating the periodic regeneration of the action potential as it travels the long distance down the axon. The synaptic terminals transmit the action potential as a chemical signal to adjacent cells. The specific domains of the axon, such as the axon initial segment and nodes of Ranvier, have distinct functions that are important for the proper propagation of action potentials (Kandel et al., 2013).

Myelin

Myelin wraps around the axon and acts as an insulator to ensure propagation of action potentials. In the CNS myelin is produced by oligodendrocytes, and in the PNS it is produced by Schwann cells (Raine, 1984). An oligodendrocyte extends multiple processes which wrap around a segment of the axon to form a multilayered sheath (Aggarwal et al., 2011). The unmyelinated portions of the axon between the myelin segments are the nodes of Ranvier. The edges of the myelin sheath form paranodal loops that border the nodes of Ranvier and form the paranodal junction (Kandel et al., 2013). This junction contains structures called transverse bands, which anchor the myelin to the axon's plasma membrane (axolemma) (Dupree et al., 1998) and establish protein clusters that form and maintain distinct axonal domains (Dupree et al., 1999). On the abnodal side of the paranode is the structurally ill-defined domain known as the juxtaparanode and between the juxtaparanodes are the internodes (Aggarwal et al., 2011).

Aiding in the myelin sheath's function of insulation is its unique composition. Myelin is composed of about 30% proteins and 70% lipids, an unusually high lipid concentration, as most membranes are composed of a near equal amount of protein and lipids (Aggarwal et al., 2011; Quarles et al., 2006). Galactosyl ceramide and its derivative sulfatide are two of the major lipid components of myelin, but myelin also has a high concentration of cholesterol (Marcus and Popko, 2002). These lipids

are necessary for stabilizing myelin-axon interactions, as demonstrated by galactose-ceramide galactosyltransferase (CGT) deficient mice. CGT isan enzyme necessary for the formation of galactolipids (Morell and Radin, 1969). CGT deficient mice display myelin structure abnormalities and premature death (Marcus and Popko, 2002). Of the protein in myelin, 60-80% of all protein in myelin is composed of myelin basic protein (MBP) and proteolipid protein (PLP) (Han, 2013). PLP, and its immature isoformDM20, constitute ~50% of the myelin proteins and are known to play a role in the stabilization of the intraperiod line (Boison and Stoffel, 1994; Han et al., 2013). However, ultrastructural analysis of the PLP deficient mice revealed that neither PLP nor DM20 is essential for formation of compact myelin (Coetzee et al., 1999) Additionally, these mice did not show widespread demyelination (Klugmann et al., 1997). PLP has been shown to contribute to axonal stability, however, as aged PLP deficient mice show axonal swellings and degeneration (Griffiths et al., 1998). Although it is an isoform of PLP, DM20 is not capable of rescuing PLP deficient mice from axonal degeneration, demonstrating the requirement of PLP for axonal stability (Stecca et al., 2000). MBP is the second most abundant protein in CNS myelin. It has several different isoforms that are present in different concentrations during development (Han et al., 2013). MBP is considered the major protein important in stabilizing the major dense line, as shown by the *shiverer* mouse, a spontaneously occurring murine mutant caused by a deletion in the MBP gene, resulting in the formation of both reduced and uncompacted myelin.

There are also other myelin proteins of interest that are expressed in levels lower than PLP or MBP. One of these proteins is 2',3'-cyclic nucleotide 3'-phopshodiesterase (CNP). CNP is expressed mainly in oligodendrocytes and has two isoforms that are differentially expressed during development (Scherer et al., 1994). It is associated with oligodendrocyte processes and the cytoplasmic domains of myelin (i.e. uncompacted myelin) and is found underneath the oligodendrocyte surface membrane, consistent with its role in the cytoskeletal structure of myelin (Gravel et al., 1996). Myelin-associated glycoprotein (MAG) is a component of myelin at the axo-glial interface and found to be important for

axon-glial interactions due to the presence of several Ig binding domains (Schachner and Bartsch, 2000). However, MAG is not necessary for myelin formation as MAG-deficient mice form relatively normal myelin (Schachner and Bartsch, 2000). Myelin oligodendrocyte glycoprotein (MOG) is another minor myelin protein, found on the surface of myelin membranes, but is noteworthy because MOG antibodies lead to myelin degeneration and are also found in MS patients (Menon et al., 1997). Its exact function is somewhat unclear, but it has been utilized to induce mouse models of MS, such as experimental autoimmune encephalomyelitis (EAE) (Johns et al., 1995), which our lab uses to study MS. Although antibodies to PLP, MBP, and MAG also exist in MS patients, MOG antibodies have shown specific T-cell reactivity, which suggests a role for a cell-mediated immune response to MOG in MS (Aslani et al., 2014; de Graaf et al., 2012).

Axonal Domains

There are several distinct domains of the myelinated axon that have specialized roles, ensuring proper neuronal function. These domains include the axon initial segment, nodes of Ranvier, paranode, juxtaparanode, and internode (Buttermore et al., 2013). The internode comprises most of the length of the axon and is wrapped by compacted myelin (Buttermore et al., 2013). Although it lacks many specialized structures, it is thought to a play a part in axon-glia interactions which are mediated by MAG (Buttermore et al., 2013; Marcus and Popko, 2002). The juxtaparanode lies just under the myelin between the internode and paranode and is characterized by clustering of $K_V1.1$ and $K_V1.2$ delayed rectifying potassium channels (Wang et al., 1993; Rhodes et al., 1997). Contactin-associated protein 2 (caspr2) specifically localizes with the $K_V\beta2$ subunit of these potassium channels at the juxtaparanode via a PDZ binding domain (Post synaptic density 95, Disc large, Zona occludens-1 domain), while caspr is specifically localized to the paranode (Poliak et al., 1999; Gordon et al., 2014). TAG-1 (transient axonal glycoprotein -1) also localizes to the juxtaparanode and forms a caspr2/TAG-1 complex . TAG-1 on the

glial cells binds to this TAG-1/caspr2 complex via homophilic interactions (Poliak et al., 2003; Traka et al., 2003). Mice deficient in either TAG-1 or caspr2 show a lack of protein clustering at the juxtaparanode, although these knockouts also appear phenotypically normal (Traka et al., 2003; Poliak et al., 2003). The juxtaparanode is also enriched in PSD (post synaptic density) 95 (Rasband et al., 2002). This protein clustering shows interactions similar to, but distinct from, those found at the paranode.

The paranode is the domain on either side of the node of Ranvier and consists of a caspr/contactin interaction, similar to that of the caspr2/TAG-1 complex at the juxtaparanode (Einheber et al., 1997). In caspr mutant mice, contactin is absent at the node, indicating the importance of caspr at the node (Rios et al., 2000). Without this caspr/contactin interaction, the paranode is defective, although myelin forms normally (Bhat et al., 2001; Boyle et al., 2001). Caspr is also thought to have a role in trafficking contactin to the paranode (Gollan, 2003). Once the caspr/contact complex is established, neurofascin 155, which is expressed by oligodendrocytes, binds contactin to form transverse bands (Rios et al., 2000; Charles et al., 2002). The nodes of Ranvier form the space between paranodes. The nodes of Ranvier and axon initial segment are two unmyelinated sections of the axon that are similar in protein composition and important for action potential propagation and regeneration (Buttermore et al., 2013). Because of this, they are of particular interest to our lab.

Nodes of Ranvier

The nodes of Ranvier are unmyelinated portions of the axon important for regenerating action potentials as they travel along the axon (Rasband and Peles, 2015). The nodes of Ranvier exhibit a protein composition conducive to this function, displaying several types of sodium and potassium channels clustered at the node. These ion channels include $Na_v1.1$, $Na_v1.2$, $Na_v1.6$, $Na_v1.7$, $Na_v1.8$, and $Na_v1.9$ sodium channels, which allow ion flux across the axon in order to regenerate the action potential at each node (Fjell et al., 2000; Boiko et al., 2001; Henry et al., 2005; Duflocq et al., 2008; Black et al.,

2012). Potassium channels present at the node include K_V3,1b, KCNQ2, and KCNQ3 channels (Devaux et al., 2003; Devaux et al., 2004). The potassium channels present at the node serve to regulate action potential regeneration at the node and modulate neuronal excitability (Battefeld et al., 2014; King et al., 2014). Due to the diversity of sodium and potassium channels at the node, not all nodes exhibit identical ion channel composition (Rasband and Peles, 2015). Other cytoskeletal and scaffolding proteins anchor these ion channels at the node of Ranvier. Notably, the neuronal-specific scaffolding protein ankyrinG anchors ions channels to βIV spectrin, which links to the actin cytoskeleton (Berghs et al., 2000; Kordeli et al., 1995). Neurofascin 186 and neural related cell adhesion molecule (NrCAM) are two adhesion molecules that bind to ankyrinG and form interactions with glial cells to further stabilize the node of Ranvier (Davis et al. 1996). In the PNS, gliomedin (a protein belonging to the olfactomedin family of proteins) binds neurofascin 186 and NrCAM, further stabilizing the node (Eshed et al., 2005). In the CNS a similar interaction may take place where extracellular matrix proteins, such as brevican, bind to neurofascin 186 and/or NrCAM to further stabilize the node. Studies have been conducted to determine how these various proteins cluster at the Node of Ranvier.

The formation of protein clusters at the node of Ranvier has been shown to be dependent on three factors; myelin-axon interaction, the neuronal cytoskeleton and the extracellular matrix (Susuki et al., 2013). I will first examine the myelin-axon interaction. Using a lysolecithin model of demyelination in the PNS, one study showed sodium channel clustering was lost, except at heminodes, which are composed of an unpaired paranode found at the transition of demyelinated and myelination brain regions and some isolated and dispersed regions thought to previously be nodes (Dugandzija-Novakovic et al., 1995). It has also been found that it is only after a Schwann cell begins producing MAG and is committed to myelination that there is a significant increase in sodium channel clustering (Martini and Schachner, 1986; Vabnick and Shrager, 1998). These studies indicate a role for interactions between the axons and the myelinating Schwann cells in the formation of the node in the PNS. Studies have also been

conducted to determine if the axo-glial interaction necessary for node formation in the PNS exists in the CNS. Using the *shiverer* mouse mutant, Rasband et. al. (1999) reported that axo-glial interaction was necessary for node protein clustering, as the *shiverer* mutant mice (which show uncompacted myelin and hypomyelination) displayed fewer and displaced sodium channel clusters (Rasband et al., 1999). The localization of caspr was also disrupted in these mice. In contrast, other studies have shown that axo-glial contact itself is not necessary for node formation, but the protein clustering relies on a protein secreted by the oligodendrocytes (Kaplan et al., 1997). Using a CGT-deficient mouse model, Dupree et al. (1999) further examined the importance of the axo-glial interaction for node formation. They found in CGT-deficient mice (which lack the enzyme necessary for generating galactolipids) nodal proteins (Na channels, neurofascin, AnkyrinG) clustered normally, while the potassium channels and caspr protein of adjacent regions were diffused along the internode and no longer restricted to their specific domains. Thus, not only are galactolipids important for myelin, but they are also necessary for the axo-glial interaction that form protein clusters in certain axonal domains. Other studies have shown that disrupting neurofascin 155 disrupts the paranode, eventually leading to node disruption as well (Pillai et al., 2009). Thus, studies in the CNS implicate axon-oligodendrocyte interaction as a necessary feature of node formation.

The extracellular matrix and cytoskeleton are also important in formation and maintenance of the node of Ranvier. The formation of sodium channel clusters at the edge of a growing span of myelin relies on the extracellular matrix protein gliomedin interacting with neurofascin 186 and NrCAM (Eshed et al., 2005; Feinberg et al., 2010). The gliomedin-NrCAM interaction allows for accumulation of neurofascin 186 (Feinberg et al., 2010; Eshed et al., 2007). In the CNS, it is thought that brevican, an extracellular matrix protein, serves the same role in the CNS that gliomedin plays in the PNS (Rasband and Peles, 2015). Brevican is known to localize at the node (Bekku et al., 2009), although brevican deficient mice show no major disruption of node formation (Brakebusch et al., 2002). Tamoxifen-

induced knockout of neurofascin 186 in mice also results in loss of gliomedin at PNS nodes and brevican at CNS nodes (Desmazieres et al., 2014). Neurofascin 186 also recruits the scaffolding protein ankyrinG to the node, and ankyrinG recruits the cytoskeletal protein βIV spectrin and sodium channels (Eshed et al., 2005; Lambert et al., 1997; Dzhashiashvili et al., 2007; Yang et al., 2007). Neurofascin 186 binds both ankyrinG and extracellular matrix proteins (Zonta et al., 2008; Eshed et al., 2005).

It has been reported that disruption of only one of the mechanisms of node formation, allows the other two to compensate, while disruption of two of these leads to node impairment (Susuki, 2013; Susuki et al., 2013). Creation of mutant mice with two of the following; knockout of extracellular matrix proteins (i.e. brevican knockout), caspr knockout, and mutant βIV spectrin, resulted in mice with fewer nodes, less density of proteins at the node, and severe neurological symptoms. As the node of Ranvier serves an important role in action potential conduction, maintenance of the nodes of Ranvier is important to maintain integrity of axonal function. Another important axonal domain, similar in composition to the node of Ranvier, is the axon initial segment.

The Axon Initial Segment

The axon initial segment (AIS) is an unmyelinated portion of the axon immediately distal to the soma. The AIS is similar in protein composition to the node of Ranvier (Yoshimura and Rasband, 2014). It contains multiple types of both sodium and potassium channels, the scaffolding protein ankyrinG, neurofascin 186, and βIV spectrin (Zhou et al., 1998; Kole et al., 2007; Pan et al., 2006) (Figure 2). However, unlike the node of Ranvier, ankyrinG is the master organizer of the AIS. AnkyrinG is required for sodium channel clustering at the AIS, and recruits βIV spectrin and adhesion molecules such as neurofascin and NrCAM (Zhou et al., 1998; Jenkins and Bennett, 2001; Yang et al., 2007). This has been

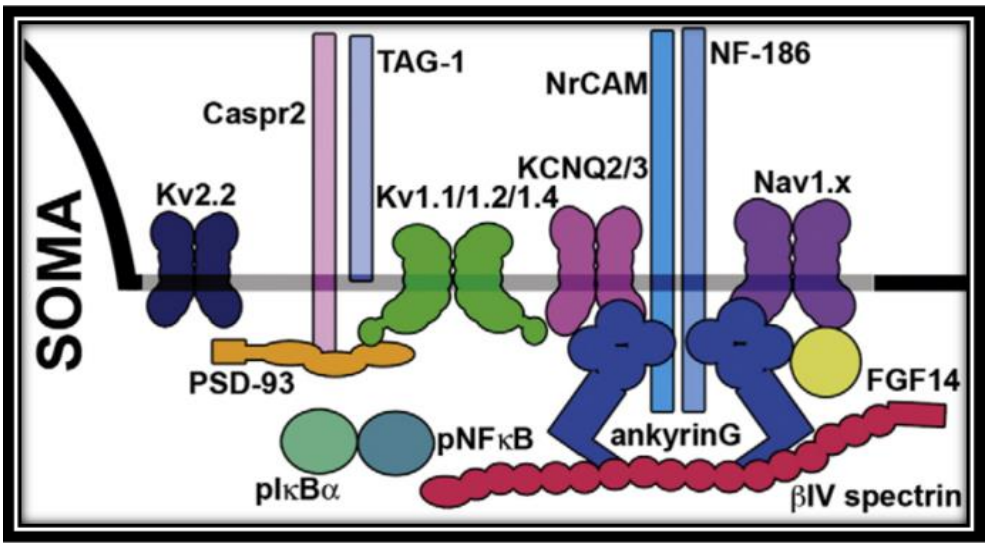

Figure 2. Schematic of proteins at the axon initial segment. AnkyrinG is a scaffolding protein that anchors sodium and potassium channels in place. AnkG also binds the adhesion molecules Neurofascin 186 and NrCAM and the cytoskeletal protein βIV spectrin.

demonstrated in ankyrinG knockout mice which do not show localization of these proteins to the initial segment and also display impaired action potential generation (Jenkins & Bennett, 2001; Zhou et al., 1998). Without ankyrinG, the AIS also cannot maintain proper neuronal polarity, causing the axon to default to a dendritic-like morphology (Hedstrom et al., 2008; Sobotzik et al., 2009). Although ankyrinG is important for the assembly and function of the AIS, other proteins contribute to maintenance of the AIS. Neurofascin 186 is not the initiator of assembly of the AIS, nor is it required for AIS assembly, however, studies have shown that it is important for the stability of the AIS (Hedstrom et al., 2008; Zonta et al., 2011). Knockout of neurofascin 186 in adult mice leads to altered action potentials and dispersion of protein clustering at the AIS (Zonta et al., 2011). Thus neurofascin is important for the stability of the AIS, but not the assembly, in contrast to its role at the node of Ranvier.

The differences between the AIS and the node of Ranvier also extend to the function of each domain. The AIS is important in to neuronal function because it is the site of action potential initiation in the neuron (Stuart and Sakmann, 1994; Mainen et al., 1995; Palmer and Stuart, 2006). Further research has found that different sodium channel compositions at the proximal and distal ends of the AIS contribute to its function (Hu et al., 2009). The distal end of the AIS, containing a dense concentration of $Na_V1.6$ channels, initiates the action potential, while the proximal end, containing a dense concentration of $Na_V1.2$ channels, back propagates the action potential to the cell body (Hu et al., 2009). In addition, the AIS maintains neuronal polarity (Hedstrom et al., 2008; Sobotzik et al., 2009). Neuronal polarity is maintained by establishing both a surface diffusion barrier and an intracellular traffic filter that allow axonal proteins through the AIS and keeps dendritic proteins out (Leterrier and Dargent, 2014). The diffusion barrier was first discovered by Winckler et al. (1999) who found that the dendritic protein GluR1 could be found in the axon hillock, but not in the AIS. Research into the selectivity filter has shown that motor protein-cargo complexes carrying dendritic proteins are restricted from entering the AIS

(Song et al., 2009). Thus the AIS serves to initiate action potentials, but also has a two-component mechanism to maintain proper axo-dendritic polarity of the neuron.

The AIS also has homeostatic mechanisms in order to protect neuron functionality after insult or injury. Using an avian model, the AIS was studied in neurons that responded to low, medium, or high frequencies (Kuba et al., 2006). Results from this study found that the AIS length and the distance from the soma were different between these types of neurons in order to optimize the threshold at which an action potential was generated (Kuba et al., 2006). This variation in AISs length and location is used in order to accurately determine interaural time differences at various frequencies (Kuba et al., 2006). Research by the same group determined that following reduced input to the neuron, the AIS increased in length in order to increase the excitability of the cell (Kuba et al., 2010). *In vitro*, another study showed that the AIS increased its distance from the soma in response to chronic depolarization, reducing the overall excitability of the cell (Grubb and Burrone, 2010). Similarly, in a mouse model of Angelman syndrome, a disorder characterized by cognitive impairment, motor abnormalities, and seizures, the AIS lengthened in response to a hyperpolarized resting membrane potential (Kaphzan et al., 2011). When the resting membrane potential was returned to normal using genetic modification, the AIS shortened (Kaphzan et al., 2013). In response to traumatic brain injury in a mouse model, the AIS shortened, suggesting altered neuronal excitability (Baalman et al., 2013). In a stroke model, the AIS shortened in response to injury, and surviving neurons were capable of sprouting a new initial segment (Hinman et al., 2013). These studies reveal that the AIS can change length and location in order to deal with hyper- or hypo-excitability. The AIS is then a plastic structure capable of adapting to its environment, making it an important domain to study in disease states affecting the axon, such as multiple sclerosis.

Multiple Sclerosis

Multiple sclerosis (MS) is a neurodegenerative disorder and one of the most common autoimmune disorders of the CNS (Files, 2015). It is diagnosed when patients have had at least two attacks and display demyelinating plaques in the brain or spinal cord (Polman et al., 2011). The cause of MS is not known, but it is thought to be caused by a mixture of genetic and environmental factors, with risk factors associated with geographic region, vitamin D levels, a first degree relative diagnosed with MS, and certain variations in the genes for the human leukocyte antigen system (HLA) (including the major histocompatibility complex (MHC)) on chromosome 6 (Files et al., 2015; Ramagopalan and Sadovnick, 2011). Clinical presentation is highly variable with patients presenting with symptoms such as limb weakness, double vision, and ataxia, which often progress to include fatigue, heat sensitivity, bladder problems, muscle spasms, cognitive deficits, depression and eventually disability (Files et al., 2015 Hauser & Oskenberg, 2006). The majority of patients (about 85%) are first diagnosed with a form of MS called relapsing-remitting MS, which is characterized by episodes of neurological disability, followed by full or partial recovery. Most of these patients eventually progress to secondary progressive MS, which is characterized by a steady decline (Dutta and Trapp, 2011). Primary progressive MS is another form of MS, characterized by a steady decline from onset of symptoms. Progressive relapsing is the least common form of MS, and is characterized by progressive neurological decline in conjunction with distinct attacks, with or without recovery (Dutta and Trapp, 2011). MS is characterized by focal inflammatory demyelination, but break down of the blood brain barrier and gliosis are also relevant components of MS pathology (Dutta and Trapp, 2011). In MS, an autoimmune response targets the myelin and oligodendrocytes and destroys them, causing widespread demyelination. However, degeneration of the axon has been proposed to be the primary cause of irreversible neurological damage (Dutta and Trapp, 2011).

Inflammation in MS

Inflammation is one significant aspect of MS. Both the innate and adaptive immune system are involved in the pathology of MS (Hemmer et al., 2015). Microglia, the innate immune cells of the CNS, and macrophages, which infiltrate from the periphery, interact with the antigen-specific CD4+ T cells and CD8+ T cells, as well as the B cells, of the adaptive immune system (Jacobsen et al., 2002; Babbe et al., 2000; Wraith and Nicholson, 2012; Ransohoff and Engelhardt, 2012). In the early stages of MS, there are two mechanisms that have been proposed that lead to the development of inflammatory lesions: 1. inflammation drives pathology, or 2. pathology occurs and inflammatory cells are recruited (Hemmer et al., 2015; Kutzelnigg et al., 2005; Trapp and Nave, 2008). The first hypothesis suggests that autoreactive T-cells become activated in the periphery by cross-reactivity, molecular mimicry, or bystander activation (Hemmer et al., 2015). It is proposed that the immune response in MS may be caused by a virus or bacteria and thus the autoimmune attack on myelin components, such as MBP, may then be the result of molecular mimicry to a viral or bacterial component (Wucherpfennig and Strominger, 1995; Sospedra and Martin, 2005; Glass et al., 2010). According to this theory, the autoreactive T-cells migrate to the lymph nodes, and produce antigen-specific T cells and B cells, which then make their way into the CNS (Henderson et al., 2009). This entry into the CNS may be mediated by chemokines from endothelial cells of the BBB which bind to receptors found on T-cells (Alt et al., 2002; Hillyer et al., 2003; Columba-Cabezas et al., 2003; Hernandez-Pedro et al., 2013). The alternative hypothesis is that an event within the CNS triggers microglia reactivity, which amplifies the immune response by recruiting innate and adaptive immune cells (Hemmer et al., 2015; Kutzelnigg and Lassmann, 2014). An inherent defect, such as a genetic mutation in oligodendrocytes, would cause spontaneous cell death and recruitment of microglia. This would explain why lesions form in normal appearing white matter, without the presence of lymphocyte infiltration (Barnett and Prineas, 2004; Mistry et al., 2011). A secondary immune response would be initiated when antigens drain out of the CNS into deep lymph nodes (Hemmer et al.,

2015). Dendritic cells would perform the role of processing the antigens and transfer them to the lymph nodes, or the antigens would drain through the cerebrospinal fluid, which would then prime T-cells (Hatterer et al., 2006; Xie et al., 2013). Regardless of the mechanism of entry, once in the CNS, T-cells release pro-inflammatory cytokines (such as TNFα and Il1β) and chemokines (such as MCP-1) that recruit other immune cells including microglia, peripheral macrophages, B cells, and astrocytes to the site of inflammation (Hemmer et al., 2015; Glass et al., 2010). The microglia and macrophages can then form an inflammatory loop by production of factors such TNFα, Il1β, and reactive oxygen species (Block et al., 2007; Haji et al., 2012; Guemez-Gamboa et al., 2011). This inflammatory loop can lead to the demyelination and axonal damage that is characteristic of MS.

Demyelination in MS

MS is characterized by areas of focal inflammatory demyelination, known as plaques, that show breakdown of the BBB, involvement of immune cells, and death of oligodendrocytes (Kutzelnigg and Lassmann, 2014). Different forms of MS show different forms of white matter plaques including acute, chronic, and remyelinated (Popescu et al., 2013). Although acute lesions can become remyelinated, chronic lesions may cause irreversible axonal damage (Kutzelnigg et al., 2005; Kutzelnigg and Lassmann, 2006). MS was initially thought to be primarily characterized by these various types of white matter lesions, but gray matter lesions are also apparent in MS and have been linked to many of the physical disabilities and cognitive impairment in MS (Pirko et al., 2007).

As previously mentioned, inflammation in MS is caused by reactive T-cells that release pro-inflammatory cytokines and chemokines (Glass et al., 2010; Hemmer, 2015). This inflammation could cause demyelination or T cells could bind MHC class I antigens on oligodendrocytes (Kutzelnigg and Lassmann, 2014; Lubetzki and Stankoff, 2014; Hoftberger et al., 2004). T cells recruit B cells, microglia, and macrophages to sites of inflammation. B cells are also adaptive immune cells, and act as antigen

presenting cells that display MHC class II molecules (Hemmer et al., 2015). B cells are thought to be responsible for production of autoantibodies. As mentioned previously, autoantibodies to myelin proteins such as MOG, MAG, PLP, MBP, and neurofascin have been found in MS patients (Menon et al., 1997; de Graaf et al., 2012; Mathey et al., 2007). Other autoantibodies against non-myelin proteins, such as Kir 4.1 (a type of potassium channel) have also been discovered (Wunsch et al., 2014; Mathey et al., 2007). B cells could attack myelin, potassium channels, or neurofascin, leading to demyelination and neurodegeneration. Several therapies targeting B cells for depletion have been successful in reducing lesions and relapses, solidifying the role of B cells in demyelinating lesions in MS (Hauser et al., 2008; Kappos et al., 2011). The idea that inflammation might results from an inherent abnormality in oligodendrocytes would implicate slightly different reasons for demyelination. In this case, oligodendrocyte cell death would recruit the inflammatory response and lead to demyelination (Barnett and Prineas, 2004). This response would rely on microglia as the resident immune cells of the CNS to initiate the response.

In addition to B cells, and T cells, microglia and macrophages are also important to consider in MS demyelination. Microglia and macrophages are phagocytic cells that could cause demyelination by phagocytosing myelin (Hendrickx et al., 2014). The reason microglia and macrophages target myelin for degradation is not entirely clear, but studies indicate there may be changes to myelin in MS patients that recruit the microglia and macrophages which in turn initiate demyelination (Hendrickx et al., 2014). The exact role of microglia in MS lesion is somewhat debated, as they may have both pro-inflammatory and beneficial effects, but this idea will be discussed further. Microglia and macrophages, along with B cells and T cells contribute to the demyelinating plaques that are the hallmark of MS. However, another important pathology to consider in MS is axonal damage.

Axonal Pathology in MS

In addition to inflammation and demyelination, axonal pathology is also present in MS patients (Haines et al., 2011) . Axonal pathology has been studied in the context of demyelinating lesions. It has been shown in MS that axons are transected at the site of demyelinating lesions (Ferguson et al., 1997; Trapp et al., 1998) . Additional studies correlated axonal injury or loss with acute demyelination and inflammation, but also found axonal injury in chronic lesions (Bitsch et al., 2000; DeLuca et al., 2004; Frischer et al., 2009). In some cases, axonal injury preceded demyelination (Marik et al., 2007). However, there appeared to be little evidence of axonal injury in remyelinated lesions (Kornek et al., 2000). Quantification of axonal number in the brain and spinal cord revealed an average reduction of 68% in axonal number in the spinal cord (Bjartmar et al., 2000) and an overall reduction of 64% in demyelinated lesions in the brain and spinal cord (Mews et al., 1998). It should be noted that both studies observed variability in axon number depending on lesion location, type of lesion, and between patients.

Amyloid precursor protein (APP) serves as a marker for axonal injury because axonal injury disrupts APP transport down the axon, causing accumulation of APP within the axon (Hayashi et al., 2015). Many studies have found accumulation of APP in axons in MS lesions. Studies have also observed Wallerian degeneration in brain tissue directly adjacent to plaques or in normal appearing white matter (NAWM) (Evangelou et al., 2000; Bjartmar et al., 2003; Dziedzic et al., 2010). Together these studies indicate that axonal pathology correlates with demyelinating lesions, but also occurs independent of myelin loss. The possibility of axonal pathology that is independent of myelin loss is further support by both animal and human studies. Marik (2007) reported that axonal injury preceded demyelination, while in human samples axonal degeneration has been observed in NAWM (absent of plaque involvement) (Kutzelnigg et al., 2005; Ramio-Torrenta et al., 2006; Siffrin et al., 2010). Furthermore, axonal

degeneration in the spinal cord is thought to contribute to spinal cord atrophy with little involvement of demyelinating lesions (Evangelou et al., 2005). Although axonal pathology is a consistent finding in MS and is observed both as consequential and independent of myelin loss, the exact mechanisms of axonal degeneration in MS are still not well understood.

Studies in animal models have shed more light on possible mechanisms of axonal degeneration in MS, both dependent and independent of demyelination. As mentioned previously, myelin is necessary for the maintenance of the node of Ranvier (Dupree et al., 2004), as demyelination leads to diffusion of protein clusters associated with the domains of the nodal region. In addition, other studies from our lab have shown that myelin is required for maintenance of axonal domains (Dupree et al., 2004; Marcus et al., 2006; Pomicter et al., 2010). However, axonal pathology in the absence of demyelination has also been studied in mouse models. Studies using CNP deficient mice, which do not exhibit myelin loss, have shown that lack of CNP leads to axon swelling and degeneration, which eventually leads to premature death (Lappe-Siefke et al., 2003). Despite absence of CNP and the presence of axonal degeneration, myelin is maintained in these mice, suggesting axonal pathology can occur independent of demyelination. Further research has shown that axonal pathology may be a primary event in MS. Comparing demyelinating and non-demyelinating strains of the mouse hepatitis virus (MHV) viral model of MS, one study revealed axonal degeneration in both the myelinating and demyelinating models (Das Sarma et al., 2009). In the non-demyelinating model, early axonal changes occurred in the absence of demyelination. Using *in vivo* imaging another study revealed focal axonal degeneration in a MOG-induced EAE mouse model of MS (Nikic et al., 2011). They tracked individual axons, using thy1-YFP mice that possessed a subset of fluorescently labeled axons, and revealed pathology that began with focal swellings and lead to axonal fragmentation. Axonal pathology was present even in axons with intact myelin sheaths. Using human MS tissue, they found axonal degeneration in axons with intact myelin sheaths that correlated with damage seen in EAE mice (Nikic et

al., 2011). In order to further elucidate the mechanisms of axon degeneration as a primary pathology, studies have looked at other potential contributors such as breakdown of the BBB and contribution of microglia. Breakdown of the BBB may contribute to inflammation and axonal pathology. In the EAE mouse model studies have shown the fibrinogen leakage into the CNS following BBB disruption can cause inflammation and axonal damage (East et al., 2005; Akassoglou et al., 2004; Davalos et al., 2012). In one study, fibrinogen leakage across the BBB correlated with axon degeneration and caused microglia clustering at the BBB (Davalos et al., 2012). The culmination of research in human MS tissue and in mouse models of MS reveals that the axon is a target of both primary and secondary pathology in MS caused by multiple factors including demyelination, inflammation, breakdown of the BBB, and immune cells such as microglia and macrophages.

Microglia

Microglia are the immune cells of the brain, however, their exact role in the CNS, especially in disease states like MS is undergoing constant revision. Microglia are the resident immune cells of the CNS and are from the myeloid progenitor cell lineage derived from the embryonic yolk sac (Ginhoux and Prinz, 2015). Non-reactive or 'surveying' microglia have long ramified processes and a small cell body, but once signaled to respond to disease or trauma they adopt a more amoeboid shape (Kettenmann et al., 2011). Microglia have a wide range of functions. They can phagocytose debris, recruit peripheral immune cells to sites of damage, produce pro-inflammatory and anti-inflammatory factors, and physically associate with damaged neurons (Kettenmann et al., 2011). Recent research has shown that microglia associate with the AIS in the developing brain (Baalman et al., 2015). Microglia possess cytokine receptors, chemokine receptors, scavenger receptors, complement receptors, and pattern recognition receptors that allow them to recognize foreign invaders (such as bacteria or viruses) or injury (Kierdorf and Prinz, 2013; Benarroch, 2013). Once reactive, microglia can recruit peripheral

immune cells to sites of damage or disease by producing chemokines, such as CCL2, which can contribute to breakdown of the BBB and recruitment of leukocytes into the CNS (Goldmann and Prinz, 2013). Microglia secrete pro-inflammatory cytokines (such as TNFα or Il1β) and reactive oxygen species that can contribute to pathology in disease states (Benarroch, 2013). However, they can also produce anti-inflammatory cytokines like Il-10 and TGFβ (Benarroch, 2013).

Corresponding to the variety of receptors microglia express and the variety of cytokines and chemokines they can produce, the exact role of microglia varies by disease state. Much discussion had been focused on the M1/M2 polarization of microglia. This terminology was originally investigated in macrophages, then adopted to microglia (Tang and Le, 2016). 'M1' or 'classically activated' microglia are generally identified by production of TNFα, Il-1β, inducible nitric oxide synthase (iNOS), and ROS. 'M2' microglia include both 'alternatively activated' and 'acquired deactivation' microglia. 'Alternatively activated' microglia are usually induced by exposure to IL-4 or Il-13 and associated with production of Arginase 1 (Arg1), anti-inflammation, and tissue and ECM repair. 'Acquired deactivation' is generally considered the result of exposure to Il-10 of TGFβ (transforming growth factor beta) and usually involved uptake of apoptotic cells (Cherry et al., 2014; Tang and Le, 2016)**.** It is thought that 'M1' microglia initiate an acute inflammatory response in the CNS by responding to invading pathogens, injury, or disease. 'M2' microglia then resolve inflammation and promote repair (Cherry et al., 2014; Tang and Le, 2016). These categorizations may be helpful in distinguishing the different roles of microglia, but may not give a full picture of all possible microglia phenotypes (Cherry et al., 2014). However, examining expression profiles of microglia may shed light on functions of microglia.

Using human microglia, research revealed *in vitro* that microglia induced by IFNγ (pro-inflammatory state) highly upregulated Il-1β and TNFα expression compared to those induced by Il-4 (anti-inflammatory state) (Peferoen et al., 2015). The induction of microglia by pro-inflammatory or anti-

inflammatory factors polarized the microglia to produce pro-inflammatory or anti-inflammatory factors (respectively). Specifically, IFNγ polarized microglia expressed the pro-inflammatory factors TNFα, Il-1β, and CXCL10 (C-X-C motif chemokine 10), while the Il-4 polarized microglia expressed the anti-inflammatory chemokine CCL22 (C-C motif chemokine 22). However, this polarization was shown to be reversible when microglia were placed in new environments, indicating that they can adapt in response to a change in external cues (Peferoen et al., 2015). Translating this observation to MS tissue, researchers found that the microglia in NAWM resembled those found in remyelinating lesions, displaying a phenotype intermediate of the IFNγ and Il-4 induced microglia *in vitro* (Peferoen et al., 2015). In studies revealing axonal pathology as a primary event in MS, the axonal degeneration was found to be mediated by microglia/macrophage release of reactive oxygen species (Nikic et al., 2011). Additional research in animal models has expanded the understanding of the various roles of microglia.

Research has shown that inhibiting activation of microglia and macrophages in a MOG-induced EAE model of MS attenuates symptoms of the disease (Bhasin et al., 2007). This study found that treating EAE induced mice with microglia inhibitory factory (MIF) at the onset of EAE symptoms decreased the severity of the disease, exhibited by decreased clinical score, and lead to complete recovery from EAE. In this study, the timing of microglia activation and inhibition was important for modulating disease course. However, protective roles have also been identified for microglia in MS. Microglia activated by IL-4 injected into the cerebrospinal fluid of EAE rodents induced oligodendrogenesis and decreased expression of TNFα (Butovsky et al., 2006b; Butovsky et al., 2006a). In contrast, microglia activated by IFNγ (interferon gamma) impeded oligodendrogenesis from adult neural stem cells (Butovsky et al., 2006b; Butovsky et al., 2006a). In a relapsing rat model of EAE, one study examined activation patterns of microglia/macrophages and their association with disease state (Mikita et al., 2011). Using iNOS as a marker for M1 microglia/macrophages, and Arg1 as a marker for M2 microglia/macrophages, the authors found that iNOS production remained higher in severe

relapsing EAE rats compared to mild EAE rats. In addition, intravenous injection of monocytes induced by Il-10/Il-13 resulted in a decrease in clinical score and a higher expression of Arg1, indicating a role for alternatively activated microglia/macrophages in resolving inflammation (Mikita et al., 2011). The complex role of microglia in MS and its mouse models highlight the need for further research in order to understand the various ways in which microglia may contribute to pathology in MS. One way they may mediate pathology in MS is via the complement system of immunity.

The Complement System of Immunity

The complement system is one aspect of immunity of particular interest in MS. Complement proteins have been found in demyelinating lesions in MS (Woyciechowska and Brzosko, 1977; Gay and Esiri, 1991; Ingram et al., 2014). As mentioned previously, microglia can also be activated by complement proteins (Benarroch, 2013). The complement system has three major pathways: the classical pathway, the alternative pathway, and the lectin pathway. Figure 3 shows the cascade of the three pathways (Dunkelberger and Song, 2010). The classical pathway is activated by antibody/antigen interaction when C1q binds the antibody/antigen complex and recruits C1s and C1r. The alternative pathway is activated by spontaneous hydrolysis of C3 to C3(H20), which is then cleaved by Factors B and D. The Lectin pathway is activated by Mannose Binding Lectin (MBL) recognizing specific carbohydrates found on the surface of pathogens. In the classical pathway, C1q activates C1r and C1s which cleave C2 and C4 into C2a, C2b, C4a, and C4b. C4b and C2a form a protease that cleaves C3 into C3a and C3b. In the alternative pathway, C3 spontaneously hydrolyzes to C3(H20) and joins with Factor B and Factor D to cleave C3 into C3a and C3b. This can create an amplification loop, continuing cleavage of C3. In both the classical and alternative pathways, cleavage of C3 leads to cleavage of C5, and a further cascade which can form the MAC-1 complex (C5b-C9) that lyses cells. A host of other complement molecules (i.e. Decay Accelerating Factor, Properdin, Factor I, Factor H, C4bp, etc.) modulate activity at various

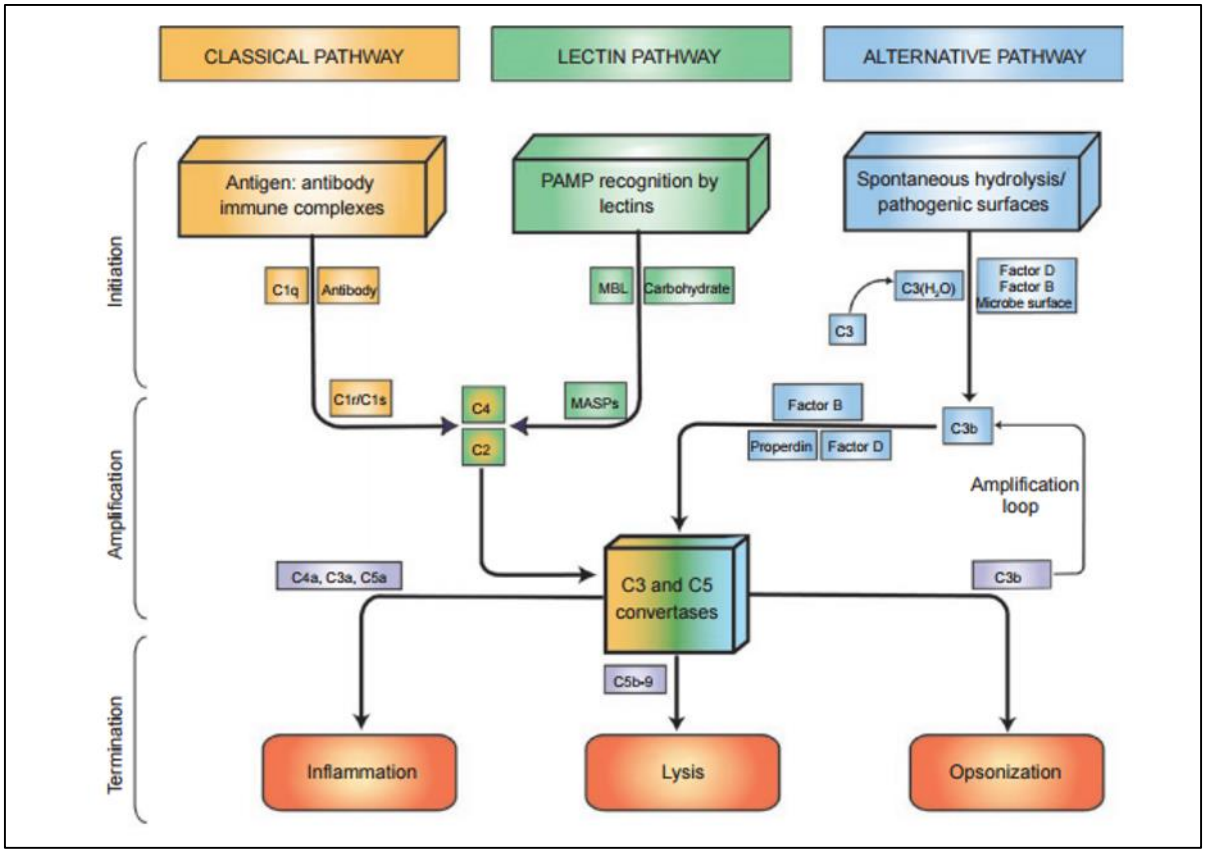

Figure 3. Diagram of the complement system. The complement system consists of the classical, lectin, and alternative pathways. The classical pathway is activated by C1q binding an antigen/antibody complex which then recruits C1r and C1s. The C1qrs complex then cleaves C2 and C4. The lectin pathway is activated mannose binding lectin (MBL) binding specific carbohydrates and activating MBL-associated serine proteases (MASPs) which also cleave C2 and C4. C2a and C4b form the C3 convertase, which cleaves C3. The alternative pathway is activated by spontaneous hydrolysis of C3 to C3(H20), which in conjunction with Cfb and Cfd cleaves C3. The C3 convertase cleaves C3, and C3b then joins C2a and C4b to form the C5 convertase. C5 is then cleaved into C5a and C5b. C5b, C6, C7, C8, and C9 form the MAC-1 complex, which causes cell lysis. C3a, C4a, and C5a, are released ad can recruit other inflammatory factors. C3b and C4b are also opsonins which can target cells for phagocytosis by microglia and macrophages. Adapted from Dunkleberger & Song, 2010.

steps of all three of the complement pathways, creating a complex, highly regulated system (Dunkelberger and Song, 2010; Merle et al., 2015a; Merle et al., 2015b).

Complement proteins play various roles in the cell. C4b, C3b, and its breakdown fragment iC3b, are molecules that can opsonize cells, and bind to complement receptors such as CR1 and CR3 to induce phagocytosis of opsonized cells by macrophages and microglia (Merle et al., 2015b; Mortensen et al., 2015). C3a and C5a are anaphylatoxins that can bind to receptors on immune cells in to recruit them and induce inflammation (Merle et al., 2015b; Klos et al., 2009). C4a is also generally considered an anaphylatoxin, but its role in recruiting inflammatory factors is debated .. The role of complement has also been studied in multiple models of neurodegeneration and neuroinflammation, particularly Alzheimer's disease. There are both detrimental and neuroprotective effects of complement proteins indicating that over activation or unrestrained production of complement proteins can contribute to disease (Bonifati and Kishore, 2007; Orsini et al., 2014; Stephan et al., 2012). In particular, binding of C3 to its receptor, CR3, has been shown to prime microglia in EAE, a necessary step for further activation of microglia (Ramaglia et al., 2012). Complement proteins, specifically C1q and C3, have been shown to have a role in synaptic plasticity, pruning synapses both during development and in disease (Stevens et al., 2007; Chu et al., 2010). Further research has determined that complement-mediated synaptic pruning involves microglia, which phagocytose synaptic proteins in response to complement signals (Schafer et al., 2012; Bahrini et al., 2015; Tremblay and Majewska, 2011). The complement-initiated pruning of synapses was studied in retinal ganglion cells (Stevens et al., 2007; Schafer et al., 2012). Initial studies found the complement proteins C1q and C3 were highly upregulated in a model of glaucoma, and were deposited at the synapse (Stevens et al., 2007). A subsequent study looked at complement in development during pruning of synapses. In this study, C3 binds to its high-affinity receptor, CR3, on microglia (Schafer et al., 2012). Where exactly the complement cascade, beginning with C1q, is activated is unclear, but both neuros and astrocytes can produce complement proteins, which were shown to be

at the synapse. The C3/CR3 interaction induces microglia to phagocytose the synapse, evidenced by synaptic proteins found inside the microglia (Schafer et al., 2012). These studies provide a new role for the microglia and the complement system in neural plasticity and disease.

Background Data

Based on previous research implicating axonal domains as targets of degeneration in MS and various models, our lab examined pathology of the AIS in MS. Preliminary data from our lab indicates a possible loss of axon initial segments in MS (Figure 4). Our research has shown that that stability of the node of Ranvier is dependent on myelin integrity (Dupree et al., 2004), and since the node of Ranvier and the AIS are very similar in protein composition, we hypothesized that the AIS might also be dependent on myelin integrity for stability. Analysis of AIS stability in the Cuprizone model of demyelination revealed that AIS stability is independent of myelin integrity (Clark et al., 2016). In the Cuprizone model, despite demyelination in the cortex, the AIS remained intact and maintained length and number similar to control mice (Figure 5). However, when we examined AIS stability in an inflammatory model of MS, we saw different results. Experimental autoimmune encephalomyelitis (EAE), is a mouse model of MS that displays CNS inflammation, but no observable cortical demyelination. In the EAE induced mice, the AIS was shortened at the early stage of EAE and lost at the late stage of EAE (Clark et al., 2016) (Figure 6 & 7).When we examined microglia morphology in both of these models, we found that reactive microglia were present in both models (Clark et al., 2016). Reactive microglia appeared in both models at an early stage of the disease, prior to any pathology, and maintained reactivity throughout the course of the disease (Figure 8). Since our hypothesis was that reactive microglia were responsible for AIS disruption, we proposed that microglia in the demyelination model exhibited a differential effect on the AIS as compared to the AISs in the inflammation model. The goal of my project was to address this hypothesis.

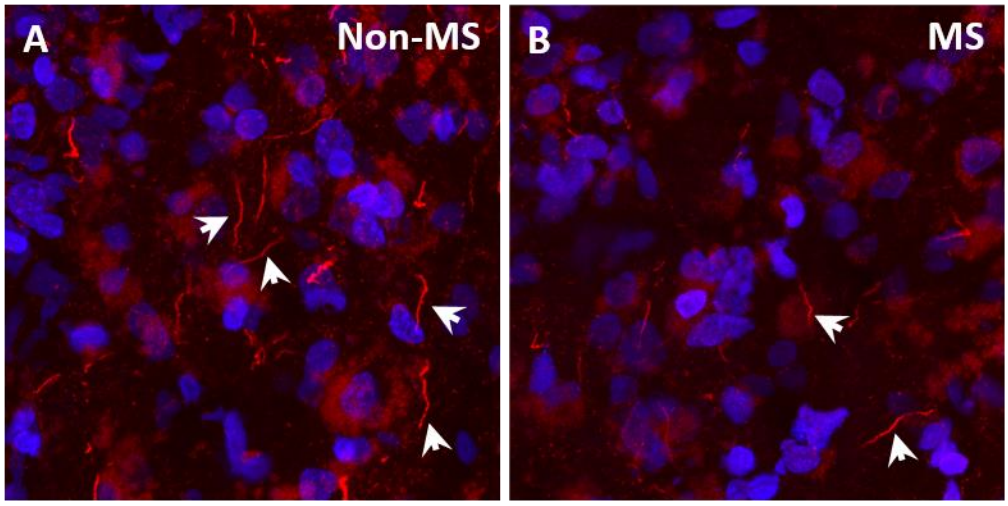

AnkyrinG-Red NeuN- Blue

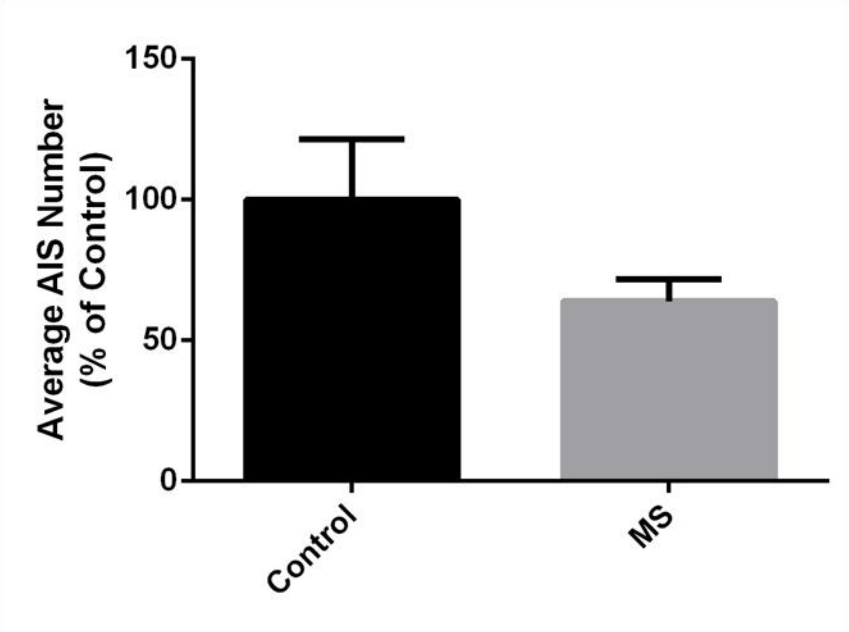

Figure 4. Preliminary data indicated loss of axon initial segments in MS tissue. Immunolabeling with an antibody directed against the AIS marker AnkyrinG exhibited decreased AIS number in human MS tissue (B) compared to non-MS tissue (A). Quantitation of AIS number in non-MS and MS tissue (C) indicated a trend toward a decreased number of AISs in MS tissue.

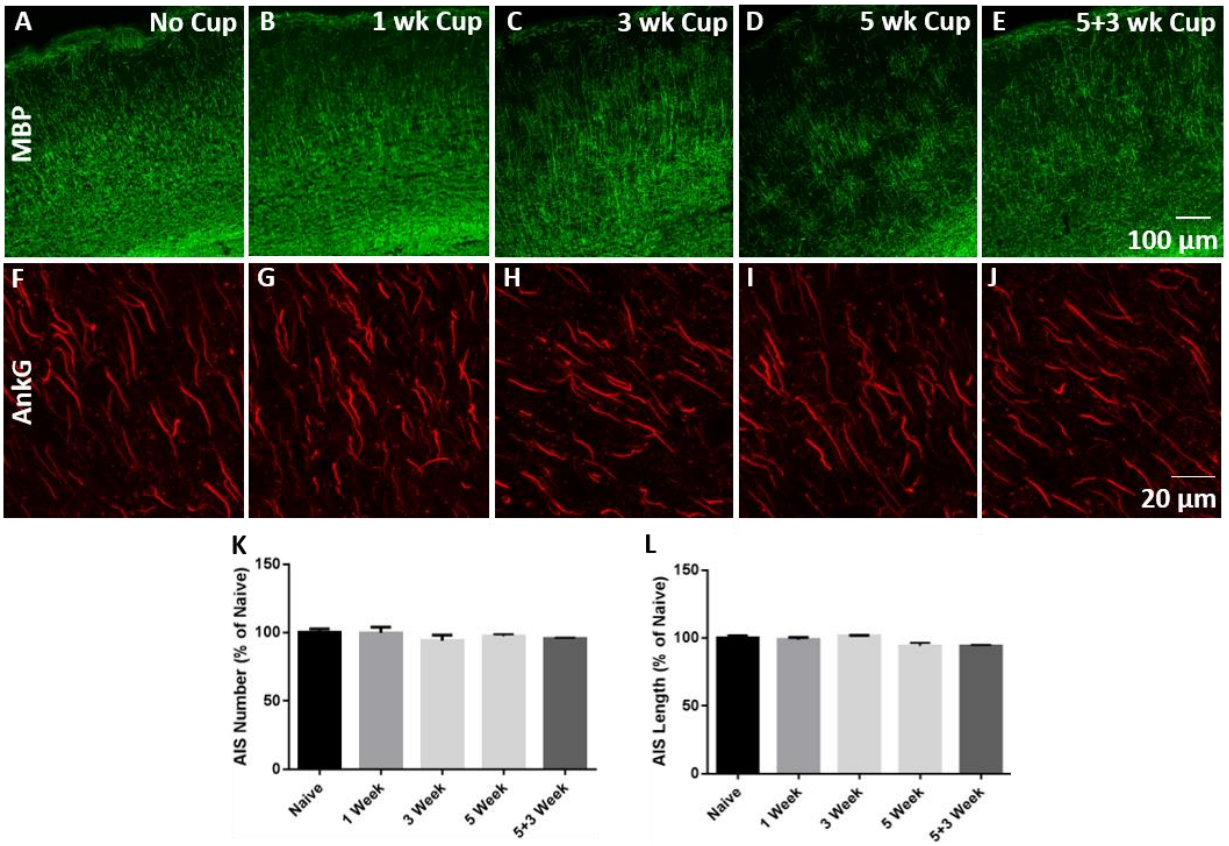

Figure 5. AIS length and number were maintained in the presence of demyelination. Immunolabeling with an antibody directed against MBP showed cortical demyelination at the 3 week (C) and 5 week time (D) time points compared to no Cuprizone treatment (A) or 1 week Cuprizone treatment (B). At the 5+3 week time point (E), remyelination was observed. Immunolabeling using an antibody directed against AnkyrinG revealed no observable change in AIS number length at the 1, 3, 5, or 5+3 week time points (G-J) compared to naïve (F). Quantitation of AIS number (K) and length (L) revealed no significant change in AIS number or length compared to naïve. Therefore the AIS remains stable despite demyelination.

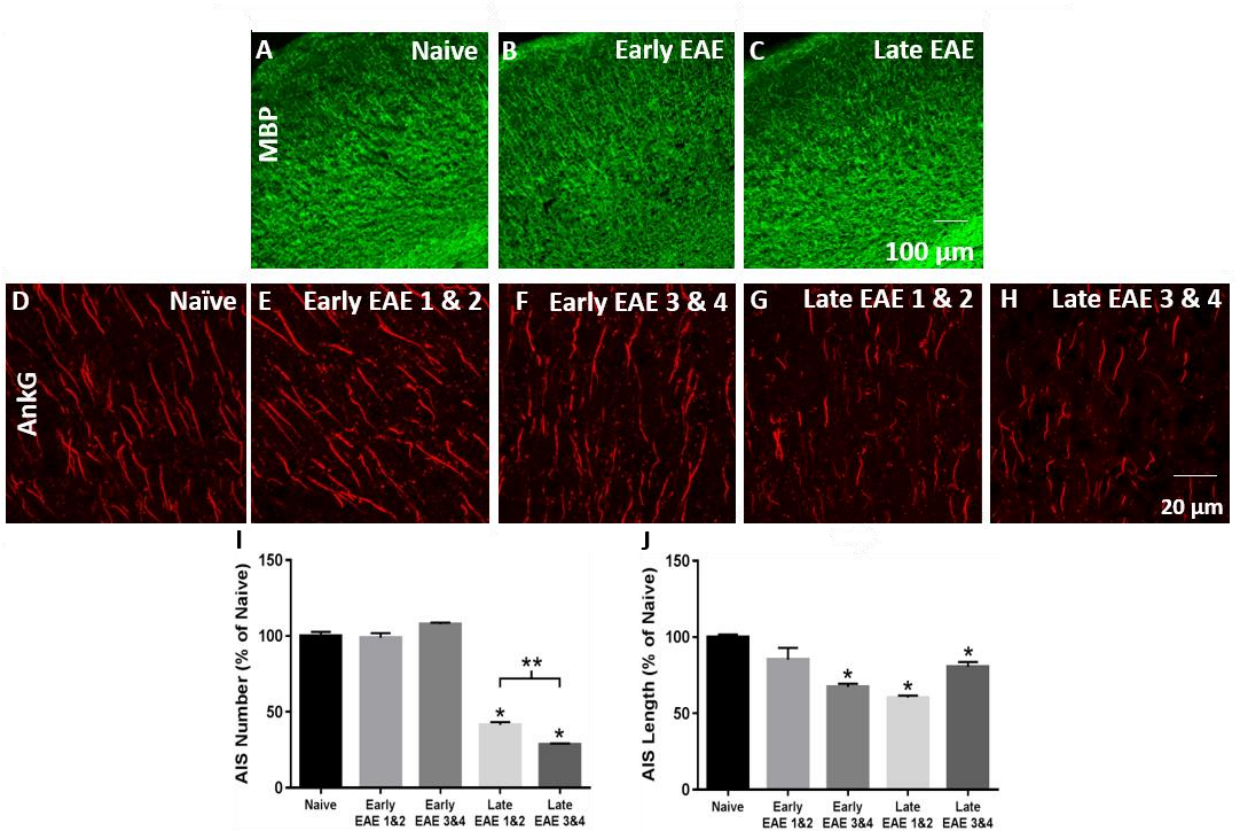

Figure 6. AIS length and number were altered in the absence of demyelination. Immunolabeling using an antibody directed against MBP revealed no observable cortical demyelination in early EAE (B) or late EAE (C) compared to naïve (A). Immunolabeling using an antibody directed against AnkyrinG revealed shortening of AIS length at the early 1&2 time point (F) and loss of AIS number at the late 1&2 (G) and late 3&4 (H) time points. Quantitation of AIS number (I) revealed a statistically significant decrease in AIS number at the late 1&2 and late 3&4 time points compared to naive. Quantitation of AIS length (J) revealed a statistically significant decrease in AIS length at the early 3&4, late 1&2, and late 3&4 time points compared to naïve. Therefore, AIS stability is altered in an inflammatory model of MS, but not in a model of demyelination.

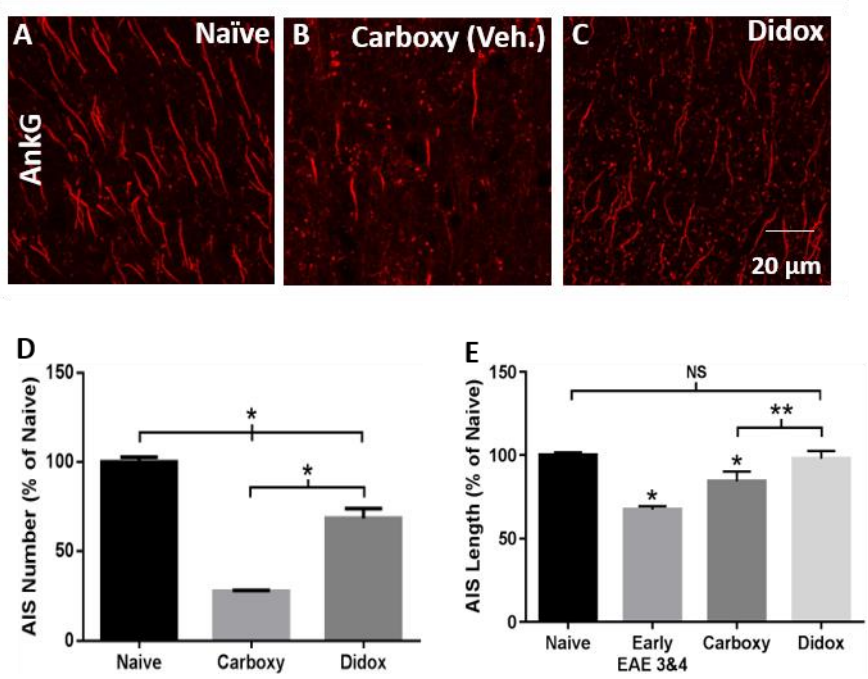

Figure 7. AIS length increases after treatment with the anti-inflammatory Didox. Immunolabeling using an antibody directed against AnkyrinG revealed an increase in AIS number in Didox treated mice (C) compared to carboxymethylcellulose vehicle control (B). The number of AISs was similar to naïve (A). Quantitation of AIS number (D) revealed the number of AISs after Didox treatment was not significantly different from naïve, but it was significantly different from vehicle treated mice. Quantitation of AIS length (E) revealed that lengths in Didox treated mice were not significantly different from Naïve, but they were significantly different between Didox treated and vehicle treated mice. Therefore, anti-inflammatory treatment may rescue AIS shortening and loss.

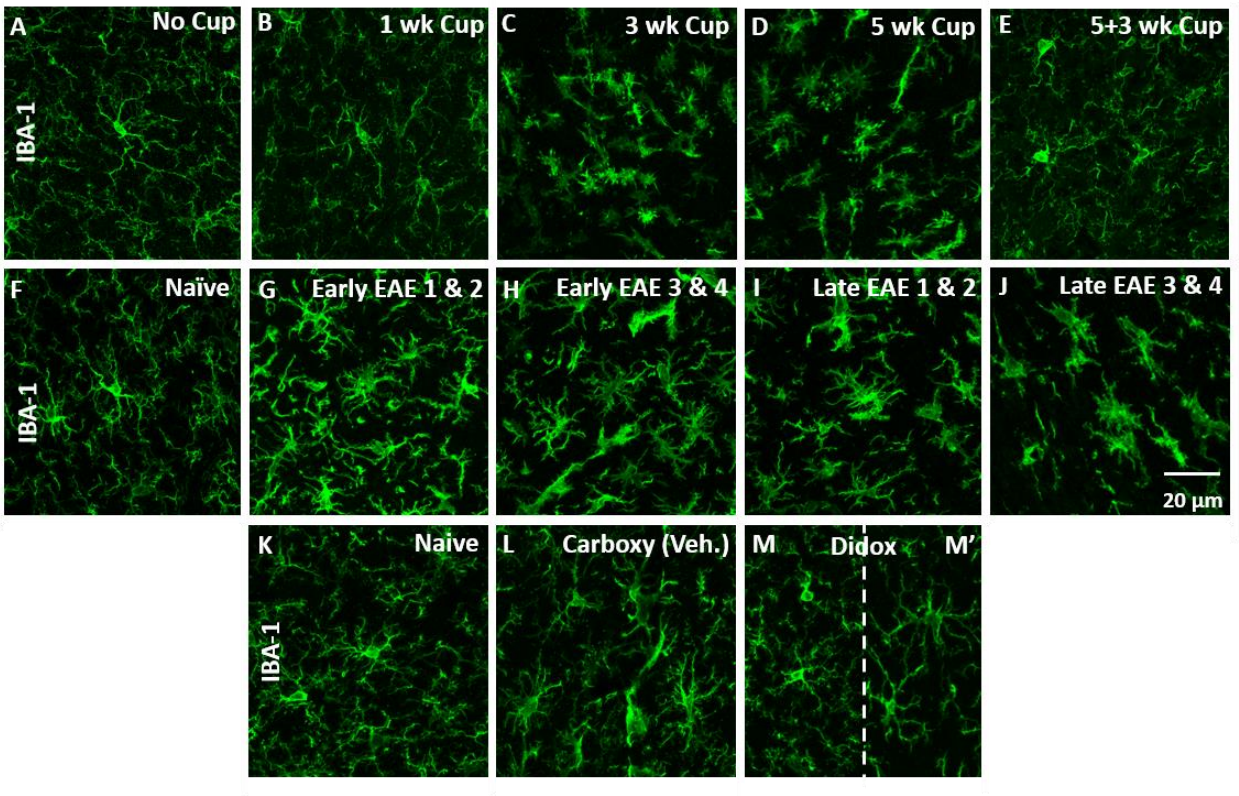

Figure 8. Microglia display reactive morphology in EAE and Cuprizone. Immunolabeling using an antibody against IBA-1 revealed reactive microglia in Cuprizone beginning at the 1 week time point (B) (before demyelination was observed) and continuing through the 3 week (C) and 5 week (D) time points. At the 5+3 week point (E) where remyelination was observed, microglia reactivity compared to that of no Cuprizone treated mice. In EAE mice, IBA-1 labeling revealed reactive microglia morphology beginning at the early 1&2 (G) time point (before AIS shortening or loss was observed) and continuing through the early 3&4 (H), late 1&2 (I), and late 3&4 (J) time points. After Didox treatment (M), microglia morphology displayed mixed reactivity, with some microglia displaying a surveying phenotype (M) and others displaying a somewhat reactive morphology (M'). Therefore, in both a model of demyelination and an inflammatory model of MS, microglia show reactivity preceding pathology and decreased reactivity with recovery.

Materials & Methods

Mice

C57bl/6 mice were purchased at five and 11 weeks of age from Jackson Laboratories (Bar Harbor, ME) and maintained in AAALAC credited facilities at the Virginia Commonwealth University Divisions of Animal Resources (VCU DAR) or the McGuire Veterans Affairs Medical Center (VAMC) vivariums, respectively. Mice were allowed to acclimate for one week before treatments began. Food and water were available *ad libitum* during all treatments. All procedures were carried out in accordance with approved IACUC protocols at VCU and VAMC.

The Cuprizone Model

Cortical demyelination was induced by mixing Cuprizone (N, N'-bis (cyclohexanone) oxalidihydrazone, 0.2% w/w) (Sigma-Aldrich, St. Louis, MO) with ground rodent chow (5001 Rodent diet; PMI Nutrition International, LLC, Brentwood, MO) as previously described(Dupree et al., 2004). Six weeks old mice were maintained on a ground chow diet without Cuprizone (0%), or with Cuprizone (0.2% w/w) for 1, 3, or 5 weeks to allow for cortical demyelination. An additional group of mice were maintained on a ground chow diet with Cuprizone for 5 weeks followed by 3 weeks on non-Cuprizone chow to allow for cortical myelin repair (5+3 weeks).

The Chronic EAE Model

An inflammatory environment was created by inducing mice with the chronic model of experimental autoimmune encephalomyelitis (EAE) as previously described (DeVries et al., 2012; Dupree et al., 2015; Secor McVoy et al., 2015; Clark et al., 2016). Twelve weeks old C57bl/6 mice were injected with 50 µL of a solution containing 3 mg/ml myelin oligodendrocyte glycoprotein peptide 35-55 (MOG_{35-55}, MEVGWYRSPFSRVVHLYRNGK) (AnaSpec, Inc., Fremont, CA), mixed with complete Freud's adjuvant

with 2mg/ml heat killed *M. Tuberculosis* (Invitrogen Life Technologies, Grand Island, NY). On the same day, mice were injected intraperitoneal (IP) with 300ng Pertussis toxin (List Biological Labs, Campbell, CA) in 200 µL phosphate buffered saline (PBS). A booster IP injection of Pertussis toxin was given 48 hours later. Animals were weighed and monitored daily for dehydration. Animals were euthanized if they experienced loss of more than 15% body weight or an inability to eat/drink. Food/drink was supplied by oral gavage during peak clinical symptoms as necessary. Clinical motor symptoms were scored and recorded daily following injection. Clinical scores were assigned as follows: 0- no symptoms, 1- limp tail, 2- limp tail with loss of righting reflex, 3- paralysis of a single hind limb, 4- paralysis of both hind limbs, 5- death. Peak clinical symptoms were reached approximately 15 days post injection. Following peak clinical symptoms mice were taken 3 days (early) and 9 days (late) for further analysis (Figure 9). Only mice that maintained consistent clinical score for 3 or 9 days were used for analysis. Not all mice reached severe clinical symptoms. This variation in clinical score was used to group mice into two categories for each time point: EAE 1&2 and EAE 3&4. Thus 4 categories were created that represent mild and severe clinical symptoms at both early and late time points (early EAE 1&2, early EAE 3&4, late EAE 1&2, late EAE 3&4).

Didox treatment

Didox (N-3,4-tridhydroxy-benzamide) (Molecules for Health, Richmond, VA) is a multifunctional compound that inhibits DNA replication, inhibits T cell proliferation, reduces oxidative injury and inflammation, and inhibits microglia/macrophage production of inflammatory factors (Bhave et al., 2013; Inayat et al., 2010; Matsebatlela et al., 2015; Turchan et al., 2003). Following procedures previously established (DeVries et al., 2012), 550 mg/kg of Didox was administered in 200 µL carboxymethylcellulose via oral gavage to a separate cohort of mice at the early EAE time point. Vehicle solution (0.5% w/v carboxymethylcellulose, 0.9% w/v sodium chloride, 0.4% w/v polysorbate 30, and

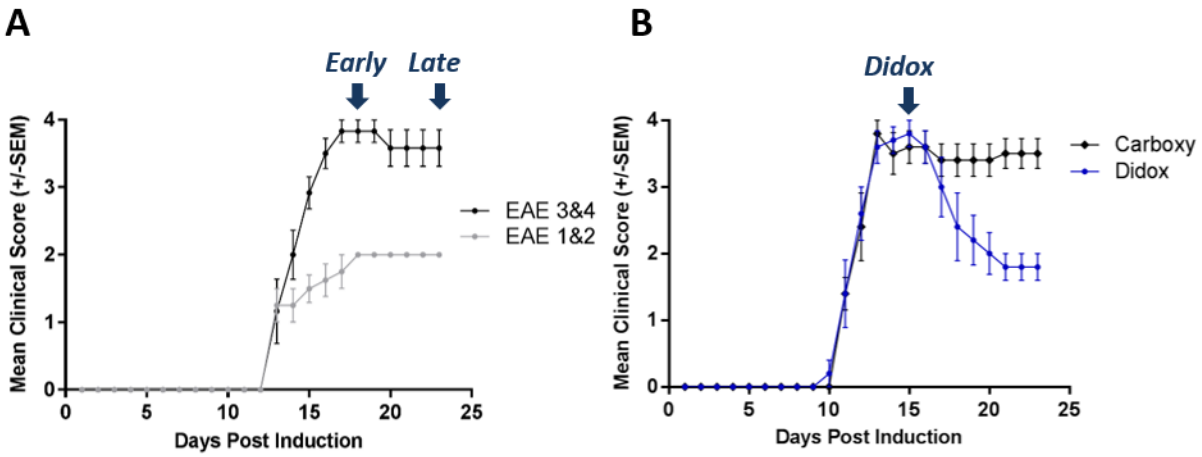

Figure 9. Graph of EAE progression. Mice show symptoms approximately 12 days after injection (A). Three days after peak clinical symptoms mice are sacrificed to represent the 'early' time point. Mice at the 'late' time point are sacrificed nine days after the peak of clinical symptoms. Mice are grouped into category based on clinical score: EAE 1&2 or EAE 3&4. Didox treatment began at the early time point and continued for 6 days (B).

0.9%w/v benzyl alcohol in deionized water) was also administered to a separate cohort of mice at the early EAE time point as a vehicle control. Didox or vehicle control were administered daily for 6 days.

Tissue Preparation

For immunohistochemistry mice were anesthetized using 15 µL/g body weight of 2.5% Avertin (2,2,2 tribromoethanol) (Sigma-Aldrich) in 0.9% sodium chloride (Sigma-Aldrich) and perfused with 4% paraformaldehyde (Ted Pella, Redding, CA). After perfusion the cortex was removed, cryopreserved in 0.1M PBS containing 30% sucrose for 48 hours at 4^{o}C, frozen in Optimal Cutting Temperature compound (Sajura Finetek, Torrance, CA) and sectioned at 40 µm in a coronal orientation using a Leica CM 1850 cryostat (Leica Biosystems, Inc., Buffalo Grove, IL). The cortex was serially sectioned spanning the region from 1.1 mm anterior to Bregma to 2.5 mm posterior to Bregma. Fifteen sets of 6 sections were collected and placed on Fisherbrand ProbeOn Plus slides (Fisher Scientific, Loughborough, UK) then stored at -80^{o}C. One additional mouse brain was sectioned transversely to observe microglia/AIS interaction from a different orientation.

Antibodies

For immunohistochemistry, axon initial segments were visualized using a mouse monoclonal antibody directed against AnkyrinG (AnkG) (N106/36; mouse monoclonal) (Neuro Mab, Davis, CA) at a dilution of 1:200. Microglia were visualized using a rabbit polyclonal antibody directed against ionized calcium binding adaptor molecule 1 (IBA-1) (Wako Chemical USA, Richmond, VA) at a dilution of 1:1000. C3 was visualized using a rat IgG2a antibody directed against Complement Component 3 (C3), particularly the C3b and iC3b fragments (clone 3/26 HM1078; Hycult, Plymouth Meeting, PA) at a dilution of 1:20. Secondary antibodies were obtained from Invitrogen Life Technologies (Alexa^{TM} Flour; Grand Island, NY) and used at a dilution of 1:500. For western blot, the C3 antibody was used at a

dilution of 1:1000. Glyceraldehyde-3-phosphate dehydrogenase (loading control) was visualized using a monoclonal mouse antibody (clone 6C5 MAD374; EMD Millipore Billerica, MA) at a dilution of 1:10,000. Appropriate secondary antibodies were conjugated to horseradish peroxidase (HRP) and used at a concentration of 1:10,000 (Santa Cruz Biotechnology, Inc., Dallas, TX). Precision Protein™ StrepTactin-HRP conjugate (1:50,000, Bio-Rad) was used along with secondary antibodies to visualize protein molecular weight markers.

Immunohistochemistry

To observe microglia-AIS contact, sections were double immunolabeled with AnkyrinG and IBA-1 using antigen retrieval. In order to visualize C3 in tissue, sections were double immunolabeled with C3 and AnkyrinG. To facilitate retrieval, slides were placed in 10mM sodium citrate (pH 8.5) for 5 minutes at room temperature. They were then placed in 10 mM sodium citrate (pH 8.5) already warmed to 80^{o}C and incubated at 80^{o}C for 30 minutes. Slides were removed from the oven, left at room temperature for 5 minutes, then rinsed in 0.1M PBS. Sections were blocked in 0.1M PBS containing 0.5% Triton X-100 (Fisher Scientific, Pittsburgh, PA) and 2% cold water fish gelatin (Aurion, The Netherlands). Primary antibodies were diluted in blocking buffer and applied to slides, incubated overnight at 4^{o}C, washed in 0.1M PBS, and blocked a second time. Sections were incubated with appropriate fluorescently labeled secondary antibodies for 90 minutes, incubated with BisBenzamide (Sigma-Aldrich) diluted 1:1000 in 0.1M PBS for 3 minutes, and rinsed with 0.1M PBS. BisBenzamide is a nuclear label that was used to visualize cortical layers. Slides were mounted with VectaShield™ (Vector Laboratories, Burlingame, CA), cover slipped, and imaged using confocal microscopy.

Confocal Microscopy & Quantitation

Confocal microscopy was performed using a Zeiss LSM 710 confocal laser scanning microscope (Carl Zeiss Microscopy, LLC, Thornwood, NY). Images were collected as confocal z-stacks 25 µm in depth, using a pinhole of 1 Airy disc unit and Nyquist sampling. Images were taken in layer V of the cortex using a 40X oil immersion objective with numerical aperture 1.3. The gain and offset values were kept constant for all images. Two images were collected for each of the six sections on a slide, resulting in 12 images per mouse for quantitation of microglia/AIS contact. Microscopy was performed in the Virginia Commonwealth University Department of Anatomy and Neurobiology Microscopy Facility.

Quantitation of contact between AISs and IBA-1+ cells was performed using the Volocity™ 3D Image Analysis Software (v6.3, PerkinElmer, Waltham, MA). The Volocity™ software allowed each confocal z-stack to be represented as a three dimensional image which could be rotated 360^{o} in order to confirm that apparent contact in two dimensions was not the result of an AIS and an IBA-1+ cell on different planes in the z axis. Contact was quantified in naïve, Cuprizone treated (1, 3, 5, and 5+3 weeks), EAE induced (early 1&2, early 3&4, late 1&2, and late 3&4), EAE induced + Didox treated, and EAE induced + vehicle treated mice (n=3 mice for each). For each image the total number of IBA-1+ cells, AISs, and contact points per field of view (FOV) were counted manually. IBA-1+ cells were counted only if the cell body was visible in the FOV. AISs and contact points along any of the six edges of the z-stack were excluded from analysis so that the type of contact could be accurately categorized. If one IBA-1+ cell contacted multiple initial segments, each contact point was counted individually. If one AIS was contacted by multiple IBA-1+ cells, each contact point was counted individually. Contact was divided into three different categories labeled ‘touching’, ‘resting’, and ‘wrapping’. ‘Touching’ contact occurred when a process from an IBA-1+ cell made contact with any part of the AIS. This type of contact was characterized by an IBA-1+ cell that extended a process toward an AIS and the end of the process wrapped around a small portion of the AIS. This was the least extreme type of contact, with only a

portion of a process from an IBA-1+ cell making contact with a portion of the AIS. 'Resting' contact occurred when the cell body of an IBA-1+ cell made contact with any part of the AIS. Frequently, 'resting' contact was shown by the cell body of the IBA-1+ cell sitting on top of the initial segment with a process extending down the length of the AIS, although the cell body was also seen resting on the middle of the AIS with processes extended in either direction along the length of the AIS.. 'Wrapping' contact occurred when the cell body or a process from an IBA-1+ cell completely engulfed an AIS. The 'wrapping' contact meant the cell body or a process of the IBA-1+ cell surrounded the entire AIS in 360 degrees. Representative images of each type of contact are shown in figure 10. The numbers of each type of contact were recorded for each image. Graphing and one way ANOVAs with Tukey's HSD post-hoc tests were performed using GraphPad Prism version 6.03 for Windows. Data are represented as number of contacts per FOV as a percent of naïve.

Isolation of Mouse Cortical Microglia & RNA

Isolation of cortical microglia was performed using the Miltenyi Neural Dissociation Kit (Miltenyi Biotec, San Diego, CA). Naïve, 3 weeks Cuprizone treated, and EAE mice (early 1&2 and early 3&4) were anesthetized with 15µL/g body weight 2.5% Avertin injected IP and perfused with 50 mL cold sterile 0.1M PBS. Brains were dissected out, meninges removed, and cortices placed in Hank's Buffered Saline Solution without $CaCl_2$ and $MgCl_2$ (HBSS w/o) (Corning, Corning, NY). Cortices of three mice were pooled to generate one sample. Cortices were diced with a razor blade and centrifuged at 300xg for 2 minutes at room temperature. A single cell suspension was prepared following manufacturer's instructions, washed with HBSS with $CaCl_2$ and $MgCl_2$ (HBSS w/) (Corning, Corning, NY) and centrifuged at 300xg for 10 minutes at 4^{o}C. Myelin depletion was performed by suspending the pellet in 3mL of 30% Percoll^{TM} (GE Healthcare Life Sciences, Pittsburgh, PA) and centrifuging at 700xg for 10 minutes at 4^{o}C. Cells were then washed with HBSS w/o and centrifuged at 300xg for 10 minutes at 4^{o}C. Microglia isolation was

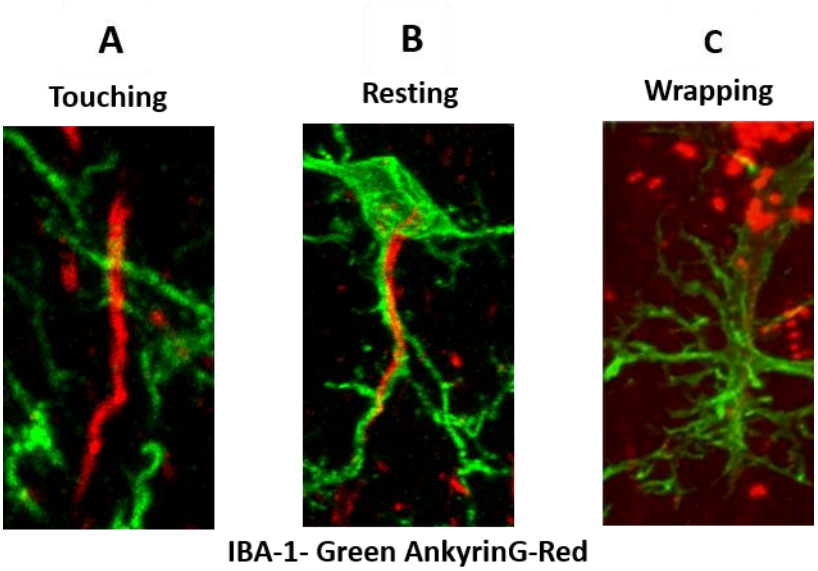

Figure 10. Representative images of the three types of contact. Touching is represented by a process from an IBA-1+ cell touching a small portion of the AIS (A). Resting is represented by the cell body resting on the AIS, often resting at the top of the AIS with a process extending down the AIS (B). Wrapping is shown by an AIS being completely engulfed within the IBA-1+ cell (C).

performed by labeling with Cd11b beads (Miltenyi), washing with MACS buffer (Miltenyi), and passing cells through a MACS LS column and magnetic separator (Miltenyi). RNA was isolated from the Cd11b+ cells using the Qiagen RNeasy Kit (Qiagen, Germantown, MD). RNA was then DNase treated using the Ambion DNase I Kit (Invitrogen Life Technologies, Grand Island, NY) following manufacturer's instructions. To ensure RNA purity, all samples had a 260/280 ratio greater than or equal to 1.8.

Microarray Procedure & Data Analysis

A microarray was used to determine RNA expression levels in multiple disease states. Twelve samples were used, three each for the following time points: Naïve, Early EAE 1&2, Early EAE 3&4, and 3 Weeks Cuprizone. RNA obtained from Cd11b+ cells was DNase treated and sent to the Gene Expression Analysis Laboratory at the University of Tennessee Health Science Center in Memphis, Tennessee for analysis. This laboratory uses the nCounter Gene Expression Analysis System (NanoString Technologies, Inc., Seattle, WA). RNA was analyzed using the nCounter mouse inflammation panel version 2 (NanoString Technologies) which contains 248 inflammation related genes in addition to six housekeeping genes, six positive controls, and eight negative controls. Table 1 contains a full list of the target and housekeeping genes included in the microarray. Data was normalized using the nSolver™ Analysis Software version 2.5 (NanoString Technologies). Background subtraction was performed using the mean of the negative controls plus two standard deviations and normalization was performed using the geometric mean of the positive controls and internal reference genes. The normalized data were used for functional enrichment analysis. Functional enrichment analysis was performed using the ToppFun (from the ToppGene Suite) (http://toppgene.cchmc.org) and EnrichR (http://amp.pharm.mssm.edu/Enrichr/) programs, which are freely available online, and Ingenuity Pathway Analysis (Qiagen, Redwood City, CA). Both the ToppFun and EnrichR programs analyze a gene list provided by the user to determine functions, phenotypes, or pathways overrepresented in that list

of genes (Chen et al., 2009b; Chen et al., 2007; Chen et al., 2009a; Chen et al., 2013). A p-value is given to display functional enrichment. For ToppFun, the Bonferroni correction method is applied, while EnrichR uses the Fisher's exact test. For both programs the list of genes imported was a list of genes upregulated or downregulated with a fold change of at least 2.0 (as determined by the nSolver software). For example, all genes upregulated in EAE early 1&2 as compared to 3 weeks Cuprizone, by at least 2.0 fold (as determined by the nSolver software) were uploaded into the functional enrichment program to determine the functions enriched in EAE early 1&2. The Ingenuity Pathway Analysis program analyzes an entire set of data uploaded into the software. Data was uploaded as a fold change compared to naïve, and the program was set to analyze only genes with at least a 2.0-fold change. The 2.0-fold cutoff for all programs was set based on the detection level of the nCounter instrument. Ingenuity Pathway Analysis also displays a p-value to show functional enrichment. Upregulation and downregulation are based on an activation z-score, with a z-score greater than 2.0 indicating increased activation and z-score less than negative 2.0 indicating decreased activation. The goal of functional enrichment was to find biological functions or pathways that varied by disease state. Pathways with several genes from the microarray that were all upregulated or downregulated would provide a basis to find candidate genes that contribute to pathology. Using functional enrichment tools and knowledge derived from current literature, further research can be conducted to examine the impact of specific genes or pathways, particularly in relation to AIS pathology in EAE.

Western Blot Protocol

Tissue for western blot analysis was obtained from mouse cortex and placed in RIPA buffer (1% Nonidet P-40, 0.5% Sodium deoxycholate, 0.1% sodium dodecyl sulfate, and 0.1 M phosphate buffered saline). Then 10µL/mL of Proteinase Inhibitor Cocktail (PIC) (Sigma- Aldrich, St. Louis, MO) was added. The sample was homogenized and centrifuged at 600xg for 10 minutes at 4˚C and the soluble fraction

was collected. A protein assay was performed to determine protein concentrations in each sample. Bovine Serum Albumin (BSA) standards were prepared using the Micro BCA Kit (Thermo #23235, Thermo Scientific, Rockford, IL). 25µL of each BSA standard and 25 µL of each sample (samples diluted 1:100 in 0.1M PBS) were added in duplicate to a 96 well plate. Reagents A, B, and C from the Micro BCA kit were mixed in a ratio of 25:24:1 and 200 µL of the reagent mix was added to the wells containing each sample and standard. The plate was incubated at 37˚C for 15 minutes and cooled for 5 minutes before reading. The plate was then read in a spectrophotometer. The standard curve was determined ($R^2 \geq 0.99$) and used to calculate protein concentrations.

Samples were appropriately diluted in Laemmli Sample buffer (Bio-Rad, Hercules, CA) to ensure 20 µg of each sample was loaded in each lane on the gel. No β-mercaptoethanol was added to create non-reducing conditions per previous protocols for the C3 antibody (Mastellos et al., 2004). Samples were boiled for 5 minutes, placed on ice and vortexed and centrifuged briefly. The gel (Criterion™ TGX 10™ well precast gel, 4-15%; Bio-Rad, Hercules, CA) was loaded with 10 µL of each sample and 10µL of protein molecular weight ladder (Precision Plus Protein™ Kaleidoscope™, Bio-Rad, Hercules, CA). The western blot apparatus (Miniprotean Tetracell, Bio-Rad, Hercules, CA) was filled with running buffer (10% Tris-Glycine, 1 g/L SDS in deionized water, pH 8.3) The gel was run at 70V for 30 minutes, then 180 V for an additional hour. The gel was removed, cut to appropriate size, placed in cold transfer buffer (10% Tris-Glycine and 20% methanol in deionized water, pH 8.3) and rocked for 15 minutes. Nitrocellulose membrane was cut to the size of the gel and also rocked in cold transfer buffer for 15 minutes. The transfer cassette was assembled with the gel and nitrocellulose clamped between two pieces of botting paper and two sponges. The gel was transferred in the western blot apparatus for 2 hours at 100V. After transfer the nitrocellulose was washed three times in PBS. The nitrocellulose was cut in two in order to probe for both the housekeeping protein and protein of interest, and blocked for 40 minutes in blocking solution (3% non-fat dry milk in PBST, 1.5g/50mL). Primary antibodies were

diluted in the same blocking solution and the nitrocellulose membranes were placed in primary solution overnight on a rocker at 4˚C. The nitrocellulose membranes were then washed in PBS and blocked for 20 minutes. Secondary antibodies were diluted in blocking solution and the nitrocellulose membranes were incubated in secondary solution for 1.5 hours. Nitrocellulose membranes were washed twice in PBST (0.05% Tween in PBS), then washed three times in PBS. Chemiluminescent reagent was prepared using the Immobilon Western Chemiluminescent HRP substrate according to manufacturer's instructions (EMD Millipore, Billerica, MA). Nitrocellulose membranes were incubated with chemiluminescent substrate for 5 minutes. The membranes were then imaged using a ChemiDoc™ Touch imaging system (Bio-Rad, Hercules, CA).

Quantitative Reverse Transcriptase Polymerase Chain Reaction

RNA samples previously isolated from Cd11b+ cells and DNase treated were reverse transcribed to form cDNA using the iScript Reverse Transcription Supermix (Bio-Rad, Hercules, CA) per manufacturer's instructions. Quantitative RT-PCR was performed with CFX96 RT-PCR detection system (Bio-Rad, Hercules, CA) using 1 µL of cDNA, SsoFast Evagreen Supermix (Bio-Rad, Hercules, CA), and forward and reverse primers (500 nM) per manufacturer's instructions. Primers were designed for C1qA (forward: 5'-AGGACTGAGGGCGTGAAAG-3'; reverse: 5'-CAAGCGTCATTGGGTTCTGC-3'), C1qB (forward: 5'-GGACCCAGACTTCCGCTTTC-3'; reverse: 5'-GGGCTTGTGTATGGAATC-3'), C2 (forward: 5'-TGCCGACAGCCTTACTCTTAC-3'; reverse: 5'-AAGGTTCTGGGTGGGATTGG-3'), and C3 (forward: 5'-AGCAACGCAAGTTCATCAGC-3'; reverse: 5'-TGTAGCTGGTGTTGGGCTTT-3'). Cycle parameters were as follows: 95˚C for 30 seconds; 40 cycles of 95˚C for 5 sec, 56˚C for 5 sec; melt curve measurement of 5 sec 0.5˚C incremental increases from 65˚C to 95˚C. Fold changes in gene expression were calculated for C1qA, C1qB, C2, and C3 compared to Cyclophilin A (forward: 5'- CTAGAGGGCATGGATGTGGT-3'; reverse: 5'- TGACATCCTTCAGTGGCTTG-3') as an endogenous reference gene using the formula $RQ = 2^{-\Delta\Delta Ct}$.

Gene expression levels were represented as fold changes in early EAE 1&2 (n=3) and early EAE 3&4 (n=3) compared to naïve (n=1). Graphing was performed using GraphPad Prism version 6.03 for Windows.

Table 1. List of Genes in Included in Microarray

complement component 1, s subcomponent
complement component 4A (Rodgers blood group)
complement component 7
chemokine (C-C motif) ligand 19
chemokine (C-C motif) ligand 21A (serine)
chemokine (C-C motif) ligand 8
chitinase 3-like 3
defensin, alpha, related sequence 1
interferon-induced protein with tetratricopeptide repeats 3
interferon alpha 1
interleukin 1 alpha
interleukin 22
ras homolog gene family, member A
advanced glycosylation end product-specific receptor
arachidonate 12-lipoxygenase
arachidonate 15-lipoxygenase
arachidonate 5-lipoxygenase
amphiregulin
arginase, liver
activating transcription factor 2
BCL2-like 1
B cell leukemia/lymphoma 6
baculoviral IAP repeat-containing 2
complement component 1, q subcomponent, alpha polypeptide
complement component 1, q subcomponent, beta polypeptide
complement component 1, r subcomponent A
complement component 2 (within H-2S)
complement component 3
complement component 3a receptor 1
complement component 6

complement component 8, alpha polypeptide
complement component 8, beta polypeptide
complement component 9
chemokine (C-C motif) ligand 11
chemokine (C-C motif) ligand 17
chemokine (C-C motif) ligand 2
chemokine (C-C motif) ligand 20
chemokine (C-C motif) ligand 22
chemokine (C-C motif) ligand 24
chemokine (C-C motif) ligand 3
chemokine (C-C motif) ligand 4
chemokine (C-C motif) ligand 5
chemokine (C-C motif) ligand 7
chemokine (C-C motif) receptor 1
chemokine (C-C motif) receptor 2
chemokine (C-C motif) receptor 3
chemokine (C-C motif) receptor 4
chemokine (C-C motif) receptor 7
CD163 antigen
CD4 antigen
CD40 antigen
CD40 ligand
CD55 antigen
CD86 antigen
cell division cycle 42
CCAAT/enhancer binding protein (C/EBP), beta
complement factor B
complement factor D (adipsin)
cofilin 1, non-muscle
cAMP responsive element binding protein 1
C-reactive protein, pentraxin-related
colony stimulating factor 1 (macrophage)

colony stimulating factor 2 (granulocyte-macrophage)
colony stimulating factor 3 (granulocyte)
chemokine (C-X-C motif) ligand 1
chemokine (C-X-C motif) ligand 10
chemokine (C-X-C motif) ligand 2
chemokine (C-X-C motif) ligand 3
chemokine (C-X-C motif) ligand 5
chemokine (C-X-C motif) ligand 9
chemokine (C-X-C motif) receptor 1
chemokine (C-X-C motif) receptor 2
chemokine (C-X-C motif) receptor 4
cysteinyl leukotriene receptor 1
cysteinyl leukotriene receptor 2
Fas death domain-associated protein
DNA-damage inducible transcript 3
ELK1, member of ETS oncogene family
Fas ligand (TNF superfamily, member 6)
FMS-like tyrosine kinase 1
FBJ osteosarcoma oncogene
FXYD domain-containing ion transport regulator 2
guanine nucleotide binding protein, alpha q polypeptide
GNAS (guanine nucleotide binding protein, alpha stimulating) complex locus
guanine nucleotide binding protein (G protein), beta 1
guanine nucleotide binding protein (G protein), gamma transducing activity polypeptide 1
G protein-coupled receptor 44
growth factor receptor bound protein 2
histocompatibility 2, class II antigen E alpha, pseudogene

histocompatibility 2, class II antigen E beta
hemolytic complement
histone deacetylase 4
hypoxia inducible factor 1, alpha subunit
high mobility group box 1
high mobility group box 2
high mobility group nucleosomal binding domain 1
Harvey rat sarcoma virus oncogene
hematopoietic SH2 domain containing
heat shock protein 1
heat shock protein 2
interferon, alpha-inducible protein 27 like 2A
interferon-induced protein 44
interferon-induced protein with tetratricopeptide repeats 1
interferon-induced protein with tetratricopeptide repeats 2
interferon beta 1, fibroblast
interferon gamma
interferon inducible GTPase 1
interleukin 10
interleukin 10 receptor, beta
interleukin 11
interleukin 12a
interleukin 12b
interleukin 13
interleukin 15
interleukin 17A
interleukin 18
interleukin 18 receptor accessory protein
interleukin 1 beta
interleukin 1 receptor, type I
interleukin 1 receptor accessory protein
interleukin 1 receptor antagonist
interleukin 2
interleukin 21
interleukin 22 receptor, alpha 2

interleukin 23, alpha subunit p19
interleukin 23 receptor
interleukin 3
interleukin 4
interleukin 5
interleukin 6
interleukin 6 receptor, alpha
interleukin 7
interleukin 9
interferon regulatory factor 1
interferon regulatory factor 3
interferon regulatory factor 5
interferon regulatory factor 7
integrin beta 2
jun proto-oncogene
kelch-like ECH-associated protein 1
kininogen 1
LIM-domain containing, protein kinase
lymphotoxin A
lymphotoxin B
leukotriene B4 receptor 1
leukotriene B4 receptor 2
lymphocyte antigen 96
v-maf musculoaponeurotic fibrosarcoma oncogene family, protein F (avian)
v-maf musculoaponeurotic fibrosarcoma oncogene family, protein G (avian)
v-maf musculoaponeurotic fibrosarcoma oncogene family, protein K (avian)
mitogen-activated protein kinase kinase 1
mitogen-activated protein kinase kinase 4
mitogen-activated protein kinase kinase 6
mitogen-activated protein kinase kinase kinase 1
mitogen-activated protein kinase kinase kinase 5
mitogen-activated protein kinase kinase kinase 7

mitogen-activated protein kinase kinase kinase 9
mitogen-activated protein kinase 1
mitogen-activated protein kinase 14
mitogen-activated protein kinase 3
mitogen-activated protein kinase 8
MAP kinase-activated protein kinase 2
MAP kinase-activated protein kinase 5
mannan-binding lectin serine peptidase 1
mannan-binding lectin serine peptidase 2
Max protein
mannose-binding lectin (protein C) 2
myocyte enhancer factor 2A
myocyte enhancer factor 2B
myocyte enhancer factor 2C
myocyte enhancer factor 2D
MAP kinase-interacting serine/threonine kinase 1
matrix metallopeptidase 3
matrix metallopeptidase 9
mannose receptor, C type 1
myxovirus (influenza virus) resistance 1
myxovirus (influenza virus) resistance 2
myelocytomatosis oncogene
myeloid differentiation primary response gene 88
myosin, light polypeptide 2, regulatory, cardiac, slow
nuclear factor of activated T cells, cytoplasmic, calcineurin dependent 3
nuclear factor, erythroid derived 2, like 2
nuclear factor of kappa light polypeptide gene enhancer in B cells 1, p105
NLR family, pyrin domain containing 3

nucleotide-binding oligomerization domain containing 1
nucleotide-binding oligomerization domain containing 2
nitric oxide synthase 2, inducible
NADPH oxidase 1
nuclear receptor subfamily 3, group C, member 1
2'-5' oligoadenylate synthetase 1A
2'-5' oligoadenylate synthetase 2
2'-5' oligoadenylate synthetase-like 1
platelet derived growth factor, alpha
phosphatidylinositol 3-kinase, C2 domain containing, gamma polypeptide
phospholipase A2, group IVA (cytosolic, calcium-dependent)
phospholipase C, beta 1
protein phosphatase 1, regulatory (inhibitor) subunit 12B
protein kinase C, alpha
protein kinase C, beta
prostaglandin E receptor 1 (subtype EP1)
prostaglandin E receptor 2 (subtype EP2)
prostaglandin E receptor 3 (subtype EP3)
prostaglandin E receptor 4 (subtype EP4)
prostaglandin F receptor
prostaglandin I receptor (IP)
prostaglandin-endoperoxide synthase 1
prostaglandin-endoperoxide synthase 2
PTK2 protein tyrosine kinase 2
RAS-related C3 botulinum substrate 1
v-raf-leukemia viral oncogene 1
Rap guanine nucleotide exchange factor (GEF) 2

v-rel reticuloendotheliosis viral oncogene homolog A (avian)
avian reticuloendotheliosis viral (v-rel) oncogene related B
resistin like alpha
receptor (TNFRSF)-interacting serine-threonine kinase 1
receptor (TNFRSF)-interacting serine-threonine kinase 2
Rho-associated coiled-coil containing protein kinase 2
ribosomal protein S6 kinase, polypeptide 5
src homology 2 domain-containing transforming protein C1
SMAD family member 7
signal transducer and activator of transcription 1
signal transducer and activator of transcription 2
signal transducer and activator of transcription 3
thromboxane A2 receptor
transcription factor 4
transforming growth factor, beta 1
transforming growth factor, beta 2
transforming growth factor, beta 3
transforming growth factor, beta receptor I
toll-like receptor 1
toll-like receptor 2
toll-like receptor 3
toll-like receptor 4
toll-like receptor 5
toll-like receptor 6
toll-like receptor 7
toll-like receptor 8
toll-like receptor 9
tumor necrosis factor
tumor necrosis factor, alpha-induced protein 3
tumor necrosis factor (ligand) superfamily, member 14
toll interacting protein

TNFRSF1A-associated via death domain
TNF receptor-associated factor 2
triggering receptor expressed on myeloid cells 2
thymic stromal lymphopoietin
twist basic helix-loop-helix transcription factor 2
TYRO protein tyrosine kinase binding protein
Internal Reference Genes
clathrin, heavy polypeptide (Hc)
glyceraldehyde-3-phosphate dehydrogenase
glucuronidase, beta
hypoxanthine guanine phosphoribosyl transferase
phosphoglycerate kinase 1
tubulin, beta 5 class I

Results

Our laboratory has previously shown that following EAE induction, the AISs are shortened and eventually lost with disease progression (Clark et al., 2016). Interestingly, in these EAE induced mice, reactive microglia accompany AIS disruption. Since these cells are known to modulate cellular morphology and shape neural circuity in development and in neurodegeneration, we hypothesized that microglia are responsible for this AS disruption. In apparent contrast to our hypothesis, reactive microglia are prevalent in the demyelinated cortex of Cuprizone treated mice, indicating that just the presence of reactive microglia is not sufficient to drive AIS disruption. Therefore, we further proposed that reactive microglia have distinct expression profiles that coincide with their apparent functions.

Contact between IBA-1+ Cells and the AIS is similar in EAE and Cuprizone

Although microglia presented with reactive phenotypes in both the EAE and Cuprizone models, AISs were only disrupted in EAE. Therefore, we propose that EAE- induced reactive microglia mediated AIS disruption by establishing and maintaining contact with the AIS. To test this hypothesis, we quantified the amount of contact between the AISs and the IBA-1+ cells in the two models. Double immunolabeling with IBA-1 and AnkyrinG revealed that IBA-1+ cells contacted the AIS in both the EAE and Cuprizone models (Figure 11A-C). Quantitative analysis of contact revealed that contact increased with disease progression compared to naïve mice in both models (Figure 11D-F). In Cuprizone treated mice, contact significantly increased at the 3 week, 5 week, and 5+3 week time points compared to naive, and decreased at the 5+3 week time point compared to the 5 week time point, correlating with

Figure 11. IBA-1+ cells contact the AIS in EAE and Cuprizone. Double immunolabeling with AnkG and IBA-1 in Naïve (A), Cuprizone (B) and EAE tissue (C) revealed contact between IBA-1+ cells and AIS in all three conditions (arrows signify points of contact). Quantification of contact in 3D using Volocity™ software revealed that the amount of contact increased in Cuprizone compared to naïve (D), and increased in EAE compared to naïve (E). In Cuprizone, contact significantly increased compared to naïve after 3, 5, and 5+3 weeks of treatment (*, p value < 0.05). Contact significantly decreased at the 5+3 weeks treatment compared to the 5 weeks treatment (**, p value < 0.05) correlating with myelin repair. In EAE, contact significantly increased at the early 3&4 and late 1&2 time points compared to naive (* p value < 0.05) correlating with AIS shortening and loss. Contact increased compared to naïve at the late 3&4 time point, although the increase was not statistically significant, likely due to variability in EAE mice observed at this time point. Didox treatment results in a significant decrease in contact compared to vehicle control (F), correlating with recovery in AIS number (** p value <0.05). Therefore, morphological analysis of amount of contact between microglia and AISs revealed similarities between EAE and Cuprizone.

Figure 11.

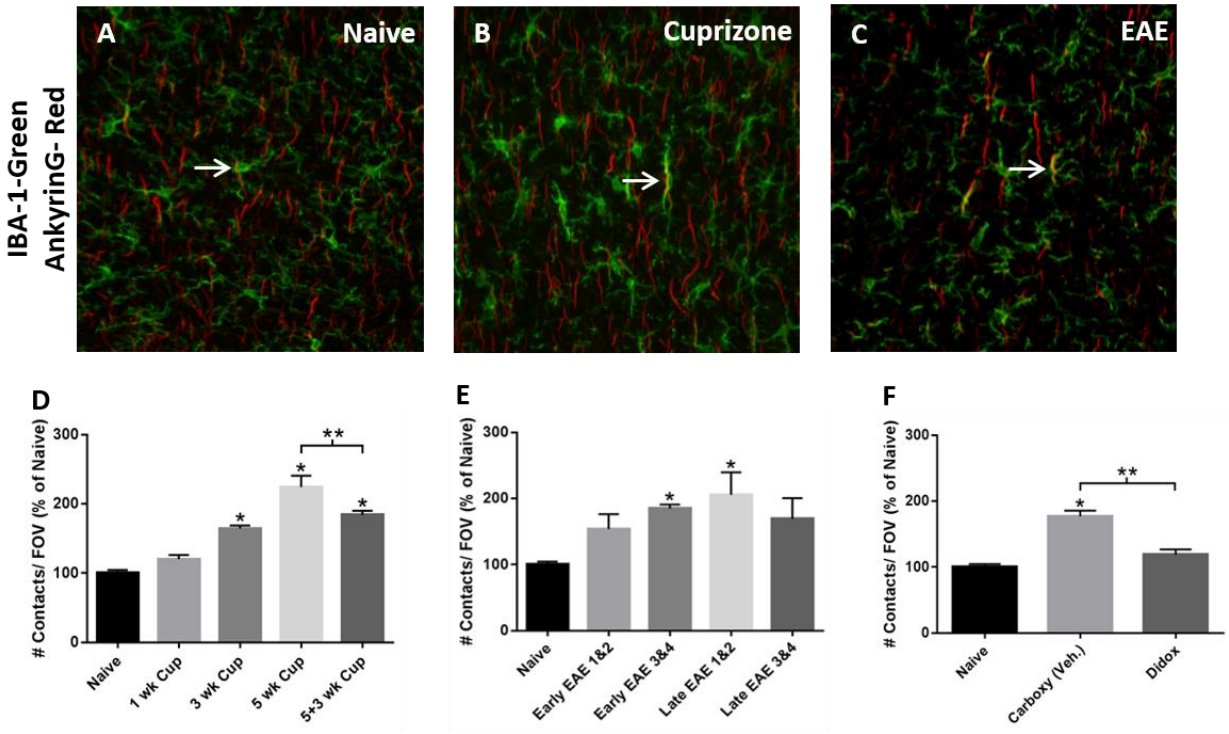
A
Naive
B
Cuprizone
C
EAE
IBA-1-Green
AnkyrinG- Red
D
Contacts/ FOV (% of Naive)
300
200
100
0
Naive
1 wk Cup
3 wk Cup
5 wk Cup
5+3 wk Cup
E
Contacts/ FOV (% of Naive)
Naive
Early EAE 1&2
Early EAE 3&4
Late EAE 1&2
Late EAE 3&4
F
Contacts/ FOV (% of Naive)
Naive
Carboxy (Veh.)
Didox

demyelination and repair (Figure 11D) (Contact as a percent of naïve in Cuprizone: 1 week- 122.9 ± 4.3 %, 3 week- 145.3 ± 5.9%, 5 week- 216.4 ± 8.5%, 5+3 week- 179.7 ± 6.3%). In EAE, contact also increased with disease progression and decreased following Didox treatment, correlating with AIS pathology (Figure 11E-F) (Contact as a percent of naïve in EAE: Early 1&2- 153.8 ± 22.5%, Early 3&4- 185.0 ± 5.9%, Late 1&2- 205.6 ± 33.9%, Late 3&4- 169.4 ±31.2%). Although contact increased in both models, the increase in contact was similar between the two models.

Different types of contact were also observed and quantified. Contact was divided into three categories termed 'touching', 'resting', and 'wrapping'. IBA-1+ cells can contact multiple initial segments at the same time and exhibit multiple types of contact (Figure 12A-D). The 'touching' contact was the most prominent type of contact in both EAE and Cuprizone, but did not change with disease progression (Figure 12E, H). 'Resting' and 'wrapping' contact constituted a smaller percent of total contact and also did not vary significantly with disease state in either model (Figure 12F-G, I-J). Despite the fact that the two models exhibit different axonal pathology, contact between IBA-1+ cells and the AIS was similar between the two models. This led to the hypothesis that a functional component of the IBA-1+ cells may be different between the two models.

Reactive Microglia from EAE and Cuprizone mice present distinct RNA profiles

Since no differential IBA-1/AIS contact was observed between the two models, we further proposed that differential expression profiles of the microglia may help to explain the different stabilities of AISs. To address this hypothesis, a microarray was performed using RNA isolated from microglia in naïve, early EAE 1&2, early EAE 3&4, and 3 weeks Cuprizone treated mice. These time points were chosen because they correlated with the beginning of pathology and microglial activation. Thus, expression levels of genes at the onset of pathology were being examined, rather than expression levels following pathology. A heat map generated using the NanoString nSolver software revealed clear

Figure 12. Type of contact does not change with disease state. Coronal sections of mouse cortices show examples of IBA-1+ cells making multiple contacts with AISs (A-C). A horizontal section revealed that the IBA-1+ cell completely engulfed the AIS (D). Quantification of the 3 types of contact, represented as a percent of total contact, revealed no significant changes across time points or between the two models. 'Touching' contact accounted for approximately 80% of total contact across all time points in both models (E, H). 'Resting' contact accounted for approximately 20% of total contact across all time points in both models (F, I). 'Wrapping' contact was the least frequent, constituting approximately 5% of total contact across all time points (G, J). Type of contact did not change with disease progression. Amount of contact also did not change with disease. Morphological analysis of microglia revealed similarities between microglia in EAE and Cuprizone. However, microglia may be performing different function in EAE and Cuprizone.

Figure 12.

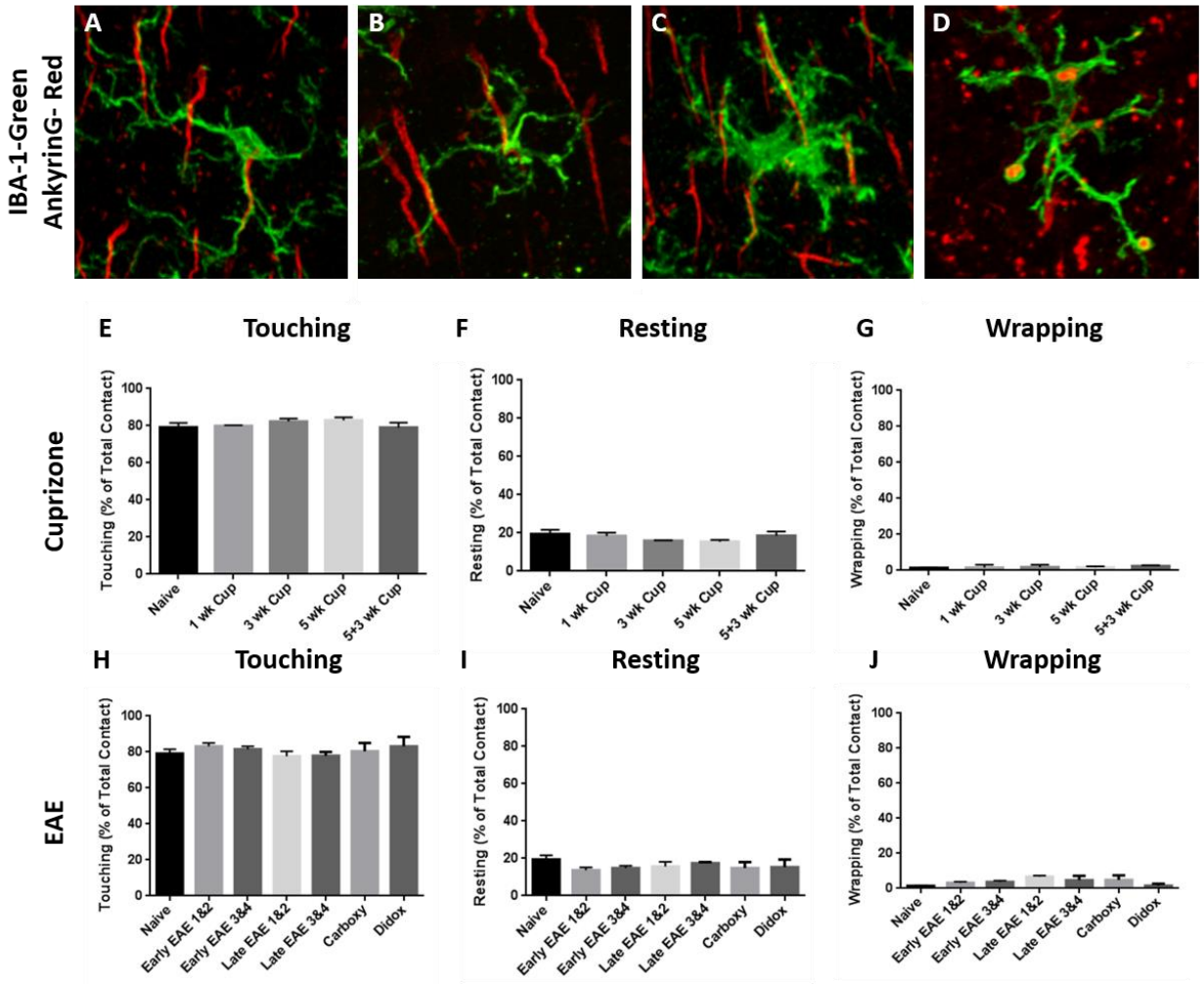
IBA-1-Green
AnkyrinG- Red
A
B
C
D
Cuprizone
E
Touching
F
Resting
G
Wrapping
Touching (% of Total Contact)
Resting (% of Total Contact)
Wrapping (% of Total Contact)
Naive
1 wk Cup
3 wk Cup
5 wk Cup
5+3 wk Cup
EAE
H
Touching
I
Resting
J
Wrapping
Naive
Early EAE 1&2
Early EAE 3&4
Late EAE 1&2
Late EAE 3&4
Carboxy
Didox

differences in RNA expression between EAE and Cuprizone (Figure 13). Of the 248 genes in the microarray, 90 were upregulated by at least 2 fold in early EAE 1&2 mice compared to naïve mice and 86 were downregulated. In early EAE 3&4 mice 76 genes were upregulated by at least 2 fold compared to naïve mice and 83 were downregulated. In Cuprizone mice 26 genes were upregulated by at least 2 fold compared to naïve mice and 163 were downregulated. Further categorization of the data using the nSolver software revealed the ten genes with the most positive and most negative changes in expression (compared to naïve) in each category (Figure 14). Maff (v-maf avian musculoaponeurotic fibrosarcoma oncogene homolog F) was the most upregulated gene in Cuprizone mice, showing an increase of 12.5 compared to naïve mice. Arg1 (Arginase 1) was the gene most upregulated in both EAE 1&2 and EAE 3&4 mice, showing an increase of 6424 fold in EAE 1&2 and an increase of 1103 fold in EAE 3&4 compared to naïve mice. Tlr5 (toll-like receptor 5) was the gene most downregulated in Cuprizone mice, showing a decrease of 87 fold compared to naïve mice. In early EAE 1&2 mice, Ptger3 (prostaglandin E receptor 3) was the most downregulated gene, showing a decrease of 22 fold compared to naïve mice. In early EAE 3&4 Retnla (resistin-like alpha) was the most downregulated down, showing a decrease of 93 fold compared to naïve mice. Some genes, for example toll-like receptor 5 (Tlr5), were downregulated compared to naïve in both EAE and Cuprizone. Other genes were downregulated in Cuprizone and upregulated in EAE: for example, Chi3l3 was downregulated 23 fold in Cuprizone, and upregulated 144 fold in EAE early 1&2. Although EAE early 1&2 and early 3&4 displayed many similarities, there were some genes that are differentially regulated between the two conditions; for example, Arginase 1 (Arg1) was the most upregulated gene compared to naive in both EAE early 1&2 and EAE early 3&4, but it was upregulated 6,424 fold in EAE 1&2 and 1,103 fold in EAE 3&4.

Analysis using functional enrichment tools was used to gain insight into the changes in gene expression. The ToppFun and EnrichR programs provided data about pathways/functions enriched in different disease states. Ingenuity Pathway Analysis also provided information about

Figure 13. A heat map of microarray results. The heat map displays genes whose expression was upregulated (red), downregulated (green), and unchanged (black) compared to naive. The heat map was generated using the Nanostring nSolver software (v. 2.5) from the previously normalized data. A brighter red signifies more upregulation, while a brighter green signifies more downregulation. Representing the expression results this way revealed clear differences between the expression profiles of microglia in EAE and Cuprizone treated mice. Compared to naïve, 185 genes were downregulated in the 3 weeks Cuprizone treatment group, 114 in early EAE 1&2, and 111 in early EAE 3&4. Alternatively, 33 were upregulated in the 3 week Cuprizone treatment group, 96 in early EAE 1&2, and 85 in early EAE 3&4 (compared to naïve). The results indicated that there are differences in RNA expression between microglia in EAE and Cuprizone, indicating possible functional differences in microglia between EAE and Cuprizone.

Figure 13.


3 Weeks Cuprizone vs. Naive
Early EAE 1&2 vs. Naive
Early EAE 3&4 vs. Naive
Daxx
Mx2
Mx1
Cebpb
Bcl6
Relb
Cysltr2
Il10
Il15
Mafk
Max
Tlr1
Tnfaip3
Il1a
Keap1
Hif1a
Cfl1
Mapkapk2
Fxyd2
Tlr2
Cxcl3
Tnf
Irf1
Stat2
Cd40lg
Il23r
Ccl2
Ifnb1
Lta
Fos
Ccl19
Il22
Mapkapk5
Il17a
Ddit3
Tradd
Map3k9
Ccr4
Areg
Gngt1
Hras1
Il7
C7
C8b
Alox15
Ifna1
C8a
Ccl24
Mafg
Jun
Il6ra
Tcf4
Rock2
Ptgs1
Ptk2
Tslp
Tlr9
Tgfb3
Irf3
Mrc1
Hc
Ccl11
Ptger1
Il21
Il23a
Kngl
Il22ra2
Hspb2
Cxcl5
Twist2
Pik3c2g
Il9
Mbl2
H2-Ea-ps
Csf3
Cfd
C9
Tbxa2r
Alox12
Il13
Tgfb1
Mef2b
Gpr44
Il4
Map2k1
Ly96
Tollip
Il10rb
Traf2
Limk1
Cd86
Myc
Prkcb
Pla2g4a
Ccl20
Il3
Masp2
Nox1
Il2
Ccr3
Crp
Defa-rs1
Mmp3
Il5
Rhoa
Mapk3
Bcl2l1
Hmgb1
Rac1
Hmgn1
C1qa
C1qb
Cdc42
Elk1
Il1r1
Shc1
Nfe2l2
Gnb1
Itgb2
C3ar1
Map3k7
Atf2
Tlr6
Rela
Map2k4
Mapk1
Nfkb1
Irf5
Grb2
Raf1
Ripk1
Ripk2
Map3k1
Stat3
Myd88
Trem2
Mknk1
Gnaq
Mapk14
Smad7
Nr3c1
Tlr7
Flt1
Mef2d
Map2k6
Hdac4
Rapgef2
Mapk8
Nlrp3
Cysltr1
Map3k5
Il1rap
Tlr4
Il18
Nfatc3
Rps6ka5
Birc2
Alox5
Creb1
Ptgfr
Ltb4r2
Mef2c_Mm
Ccl21a
Tyrobp
Ccl3
Gnas
Pdgfa
Ccl4
Myl2
Tgfbr1
Hspb1
Masp1
Tgfb2
Ager
Cd55
Ccl7
Ltb
Nod1
Tlr8
Mmp9
Tlr3
Csf1
Ifit1
Ifit3
Oasla
C2
Stat1
Csf2
Ccrl
Ptgir
Cxcr4
Cxcl2
Cxcl1
Ptger4
Ifi27l2a
Ifit2
Oas2
Cls
Nod2
Ccr2
Cd4
Hsh2d
Il1l
Maff
Fasl
Il12a
Irf7
H2-Eb1
Hmgb2
Cd163
Il6
Prkca
Plcb1
Mef2a
Ptger3
Il1b
Il18rap
Ifng
Cxcr2
Ltb4r1
Ifi44
Il12b
C4a
Cxcl10
Oasl1
Clra
Iigp1
Ccl17
Cxcr1
Ptger2
Tlr5
Ppp1r12b
Retnla
C6
Ccl8
Ccl5
Cd40
Tnfsf14
Chi3l3
Il1rn
Nos2
Ptgs2
Ccl22
Ccr7
C3
Cxcl9
Cfb
Arg1

Figure 14. Top 10 upregulated and downregulated genes in EAE and Cuprizone. The Top 10 genes upregulated (blue) and downregulated (red), compared to naïve, in 3 weeks Cuprizone (A), EAE Early 1&2 (B), and EAE Early 3&4 (C). All genes had a significant positive or negative fold change compared to naïve according to the nSolver software (p value <0.05). All genes demonstrated a greater than 2.0 fold change. Note the axis breaks in graphs B and C due the very large fold change in the top two genes displayed. In Cuprizone, the highest upregulated gene (Maff) was upregulated by 12.6 fold compared to naïve. In EAE, the highest upregulated gene (Arg1) as upregulated by 6424 fold compared to naïve in early 1&2 and 1104 fold compared to naïve in early 3&4. In Cuprizone, Tlr5 was the most downregulated gene, decreased by 87 fold compared to naïve. In early EAE 1&2 Ptger3 was the most downregulated gene (22 fold decrease compared to naive) and in early EAE 3&4 Retnla was the most downregulated gene (93 fold decrease compared to naïve). This data further confirms differences in RNA expression between EAE and Cuprizone.

Figure 14.

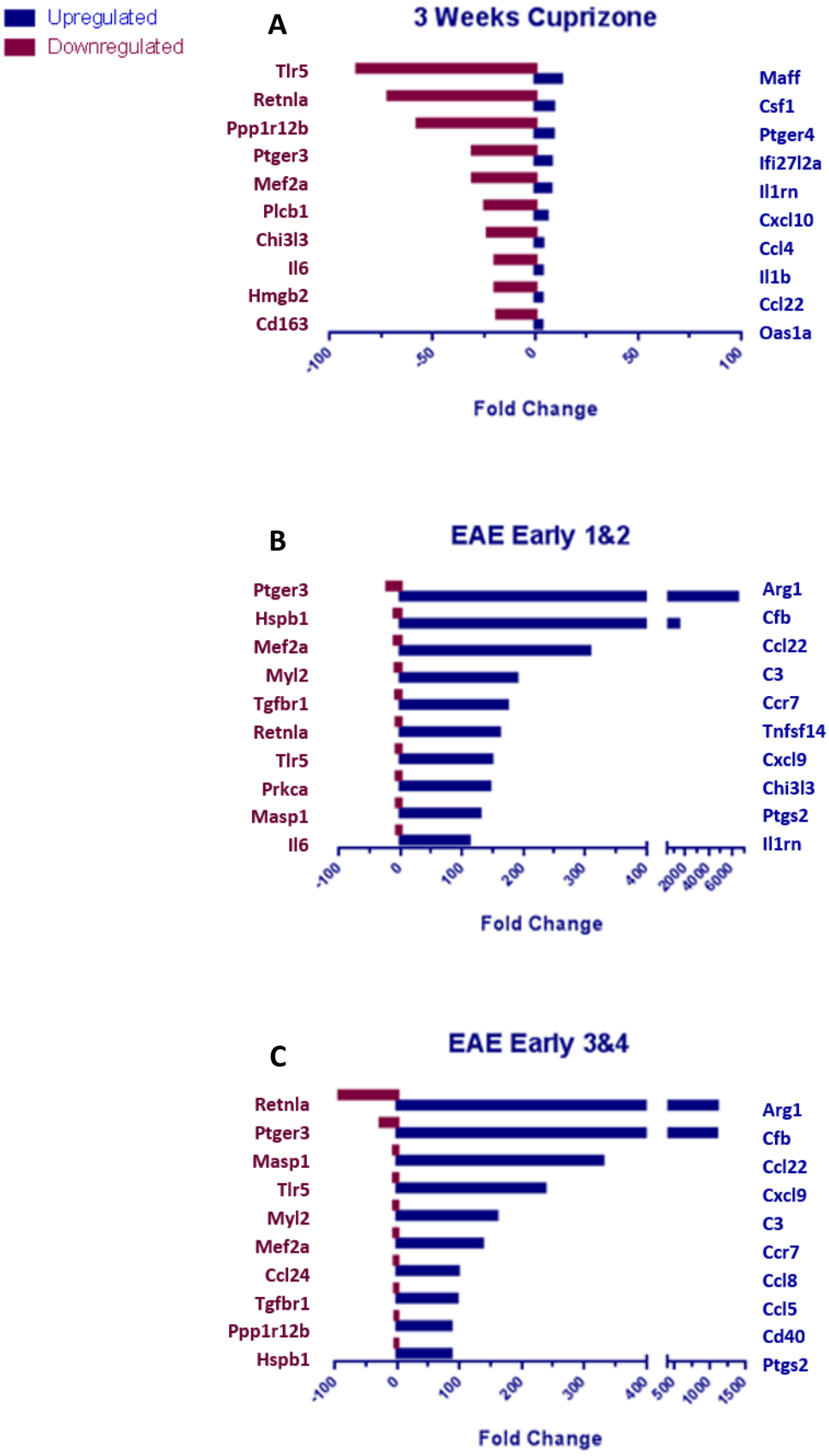
Upregulated
Downregulated
A
3 Weeks Cuprizone
Tlr5
Retnla
Ppp1r12b
Ptger3
Mef2a
Plcb1
Chi3l3
Il6
Hmgb2
Cd163
Maff
Csf1
Ptger4
Ifi27l2a
Il1rn
Cxcl10
Ccl4
Il1b
Ccl22
Oas1a
-100
-50
0
50
100
Fold Change
B
EAE Early 1&2
Ptger3
Hspb1
Mef2a
Myl2
Tgfbr1
Retnla
Tlr5
Prkca
Masp1
Il6
Arg1
Cfb
Ccl22
C3
Ccr7
Tnfsf14
Cxcl9
Chi3l3
Ptgs2
Il1rn
-100
0
100
200
300
400
2000
4000
6000
Fold Change
C
EAE Early 3&4
Retnla
Ptger3
Masp1
Tlr5
Myl2
Mef2a
Ccl24
Tgfbr1
Ppp1r12b
Hspb1
Arg1
Cfb
Ccl22
Cxcl9
C3
Ccr7
Ccl8
Ccl5
Cd40
Ptgs2
-100
0
100
200
300
400
500
1000
1500
Fold Change

pathways/functions enriched in specific disease states, but was more specific to neuronal tissue than either ToppFun or EnrichR. According to Ingenuity Pathway analysis, functions relating to demyelination and lymphocyte movement showed the most increase in activation in Cuprizone, while the inflammatory response, cell proliferation/cell number, and growth and branching of neurites showed decreased activation (Figure 15). In EAE both EAE 1&2 and 3&4, leukocyte migration/movement, cell migration, and cell death of neuroglia showed increased activation. In EAE, similar to Cuprizone, growth of neurites, and cell number/viability showed decreased activation (Figure 16). Although each program gave results for pathways that were enriched in each category, there were three pathways that appeared specifically enriched in EAE in all three programs: the complement cascade, toll-like receptor signaling, and p38 MAP kinase signaling (Figure 16). Ingenuity Pathways Analysis also provided the 'Top Analysis Ready Molecules', which are molecules that were highly upregulated or downregulated, but also related to the enriched functions/pathways. Of note, in EAE Early 1&2 three of the top analysis ready molecules are C3, Cfb (complement factor B), and C6, and in EAE Early 3&4 Cfb and C3 both appear in the list. Cfb, C3, and C6 are all molecules part of the Complement pathway (part of innate immunity). Data from the microarray indicated an increase in expression of C1r, C1s, C2, C3, C4, C6, and Factor B indicating involvement of the classical and alternative complement pathways. Decrease of MASP1 (mannose-associate serine protease 1) indicated the lectin pathway was not activated in EAE. High levels of C3 and Complement Factor B indicated a possible amplification loop, resulting in cleavage of C3 into C3a and C3b. Although C1qa or C1qb were not upregulated, which is necessary to activate the classical complement pathway, high levels of C3 and Cfb indicated the alternative pathway initiated the activation of the cascade in the EAE samples. Although the gene data does not differentiate between the different protein subunits of C2, C3, and C4, inflammation in EAE would indicate that C3a and C4a may be recruiting other inflammatory factors.

Figure 15. Ingenuity Pathway Analysis (IPA) results for functions upregulated and downregulated in EAE and Cuprizone. The top five functions designated as having increased and decreased activation are listed for each disease state. In EAE increased activation functions included leukocyte migration, leukocyte cell movement, and cell death of neuroglia. In Cuprizone increased activation functions included demyelination of the CNS and cell movement of lymphocytes. Decreased activation functions in both EAE and Cuprizone included growth of neurites. In EAE cell viability of neurons and quantity of neuronal cells were decreased. In Cuprizone, branching of neurites, quantity and proliferation of neuronal cells, and the inflammatory response revealed decreased activation. Rank was based on p-values provided by IPA, with the smallest p-value indicating the most enriched function. Determination of increased or decreased activation was based on z-score (z-score >2.0= increased activation, z-score <-2.0= decreased activation). Not all disease states had five functions classified as showing increased or decreased activation, in which case all of the functions with increased or decreased activation were listed. The data revealed alternatively activated functions in EAE and Cuprizone.

Figure 15.

EAE Early 3&4	
Increased Activation	**Decreased Activation**
Leukocyte migration	Growth of neurites
Cell movement of leukocytes	Outgrowth of neurites
Migration of cells	Cell viability of neurons
Cell death of neuroglia	Quantity of central nervous system cells
Apoptosis of neuroglia	

EAE Early 1&2	
Increased Activation	**Decreased Activation**
Leukocyte migration	Growth of neurites
Cell movement of leukocytes	Cell viability of neurons
Migration of cells	Quantity of central nervous system cells
Cell death of neuroglia	
Cellular infiltration by leukocytes	

3 Weeks Cuprizone	
Increased Activation	**Decreased Activation**
Demyelination	Inflammatory Response
Demyelination of spinal cord	Quantity of cells
Demyelination of central nervous system	Branching of neurites
Cell movement of lymphocytes	Growth of neurites
	Proliferation of neuronal cells

Figure 16. Top pathways shown to be enriched in EAE by ToppFun, EnrichR, and Ingenuity Pathway Analysis programs. All pathways were in the top 10 results for each program individually. All pathways were enriched in both EAE Early 1&2 and EAE Early 3&4. The Complement pathway, the toll-like receptor signaling pathway, and the p38 MAPK pathway may then contribute to AIS pathology in EAE.

Figure 16.

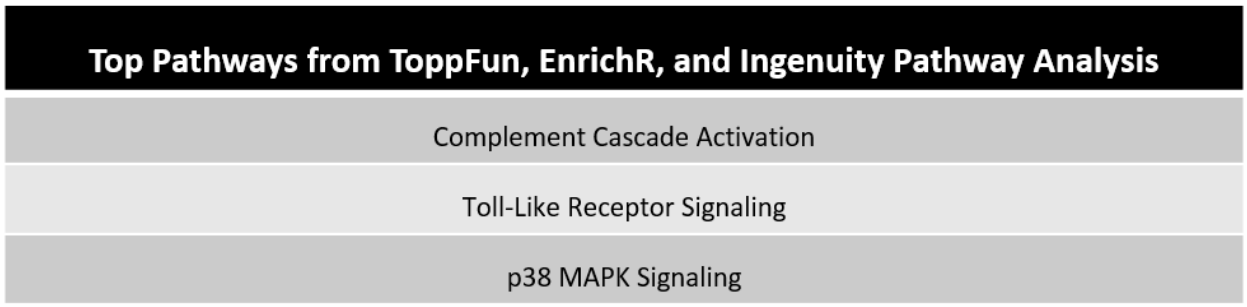
Top Pathways from ToppFun, EnrichR, and Ingenuity Pathway Analysis
Complement Cascade Activation
Toll-Like Receptor Signaling
p38 MAPK Signaling

Complement Genes are Upregulated in EAE

Due to the prevalence of evidence indicating that the complement pathway was active in the IBA-1+ cells in EAE, further studies were conducted to confirm the upregulation of complement components in EAE. Quantitative reverse transcriptase polymerase chain reaction was performed on naïve, early EAE 1&2, and early EAE 3&4 samples to validate gene expression levels. According to the microarray, the fold changes in C1qa compare to naïve were 0.52 in EAE 1&2 and 0.79 in EAE 3&4. For C1qb, the fold changes were 0.58 in EAE 1&2 and 0.81 in EAE 3&4. For C2, the fold changes were 4.9 in EAE 1&2 and 8.8 in EAE 3&4. The fold changes for C3 were 188 in EAE 1&2 and 159 in EAE 3&4. These values were confirmed by qPCR (Figure 17).

C3 Protein Expression is Upregulated in EAE

Although the qPCR results confirmed the expression changes presented by the NanoString array, neither approach assures a change in expression at the protein level, therefore, western blot analysis was performed in order to determine if protein expression levels of C3 increased in EAE mice similar to gene expression levels. Three distinct bands were observed in both naive and EAE samples. Bands were observed at approximately 185 kD, 104 kD, and 67 kD corresponding to full-length C3, C3b, and iC3b (Cunnion et al., 2004, Mastellos et al. 2004, Pangburn et al., 1977). C3 increased in EAE samples relative to controls, correlating with the already described increased in C3 gene expression (Figure 18). The cleavage fragments of C3, C3b, and iC3b, both showed higher levels in control samples than in EAE samples.

C3 Localizes at the AIS

Using immunohistochemistry to visualize complement proteins in relation to the AIS, double immunolabeling was performed with AnkyrinG and C3. Colocalization of C3 and ankyrinG was observed

Figure 17. Gene expression results for Complement genes found by microarray were confirmed by qPCR. Graphs show gene expression values as a fold change compared to naïve. Naïve expression values were set equal to 1, with fold change values less than naïve represented as fractions between 0 and 1. According to microarfigureray results C1qa (A) decreased in expression by 0.52 fold in early EAE 1&2 and 0.79 fold in early EAE 3&4. C1qb (B) decreased in expression by 0.58 fold in early EAE 1&2 and 0.81 fold in early EAE 3&4. C2 (C) increased in expression by 4.9 fold in early EAE 1&2 and 8.8 fold in early EAE 3&4. C3 (D) increased by 188 fold in early EAE 1&2 and 159 fold in early EAE 3&4. These relative expression values were confirmed by qPCR (A'-D').

Figure 17.

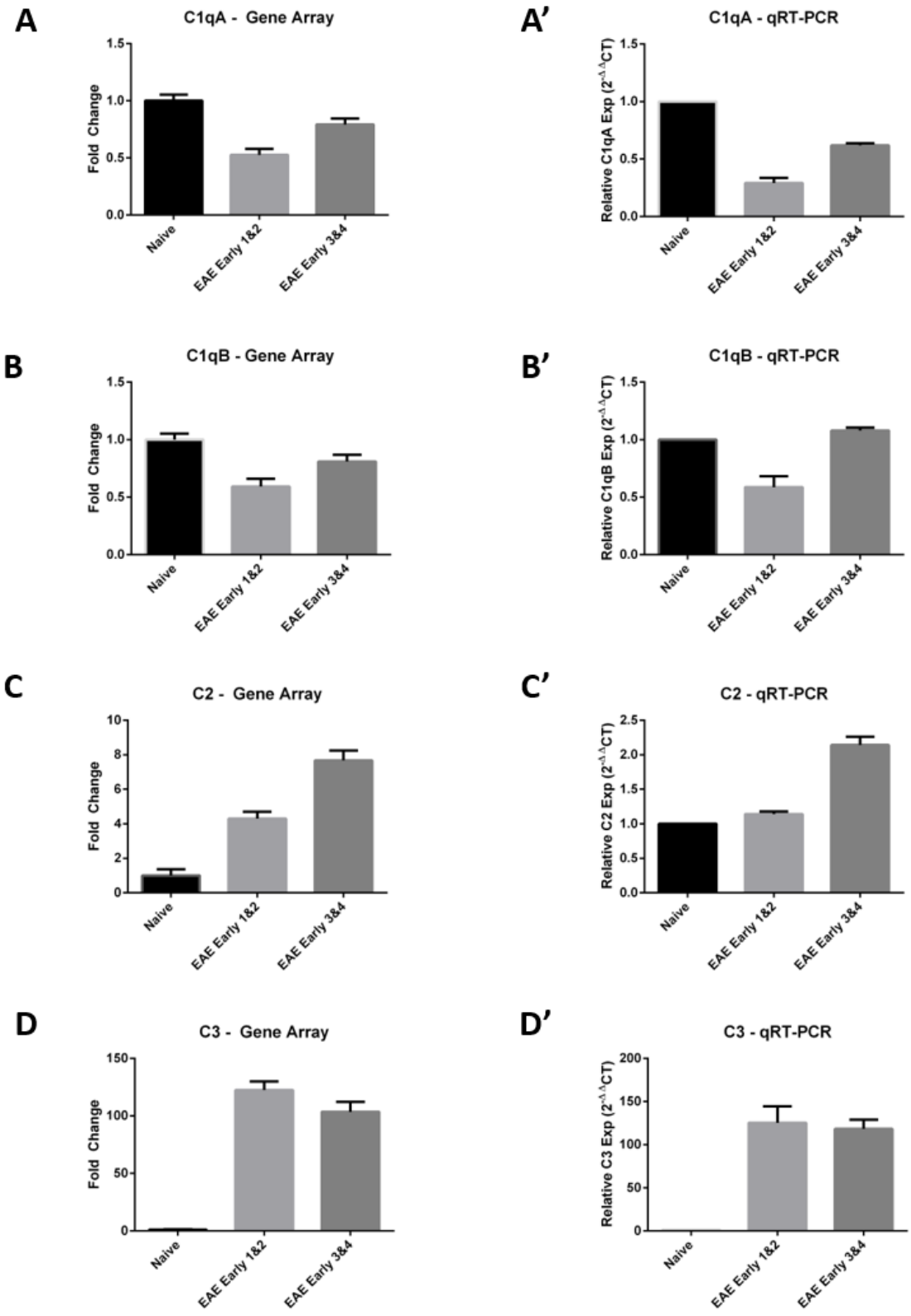
A
C1qA - Gene Array
Fold Change
1.5
1.0
0.5
0.0
Naive
EAE Early 1&2
EAE Early 3&4
A'
C1qA - qRT-PCR
Relative C1qA Exp (2^-ΔΔCT)
B
C1qB - Gene Array
B'
C1qB - qRT-PCR
Relative C1qB Exp (2^-ΔΔCT)
C
C2 - Gene Array
10
8
6
4
2
C'
C2 - qRT-PCR
2.5
2.0
1.5
Relative C2 Exp (2^-ΔΔCT)
D
C3 - Gene Array
150
100
50
D'
C3 - qRT-PCR
200
Relative C3 Exp (2^-ΔΔCT)

Figure 18. Protein expression of C3 increases in EAE. Western blot analysis was performed on whole brain lysate from naïve and EAE samples in order to determine if C3 levels increased throughout the brain and not just in microglia. Representative blots are shown with bands for C3, C3b, and iC3b. GAPDH was used a protein loading control. Densitometry results revealed that C3 (A) protein expression increased in EAE samples compared to naïve. C3b (B) and iC3b (C) protein expression levels decreased in EAE samples compared to naïve. The increase in gene expression of C3 found in microglia was confirmed at the protein level, further solidifying the possibility that C3 may be involved in AIS pathology.

Figure 18.

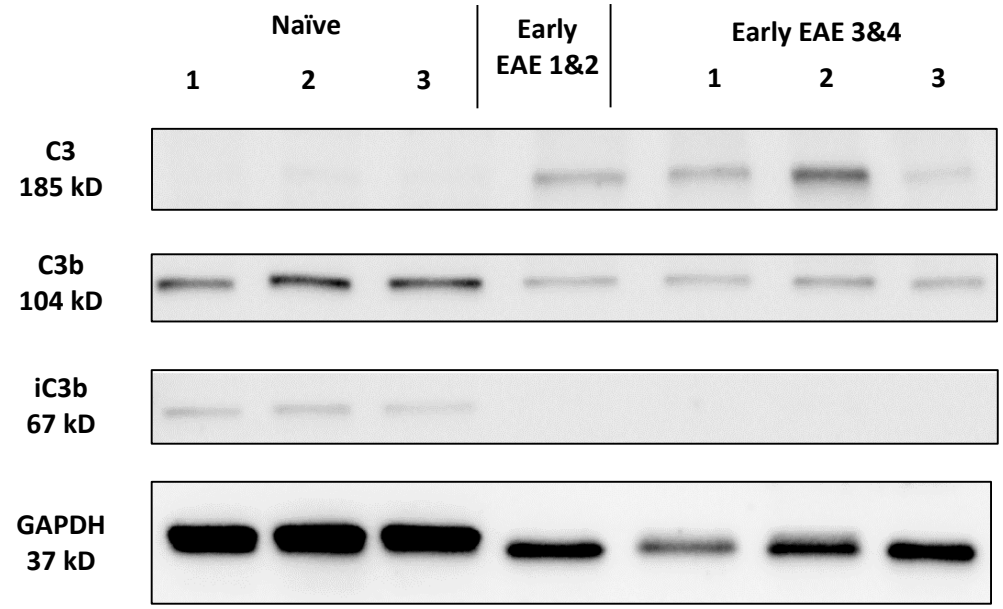
Naïve
Early EAE 1&2
Early EAE 3&4
1
2
3
1
2
3
C3
185 kD
C3b
104 kD
iC3b
67 kD
GAPDH
37 kD

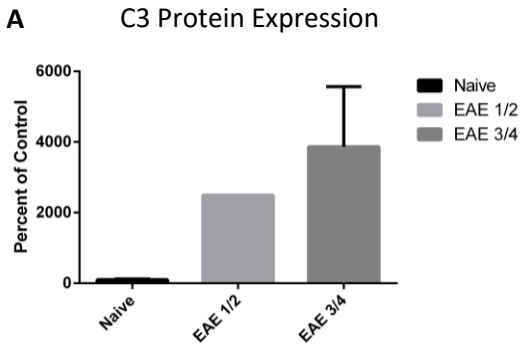
A
C3 Protein Expression
Percent of Control
6000
4000
2000
0
Naive
EAE 1/2
EAE 3/4

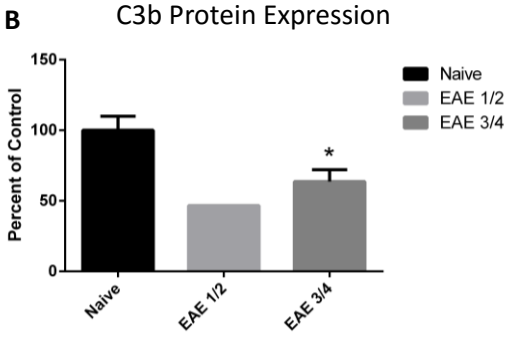
B
C3b Protein Expression
Percent of Control
150
100
50
0
*
Naive
EAE 1/2
EAE 3/4

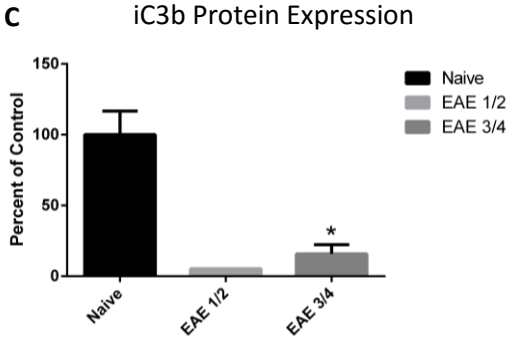
C
iC3b Protein Expression
Percent of Control
150
100
50
0
*
Naive
EAE 1/2
EAE 3/4

in EAE tissue, represented by puncta on the edge of the AIS (Figure 19). The localization at C3 at the AIS is significant because it demonstrates that not only is C3 upregulated at the gene and protein level, it also correlates with the AIS and may contribute to AIS shortening or loss.

Figure 19. C3 localizes at the AIS. Double immunolabeling with antibodies directed against C3 and AnkyrinG revealed that C3 (green) can be found at the AIS (red). In naïve tissue, C3 was not found localized at the AIS (A-C). However, in early EAE 3&4 tissue, C3 was found localized at the AIS (D-F). This indicates that upregulated C3 may play a role in mediating AIS breakdown.

Figure 19.

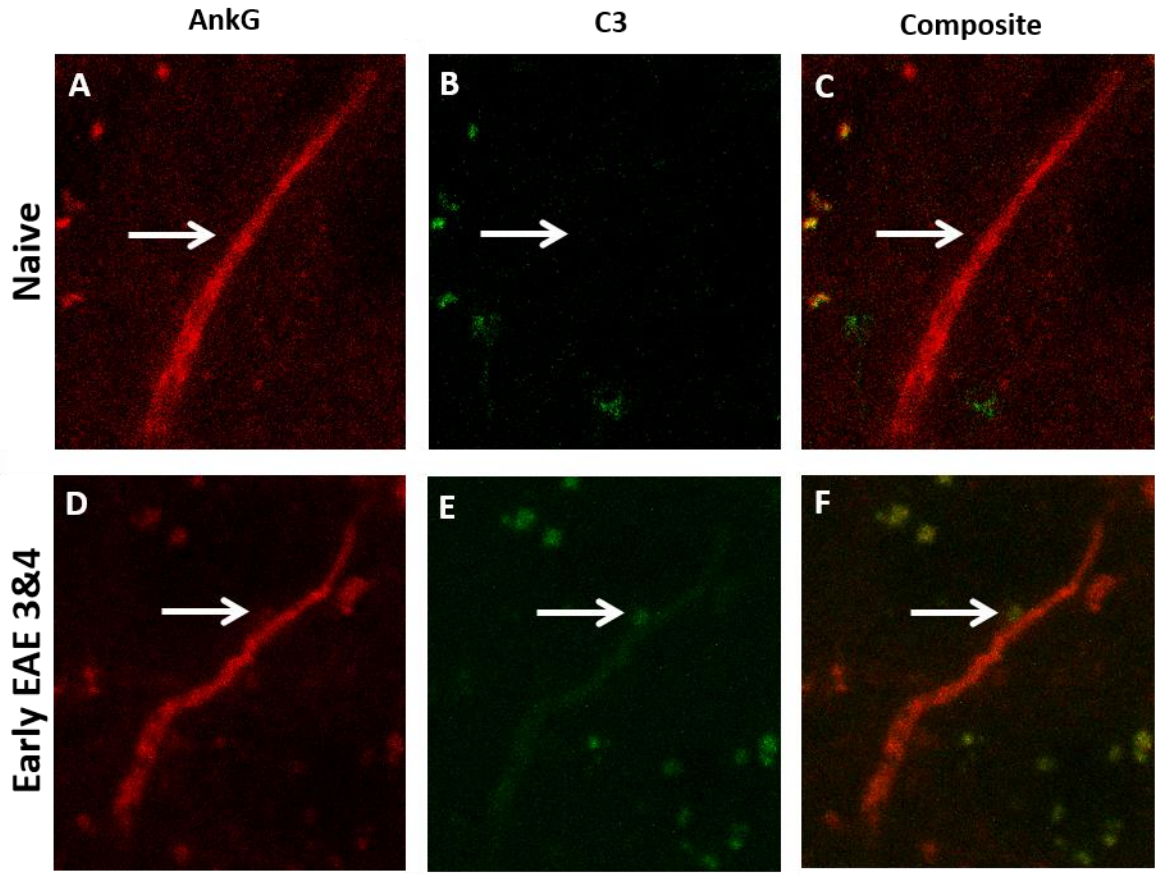

Discussion

Our laboratory has previously observed AIS disruption in cortical neurons of MS tissue. We have also observed a similar disruption in cortical layer V neurons that was coincidental with inflammation, but not demyelination. Indicative of the inflammation was the presence of reactive microglia. Therefore, we posited that reactive microglia may drive AIS disruption. Here, we have further explored that hypothesis by quantifying reactive microglia/AIS contact and microglia expression profiles in both our inflammatory and demyelinating models. Reactive microglia, as identified by a combination of morphologic changes and their immunoreactivity against the IBA-1 antibody, were present in both EAE, the inflammatory model, and in Cuprizone, the demyelinating model. The data show that microglia/AIS contact increased with disease progression with both inflammation and myelin loss. The increase was similar between the two models despite differing pathologies. Microarray data revealed different gene expression profiles in microglia between the two models, indicating possible functional differences between the microglia. Further analysis of microarray data identified the Complement pathway of innate immunity as an important pathway in EAE, suggesting a role for microglia driven complement in AIS disruption and perhaps disease progression. Consistent with our findings, IBA-1+ cells have been correlated to the progression and pathology of MS (Benveniste, 1997; Kutzelnigg and Lassmann, 2014). Modulating the microglia phenotype or inhibiting reactivity can also alter progression of disease in EAE (Heppner et al., 2005; Bhasin et al., 2007) and Cuprizone (Janssens et al., 2015). Thus, understanding the differences in microglial gene expression between EAE and Cuprizone can elucidate mechanisms of pathology distinct to each model.

Microglia Show Morphological Similarities in EAE and Cuprizone

I examined the potential role of IBA-1+ cells in the pathology of the axon initial segment in EAE and Cuprizone. Previous studies have shown that microglia target the axon in MS and mouse models of MS (Nikic et al., 2011; Rawji and Yong, 2013). Previous studies from the lab have shown that AISs are lost in EAE, but not in Cuprizone (Clark et al., 2016). Results show that IBA-1+ cells contact the AIS in naïve mice, and that contact between IBA-1+ cells and the AIS increases with disease progression in EAE and Cuprizone treated mice. Baalman et al. (2015) first published the presence of contact between cortical microglia and the AIS. These results are the first report of microglia/AIS contact in the EAE and Cuprizone models and the first to show contact between the AIS and reactive microglia. Baalman et al. found that microglia contact the AIS throughout development and in adulthood. However, using a traumatic brain injury model, they observed a loss of contact between microglia and the AIS following injury and reported that reactive microglia do not contact the AIS. Thus, the results show a contrast between models of demyelination and inflammation and traumatic brain injury, although they do confirm that IBA-1+ cells contact AISs in the naïve brain. It should also be noted that in the traumatic brain injury model, Baalman et al. saw no loss of AISs, while in EAE we observe a significant decrease in AIS number. Further studies may elucidate the role microglia/AIS contact play in various disease models.

Microglia Gene Expression Differs in EAE and Cuprizone

Despite similar contact with the AIS in EAE and Cuprizone, IBA-1+ cells showed different gene expression profiles in EAE and Cuprizone. The differences in gene expression in microglia indicate functional differences in microglia (Hanisch and Kettenmann, 2007). Genes such as TNF and NOS2, which encode TNFα and iNOS, respectively, were found to be upregulated in EAE and are associated with neurodegeneration (Block et al., 2007; Glass et al., 2010). Colony Stimulating Factor 1 (CSF1) was found to be upregulated in Cuprizone and is involved in the survival, proliferation, and differentiation of

microglia and macrophages and promotes remyelination in the lysolecithin model of demyelination (Doring et al., 2015; Stanley et al., 1997). Correlating with gene expression data, functional enrichment programs indicted the inflammatory response upregulated in EAE, but down regulated in Cuprizone. This information reveals that even though morphological studies showed similarities in IBA-1+ cells between EAE and Cuprizone, examining gene expression, which is indicative of cell function, reveals that the microglia are performing two different functions in the EAE and Cuprizone models. Although, it should be noted that some genes, such as TNF, were similarly expressed in EAE and Cuprizone, and functional analysis programs likewise indicate some overlaps between the two models, indicating the complex nature of IBA-1+ cells.

In EAE, Arginase 1 was the most highly upregulated molecule according to microarray results. Arginase 1 and iNOS compete for the same substrate (arginine) (Wu and Morris, 1998), yet both the Arginase 1 and NOS2 genes were upregulated in EAE. Others observed a similar significant increase in Arginase 1 in EAE, and found that inhibiting Arginase 1 lead to a later onset, less severe course of EAE, and quicker recovery, suggesting a negative effect of Arginase 1 in EAE (Xu et al., 2003). In contrast, Arginase 1 is also commonly used as a marker for 'M2' or 'alternatively activated' macrophages and microglia, a distinct subsets of macrophages/microglia characterized by a 'resolving' phenotype (Mills et al., 2000; Stein et al., 1992; Doyle et al., 1994; Tang and Le, 2016). However, recent data suggests that these distinctions are too narrow, and multiple activation states exist for microglia (Cherry et al., 2014; Martinez and Gordon, 2014). Our data are consistent with this interpretation because although Arginase 1 was highly upregulated, pro-inflammatory cytokines such as TNFα and IL1β were also upregulated in EAE. The high levels of Arginase 1 and pro-inflammatory cytokines may then be indicative of the presence of microglia with phenotypes that do not fall neatly into the 'M1' or 'M2' categories. In addition, the higher expression levels of Arginase 1 compared to NOS2 could indicate that Arginase 1 is outcompeting NOS2 for the same substrate and attempting to resolve inflammation in EAE.

The Complement Pathway May Mediate AIS Disruption

The Complement pathway emerged as a pathway of interest in EAE due to the high upregulation of multiple complement components, especially Complement Component 3 (C3). Three different functional enrichment programs suggested activation of the complement cascade based on the upregulation of complement genes C1r, C1s, C2, C3, C4a, and Cfb. The complement system has also been long-associated with demyelinating lesions in MS (Woyciechowska and Brzosko, 1977; Gay and Esiri, 1991; Ingram et al., 2014). Antibodies directed against neurofascin 186 have also been shown to activate complement and lead to axonal injury (Mathey et al., 2007). Recent research has shown that microglia are involved in pruning synapses in development and in a model of glaucoma via complement activation (Schafer et al., 2012). In this study, researchers propose that astrocytes produce a factor that triggers neurons to produce initiate the complement cascade via C1q. This leads to production of C3b/iC3b which bind to their receptors on microglia and induce them to phagocytose the synapse. Based on the data derived from the EAE model, it is possible that the loss of AISs in EAE occurs by a similar mechanism. A loss of synapses on the AIS could lead to AIS disruption, or the AIS could be a primary target of phagocytosis. What is causing the microglia production of complement is unclear. Complement proteins are upregulated in EAE, so the microglia may be initiating complement-mediated AIS disruption. Although the data examine the expression of complement proteins only in microglia, it is also possible that the neurons themselves are responding to distress by producing a complement-mediated signal that instructs microglia to begin phagocytosis of synapses on the axon initial segment (Figure 20). Further research examining expression of complement proteins in more than one cell type is necessary to determine if either process is occurring. In addition, examination of more molecules involved in the complement pathways would shed light on the exact role of complement in EAE and AIS pathology.

In conclusion, the loss of axon initial segments in the EAE model of MS correlates with increased microglia reactivity and microglia contact with the AIS. The expression profiles of microglia suggest that these cells are serving different roles in inflammatory and demyelinating models. The loss of axon initial segments in EAE may be mediated via the complement system of immunity.

Figure 20. Schematic of the possible role of complement in AIS breakdown. Based on published data regarding synaptic pruning, we hypothesize that microglia are pruning synapses at the AIS. Neurons produce C1q, which activates the complement cascade. Complement proteins C3b/iC3b are then released and bind to receptors on microglia. This induces microglia to prune synapses, specifically the synapses inhibitory interneurons make on the AIS. The pruning of synapses at the AIS then causes shortening of the AIS via plasticity mechanisms. A- published schematic of microglia synaptic pruning; B- Schematic of synaptic pruning at the AIS.

Figure 20.

A

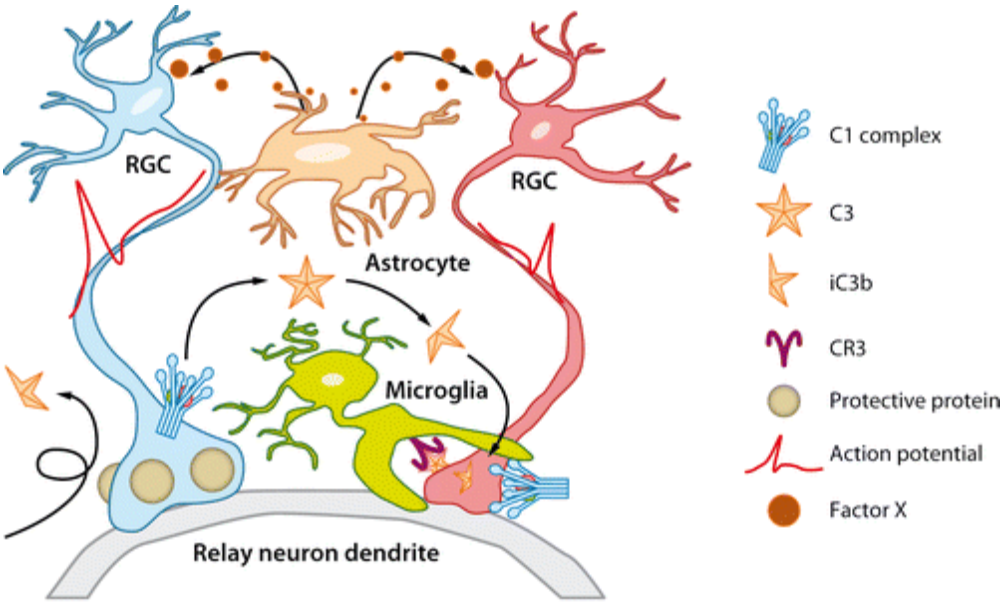

Stephan AH, et al. 2012.
Annu. Rev. Neurosci. 35:369–89

B

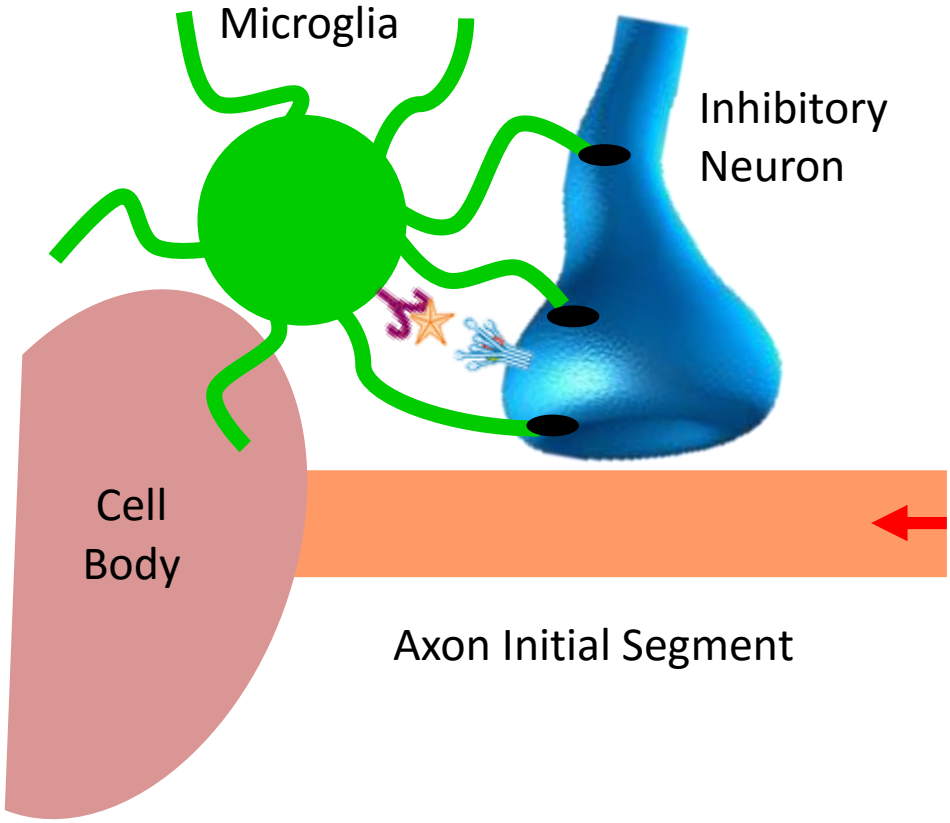

References

Aggarwal S, Yurlova L, Simons M (2011) Central nervous system myelin: Structure, synthesis and assembly. Trends Cell Biol (England) 21:585-593.

Akassoglou K, Adams RA, Bauer J, Mercado P, Tseveleki V, Lassmann H, Probert L, Strickland S (2004) Fibrin depletion decreases inflammation and delays the onset of demyelination in a tumor necrosis factor transgenic mouse model for multiple sclerosis. Proc Natl Acad Sci U S A (United States) 101:6698-6703.

Alt C, Laschinger M, Engelhardt B (2002) Functional expression of the lymphoid chemokines CCL19 (ELC) and CCL 21 (SLC) at the blood-brain barrier suggests their involvement in G-protein-dependent lymphocyte recruitment into the central nervous system during experimental autoimmune encephalomyelitis. Eur J Immunol (Germany) 32:2133-2144.

Aslani MK, Hamid KM, Nazer NH, Mirshafiey A (2014) The role of autoantibodies in diagnosis of multiple sclerosis. International Trends in Immunity 2:29.

Baalman K, Marin MA, Ho TS, Godoy M, Cherian L, Robertson C, Rasband MN (2015) Axon initial segment-associated microglia. J Neurosci (United States) 35:2283-2292.

Baalman KL, Cotton RJ, Rasband SN, Rasband MN (2013) Blast wave exposure impairs memory and decreases axon initial segment length. J Neurotrauma (United States) 30:741-751.

Babbe H, Roers A, Waisman A, Lassmann H, Goebels N, Hohlfeld R, Friese M, Schroder R, Deckert M, Schmidt S, Ravid R, Rajewsky K (2000) Clonal expansions of CD8(+) T cells dominate the T cell infiltrate in active multiple sclerosis lesions as shown by micromanipulation and single cell polymerase chain reaction. J Exp Med (UNITED STATES) 192:393-404.

Bahrini I, Song JH, Diez D, Hanayama R (2015) Neuronal exosomes facilitate synaptic pruning by up-regulating complement factors in microglia. Sci Rep (England) 5:7989.

Barnett MH, Prineas JW (2004) Relapsing and remitting multiple sclerosis: Pathology of the newly forming lesion. Ann Neurol (United States) 55:458-468.

Barnum SR (2015) C4a: An anaphylatoxin in name only. J Innate Immun (Switzerland) 7:333-339.

Battefeld A, Tran BT, Gavrilis J, Cooper EC, Kole MH (2014) Heteromeric Kv7.2/7.3 channels differentially regulate action potential initiation and conduction in neocortical myelinated axons. J Neurosci (United States) 34:3719-3732.

Bekku Y, Rauch U, Ninomiya Y, Oohashi T (2009) Brevican distinctively assembles extracellular components at the large diameter nodes of ranvier in the CNS. J Neurochem (England) 108:1266-1276.

Benarroch EE (2013) Microglia: Multiple roles in surveillance, circuit shaping, and response to injury. Neurology (United States) 81:1079-1088.

Benveniste EN (1997) Role of macrophages/microglia in multiple sclerosis and experimental allergic encephalomyelitis. J Mol Med (Berl) (GERMANY) 75:165-173.

Berghs S, Aggujaro D, Dirkx R,Jr, Maksimova E, Stabach P, Hermel JM, Zhang JP, Philbrick W, Slepnev V, Ort T, Solimena M (2000) betaIV spectrin, a new spectrin localized at axon initial segments and nodes of ranvier in the central and peripheral nervous system. J Cell Biol (UNITED STATES) 151:985-1002.

Bhasin M, Wu M, Tsirka SE (2007) Modulation of microglial/macrophage activation by macrophage inhibitory factor (TKP) or tuftsin (TKPR) attenuates the disease course of experimental autoimmune encephalomyelitis. BMC Immunol (England) 8:10.

Bhat MA, Rios JC, Lu Y, Garcia-Fresco GP, Ching W, St Martin M, Li J, Einheber S, Chesler M, Rosenbluth J, Salzer JL, Bellen HJ (2001) Axon-glia interactions and the domain organization of myelinated axons requires neurexin IV/caspr/paranodin. Neuron (United States) 30:369-383.

Bhave S, Elford H, McVoy MA (2013) Ribonucleotide reductase inhibitors hydroxyurea, didox, and trimidox inhibit human cytomegalovirus replication in vitro and synergize with ganciclovir. Antiviral Res (Netherlands) 100:151-158.

Bitsch A, Schuchardt J, Bunkowski S, Kuhlmann T, Bruck W (2000) Acute axonal injury in multiple sclerosis. correlation with demyelination and inflammation. Brain (ENGLAND) 123 (Pt 6):1174-1183.

Bjartmar C, Wujek JR, Trapp BD (2003) Axonal loss in the pathology of MS: Consequences for understanding the progressive phase of the disease. J Neurol Sci (Netherlands) 206:165-171.

Bjartmar C, Kidd G, Mork S, Rudick R, Trapp BD (2000) Neurological disability correlates with spinal cord axonal loss and reduced N-acetyl aspartate in chronic multiple sclerosis patients. Ann Neurol (United States) 48:893-901.

Black JA, Frezel N, Dib-Hajj SD, Waxman SG (2012) Expression of Nav1.7 in DRG neurons extends from peripheral terminals in the skin to central preterminal branches and terminals in the dorsal horn. Mol Pain (England) 8:82-8069-8-82.

Block ML, Zecca L, Hong JS (2007) Microglia-mediated neurotoxicity: Uncovering the molecular mechanisms. Nat Rev Neurosci (England) 8:57-69.

Boiko T, Rasband MN, Levinson SR, Caldwell JH, Mandel G, Trimmer JS, Matthews G (2001) Compact myelin dictates the differential targeting of two sodium channel isoforms in the same axon. Neuron (United States) 30:91-104.

Boison D, Stoffel W (1994) Disruption of the compacted myelin sheath of axons of the central nervous system in proteolipid protein-deficient mice. Proc Natl Acad Sci U S A (UNITED STATES) 91:11709-11713.

Bonifati DM, Kishore U (2007) Role of complement in neurodegeneration and neuroinflammation. Mol Immunol (England) 44:999-1010.

Boyle ME, Berglund EO, Murai KK, Weber L, Peles E, Ranscht B (2001) Contactin orchestrates assembly of the septate-like junctions at the paranode in myelinated peripheral nerve. Neuron (United States) 30:385-397.

Brakebusch C, Seidenbecher CI, Asztely F, Rauch U, Matthies H, Meyer H, Krug M, Bockers TM, Zhou X, Kreutz MR, Montag D, Gundelfinger ED, Fassler R (2002) Brevican-deficient mice display impaired hippocampal CA1 long-term potentiation but show no obvious deficits in learning and memory. Mol Cell Biol (United States) 22:7417-7427.

Browne P, Chandraratna D, Angood C, Tremlett H, Baker C, Taylor BV, Thompson AJ (2014) Atlas of multiple sclerosis 2013: A growing global problem with widespread inequity. Neurology (United States) 83:1022-1024.

Butovsky O, Ziv Y, Schwartz A, Landa G, Talpalar AE, Pluchino S, Martino G, Schwartz M (2006a) Microglia activated by IL-4 or IFN-gamma differentially induce neurogenesis and oligodendrogenesis from adult stem/progenitor cells. Mol Cell Neurosci (United States) 31:149-160.

Butovsky O, Landa G, Kunis G, Ziv Y, Avidan H, Greenberg N, Schwartz A, Smirnov I, Pollack A, Jung S, Schwartz M (2006b) Induction and blockage of oligodendrogenesis by differently activated microglia in an animal model of multiple sclerosis. J Clin Invest (United States) 116:905-915.

Buttermore ED, Thaxton CL, Bhat MA (2013) Organization and maintenance of molecular domains in myelinated axons. J Neurosci Res (United States) 91:603-622.

Charles P, Tait S, Faivre-Sarrailh C, Barbin G, Gunn-Moore F, Denisenko-Nehrbass N, Guennoc AM, Girault JA, Brophy PJ, Lubetzki C (2002) Neurofascin is a glial receptor for the paranodin/caspr-contactin axonal complex at the axoglial junction. Curr Biol (England) 12:217-220.

Chen EY, Tan CM, Kou Y, Duan Q, Wang Z, Meirelles GV, Clark NR, Ma'ayan A (2013) Enrichr: Interactive and collaborative HTML5 gene list enrichment analysis tool. BMC Bioinformatics (England) 14:128-2105-14-128.

Chen J, Aronow BJ, Jegga AG (2009a) Disease candidate gene identification and prioritization using protein interaction networks. BMC Bioinformatics (England) 10:73-2105-10-73.

Chen J, Bardes EE, Aronow BJ, Jegga AG (2009b) ToppGene suite for gene list enrichment analysis and candidate gene prioritization. Nucleic Acids Res (England) 37:W305-11.

Chen J, Xu H, Aronow BJ, Jegga AG (2007) Improved human disease candidate gene prioritization using mouse phenotype. BMC Bioinformatics (England) 8:392.

Cherry JD, Olschowka JA, O'Banion MK (2014) Neuroinflammation and M2 microglia: The good, the bad, and the inflamed. J Neuroinflammation (England) 11:98-2094-11-98.

Chu Y, Jin X, Parada I, Pesic A, Stevens B, Barres B, Prince DA (2010) Enhanced synaptic connectivity and epilepsy in C1q knockout mice. Proc Natl Acad Sci U S A (United States) 107:7975-7980.

Clark KC, Josephson A, Benusa S, Hartley RK, Baer M, Thummala S, Joslyn M, Elford H, Oh U, Dilsizoglu-Senol A, Lubetzki C, Davenne M, DeVries G, Dupree JL (2016) Compromised axon initial segment integrity in EAE is preceded by microglial reactivity and contact. Glia in submission:.

Coetzee T, Suzuki K, Nave KA, Popko B (1999) Myelination in the absence of galactolipids and proteolipid proteins. Mol Cell Neurosci (UNITED STATES) 14:41-51.

Columba-Cabezas S, Serafini B, Ambrosini E, Aloisi F (2003) Lymphoid chemokines CCL19 and CCL21 are expressed in the central nervous system during experimental autoimmune encephalomyelitis: Implications for the maintenance of chronic neuroinflammation. Brain Pathol (Switzerland) 13:38-51.

Das Sarma J, Kenyon LC, Hingley ST, Shindler KS (2009) Mechanisms of primary axonal damage in a viral model of multiple sclerosis. J Neurosci (United States) 29:10272-10280.

Davalos D, Ryu JK, Merlini M, Baeten KM, Le Moan N, Petersen MA, Deerinck TJ, Smirnoff DS, Bedard C, Hakozaki H, Gonias Murray S, Ling JB, Lassmann H, Degen JL, Ellisman MH, Akassoglou K (2012) Fibrinogen-induced perivascular microglial clustering is required for the development of axonal damage in neuroinflammation. Nat Commun (England) 3:1227.

Davis JQ, Lambert S, Bennett V (1996) Molecular composition of the node of ranvier: Identification of ankyrin-binding cell adhesion molecules neurofascin (mucin+/third FNIII domain-) and NrCAM at nodal axon segments. J Cell Biol (UNITED STATES) 135:1355-1367.

de Graaf KL, Albert M, Weissert R (2012) Autoantigen conformation influences both B- and T-cell responses and encephalitogenicity. J Biol Chem (United States) 287:17206-17213.

DeLuca GC, Ebers GC, Esiri MM (2004) Axonal loss in multiple sclerosis: A pathological survey of the corticospinal and sensory tracts. Brain (England) 127:1009-1018.

Desmazieres A, Zonta B, Zhang A, Wu LM, Sherman DL, Brophy PJ (2014) Differential stability of PNS and CNS nodal complexes when neuronal neurofascin is lost. J Neurosci (United States) 34:5083-5088.

Devaux J, Alcaraz G, Grinspan J, Bennett V, Joho R, Crest M, Scherer SS (2003) Kv3.1b is a novel component of CNS nodes. J Neurosci (United States) 23:4509-4518.

Devaux JJ, Kleopa KA, Cooper EC, Scherer SS (2004) KCNQ2 is a nodal K+ channel. J Neurosci (United States) 24:1236-1244.

DeVries GH, Farrer R, Padadopoulos C, Campbell C, Litz J, Paletta J, Dupree JL, Elford H (2012) Didox-A multipotent drug for treating demyelinating disease. The FASEB Journal 26:341.4.

Doring A, Sloka S, Lau L, Mishra M, van Minnen J, Zhang X, Kinniburgh D, Rivest S, Yong VW (2015) Stimulation of monocytes, macrophages, and microglia by amphotericin B and macrophage colony-stimulating factor promotes remyelination. J Neurosci (United States) 35:1136-1148.

Doyle AG, Herbein G, Montaner LJ, Minty AJ, Caput D, Ferrara P, Gordon S (1994) Interleukin-13 alters the activation state of murine macrophages in vitro: Comparison with interleukin-4 and interferon-gamma. Eur J Immunol (GERMANY) 24:1441-1445.

Duflocq A, Le Bras B, Bullier E, Couraud F, Davenne M (2008) Nav1.1 is predominantly expressed in nodes of ranvier and axon initial segments. Mol Cell Neurosci (United States) 39:180-192.

Dugandzija-Novakovic S, Koszowski AG, Levinson SR, Shrager P (1995) Clustering of na+ channels and node of ranvier formation in remyelinating axons. J Neurosci (UNITED STATES) 15:492-503.

Dunkelberger JR, Song WC (2010) Complement and its role in innate and adaptive immune responses. Cell Res (China) 20:34-50.

Dupree JL, Mason JL, Marcus JR, Stull M, Levinson R, Matsushima GK, Popko B (2004) Oligodendrocytes assist in the maintainence of sodium channel clusters independent of the myelin sheath. Neuron Glia Biology 1:179-192.

Dupree JL, Girault JA, Popko B (1999) Axo-glial interactions regulate the localization of axonal paranodal proteins. J Cell Biol (UNITED STATES) 147:1145-1152.

Dupree JL, Polak PE, Hensley K, Pelligrino D, Feinstein DL (2015) Lanthionine ketimine ester provides benefit in a mouse model of multiple sclerosis. J Neurochem (England) 134:302-314.

Dupree JL, Coetzee T, Blight A, Suzuki K, Popko B (1998) Myelin galactolipids are essential for proper node of ranvier formation in the CNS. J Neurosci (UNITED STATES) 18:1642-1649.

Dutta R, Trapp BD (2011) Mechanisms of neuronal dysfunction and degeneration in multiple sclerosis. Prog Neurobiol (England) 93:1-12.

Dzhashiashvili Y, Zhang Y, Galinska J, Lam I, Grumet M, Salzer JL (2007) Nodes of ranvier and axon initial segments are ankyrin G-dependent domains that assemble by distinct mechanisms. J Cell Biol (United States) 177:857-870.

Dziedzic T, Metz I, Dallenga T, Konig FB, Muller S, Stadelmann C, Bruck W (2010) Wallerian degeneration: A major component of early axonal pathology in multiple sclerosis. Brain Pathol (Switzerland) 20:976-985.

East E, Baker D, Pryce G, Lijnen HR, Cuzner ML, Gveric D (2005) A role for the plasminogen activator system in inflammation and neurodegeneration in the central nervous system during experimental allergic encephalomyelitis. Am J Pathol (United States) 167:545-554.

Einheber S, Zanazzi G, Ching W, Scherer S, Milner TA, Peles E, Salzer JL (1997) The axonal membrane protein caspr, a homologue of neurexin IV, is a component of the septate-like paranodal junctions that assemble during myelination. J Cell Biol (UNITED STATES) 139:1495-1506.

Eshed Y, Feinberg K, Carey DJ, Peles E (2007) Secreted gliomedin is a perinodal matrix component of peripheral nerves. J Cell Biol (United States) 177:551-562.

Eshed Y, Feinberg K, Poliak S, Sabanay H, Sarig-Nadir O, Spiegel I, Bermingham JR,Jr, Peles E (2005) Gliomedin mediates schwann cell-axon interaction and the molecular assembly of the nodes of ranvier. Neuron (United States) 47:215-229.

Evangelou N, DeLuca GC, Owens T, Esiri MM (2005) Pathological study of spinal cord atrophy in multiple sclerosis suggests limited role of local lesions. Brain (England) 128:29-34.

Evangelou N, Konz D, Esiri MM, Smith S, Palace J, Matthews PM (2000) Regional axonal loss in the corpus callosum correlates with cerebral white matter lesion volume and distribution in multiple sclerosis. Brain (ENGLAND) 123 (Pt 9):1845-1849.

Feinberg K, Eshed-Eisenbach Y, Frechter S, Amor V, Salomon D, Sabanay H, Dupree JL, Grumet M, Brophy PJ, Shrager P, Peles E (2010) A glial signal consisting of gliomedin and NrCAM clusters axonal na+ channels during the formation of nodes of ranvier. Neuron (United States) 65:490-502.

Ferguson B, Matyszak MK, Esiri MM, Perry VH (1997) Axonal damage in acute multiple sclerosis lesions. Brain (ENGLAND) 120 (Pt 3):393-399.

Files DK, Jausurawong T, Katrajian R, Danoff R (2015) Multiple sclerosis. Prim Care (United States) 42:159-175.

Fjell J, Hjelmstrom P, Hormuzdiar W, Milenkovic M, Aglieco F, Tyrrell L, Dib-Hajj S, Waxman SG, Black JA (2000) Localization of the tetrodotoxin-resistant sodium channel NaN in nociceptors. Neuroreport (ENGLAND) 11:199-202.

Frischer JM, Bramow S, Dal-Bianco A, Lucchinetti CF, Rauschka H, Schmidbauer M, Laursen H, Sorensen PS, Lassmann H (2009) The relation between inflammation and neurodegeneration in multiple sclerosis brains. Brain (England) 132:1175-1189.

Gay D, Esiri M (1991) Blood-brain barrier damage in acute multiple sclerosis plaques. an immunocytological study. Brain (ENGLAND) 114 (Pt 1B):557-572.

Ginhoux F, Prinz M (2015) Origin of microglia: Current concepts and past controversies. Cold Spring Harb Perspect Biol (United States) 7:a020537.

Glass CK, Saijo K, Winner B, Marchetto MC, Gage FH (2010) Mechanisms underlying inflammation in neurodegeneration. Cell (United States) 140:918-934.

Goldmann T, Prinz M (2013) Role of microglia in CNS autoimmunity. Clin Dev Immunol (Egypt) 2013:208093.

Gordon A, Adamsky K, Vainshtein A, Frechter S, Dupree JL, Rosenbluth J, Peles E (2014) Caspr and caspr2 are required for both radial and longitudinal organization of myelinated axons. J Neurosci (United States) 34:14820-14826.

Gravel M, Peterson J, Yong VW, Kottis V, Trapp B, Braun PE (1996) Overexpression of 2',3'-cyclic nucleotide 3'-phosphodiesterase in transgenic mice alters oligodendrocyte development and produces aberrant myelination. Mol Cell Neurosci (UNITED STATES) 7:453-466.

Griffiths I, Klugmann M, Anderson T, Yool D, Thomson C, Schwab MH, Schneider A, Zimmermann F, McCulloch M, Nadon N, Nave KA (1998) Axonal swellings and degeneration in mice lacking the major proteolipid of myelin. Science (UNITED STATES) 280:1610-1613.

Grubb MS, Burrone J (2010) Activity-dependent relocation of the axon initial segment fine-tunes neuronal excitability. Nature (England) 465:1070-1074.

Guemez-Gamboa A, Estrada-Sanchez AM, Montiel T, Paramo B, Massieu L, Moran J (2011) Activation of NOX2 by the stimulation of ionotropic and metabotropic glutamate receptors contributes to glutamate neurotoxicity in vivo through the production of reactive oxygen species and calpain activation. J Neuropathol Exp Neurol (United States) 70:1020-1035.

Haines JD, Inglese M, Casaccia P (2011) Axonal damage in multiple sclerosis. Mt Sinai J Med (United States) 78:231-243.

Haji N, Mandolesi G, Gentile A, Sacchetti L, Fresegna D, Rossi S, Musella A, Sepman H, Motta C, Studer V, De Chiara V, Bernardi G, Strata P, Centonze D (2012) TNF-alpha-mediated anxiety in a mouse model of multiple sclerosis. Exp Neurol (United States) 237:296-303.

Han H, Myllykoski M, Ruskamo S, Wang C, Kursula P (2013) Myelin-specific proteins: A structurally diverse group of membrane-interacting molecules. Biofactors (Netherlands) 39:233-241.

Hanisch UK, Kettenmann H (2007) Microglia: Active sensor and versatile effector cells in the normal and pathologic brain. Nat Neurosci (United States) 10:1387-1394.

Hatterer E, Davoust N, Didier-Bazes M, Vuaillat C, Malcus C, Belin MF, Nataf S (2006) How to drain without lymphatics? dendritic cells migrate from the cerebrospinal fluid to the B-cell follicles of cervical lymph nodes. Blood (United States) 107:806-812.

Hauser SL, Waubant E, Arnold DL, Vollmer T, Antel J, Fox RJ, Bar-Or A, Panzara M, Sarkar N, Agarwal S, Langer-Gould A, Smith CH, HERMES Trial Group (2008) B-cell depletion with rituximab in relapsing-remitting multiple sclerosis. N Engl J Med (United States) 358:676-688.

Hayashi T, Ago K, Nakamae T, Higo E, Ogata M (2015) Two different immunostaining patterns of beta-amyloid precursor protein (APP) may distinguish traumatic from nontraumatic axonal injury. Int J Legal Med (Germany) 129:1085-1090.

Hedstrom KL, Ogawa Y, Rasband MN (2008) AnkyrinG is required for maintenance of the axon initial segment and neuronal polarity. J Cell Biol (United States) 183:635-640.

Hemmer B, Kerschensteiner M, Korn T (2015) Role of the innate and adaptive immune responses in the course of multiple sclerosis. Lancet Neurol (England) 14:406-419.

Henderson AP, Barnett MH, Parratt JD, Prineas JW (2009) Multiple sclerosis: Distribution of inflammatory cells in newly forming lesions. Ann Neurol (United States) 66:739-753.

Hendrickx DA, Schuurman KG, van Draanen M, Hamann J, Huitinga I (2014) Enhanced uptake of multiple sclerosis-derived myelin by THP-1 macrophages and primary human microglia. J Neuroinflammation (England) 11:64-2094-11-64.

Henry MA, Sorensen HJ, Johnson LR, Levinson SR (2005) Localization of the Nav1.8 sodium channel isoform at nodes of ranvier in normal human radicular tooth pulp. Neurosci Lett (Ireland) 380:32-36.

Heppner FL, Greter M, Marino D, Falsig J, Raivich G, Hovelmeyer N, Waisman A, Rulicke T, Prinz M, Priller J, Becher B, Aguzzi A (2005) Experimental autoimmune encephalomyelitis repressed by microglial paralysis. Nat Med (United States) 11:146-152.

Hernandez-Pedro NY, Espinosa-Ramirez G, de la Cruz VP, Pineda B, Sotelo J (2013) Initial immunopathogenesis of multiple sclerosis: Innate immune response. Clin Dev Immunol (Egypt) 2013:413465.

Hillyer P, Mordelet E, Flynn G, Male D (2003) Chemokines, chemokine receptors and adhesion molecules on different human endothelia: Discriminating the tissue-specific functions that affect leucocyte migration. Clin Exp Immunol (England) 134:431-441.

Hinman JD, Rasband MN, Carmichael ST (2013) Remodeling of the axon initial segment after focal cortical and white matter stroke. Stroke (United States) 44:182-189.

Hoftberger R, Aboul-Enein F, Brueck W, Lucchinetti C, Rodriguez M, Schmidbauer M, Jellinger K, Lassmann H (2004) Expression of major histocompatibility complex class I molecules on the different cell types in multiple sclerosis lesions. Brain Pathol (Switzerland) 14:43-50.

Hu W, Tian C, Li T, Yang M, Hou H, Shu Y (2009) Distinct contributions of na(v)1.6 and na(v)1.2 in action potential initiation and backpropagation. Nat Neurosci (United States) 12:996-1002.

Inayat MS, El-Amouri IS, Bani-Ahmad M, Elford HL, Gallicchio VS, Oakley OR (2010) Inhibition of allogeneic inflammatory responses by the ribonucleotide reductase inhibitors, didox and trimidox. J Inflamm (Lond) (England) 7:43-9255-7-43.

Ingram G, Loveless S, Howell OW, Hakobyan S, Dancey B, Harris CL, Robertson NP, Neal JW, Morgan BP (2014) Complement activation in multiple sclerosis plaques: An immunohistochemical analysis. Acta Neuropathol Commun (England) 2:53-5960-2-53.

Jacobsen M, Cepok S, Quak E, Happel M, Gaber R, Ziegler A, Schock S, Oertel WH, Sommer N, Hemmer B (2002) Oligoclonal expansion of memory CD8+ T cells in cerebrospinal fluid from multiple sclerosis patients. Brain (England) 125:538-550.

Janssens K, Maheshwari A, Van den Haute C, Baekelandt V, Stinissen P, Hendriks JJ, Slaets H, Hellings N (2015) Oncostatin M protects against demyelination by inducing a protective microglial phenotype. Glia (United States) 63:1729-1737.

Jenkins SM, Bennett V (2001) Ankyrin-G coordinates assembly of the spectrin-based membrane skeleton, voltage-gated sodium channels, and L1 CAMs at purkinje neuron initial segments. J Cell Biol (United States) 155:739-746.

Johns TG, Kerlero de Rosbo N, Menon KK, Abo S, Gonzales MF, Bernard CC (1995) Myelin oligodendrocyte glycoprotein induces a demyelinating encephalomyelitis resembling multiple sclerosis. J Immunol (UNITED STATES) 154:5536-5541.

Kandel ER, Barres BA, Hudspeth AJ (2013) Nerve cells, neurl circuitry, and behavior. In: Principles of neural science Nerve cells, neurl circuitry, and behavior. pp21.McGraw-Hill.

Kaphzan H, Buffington SA, Jung JI, Rasband MN, Klann E (2011) Alterations in intrinsic membrane properties and the axon initial segment in a mouse model of angelman syndrome. J Neurosci (United States) 31:17637-17648.

Kaphzan H, Buffington SA, Ramaraj AB, Lingrel JB, Rasband MN, Santini E, Klann E (2013) Genetic reduction of the alpha1 subunit of na/K-ATPase corrects multiple hippocampal phenotypes in angelman syndrome. Cell Rep (United States) 4:405-412.

Kaplan MR, Meyer-Franke A, Lambert S, Bennett V, Duncan ID, Levinson SR, Barres BA (1997) Induction of sodium channel clustering by oligodendrocytes. Nature (ENGLAND) 386:724-728.

Kappos L, Li D, Calabresi PA, O'Connor P, Bar-Or A, Barkhof F, Yin M, Leppert D, Glanzman R, Tinbergen J, Hauser SL (2011) Ocrelizumab in relapsing-remitting multiple sclerosis: A phase 2, randomised, placebo-controlled, multicentre trial. Lancet (England) 378:1779-1787.

Kettenmann H, Hanisch UK, Noda M, Verkhratsky A (2011) Physiology of microglia. Physiol Rev (United States) 91:461-553.

Kierdorf K, Prinz M (2013) Factors regulating microglia activation. Front Cell Neurosci (Switzerland) 7:44.

King CH, Lancaster E, Salomon D, Peles E, Scherer SS (2014) Kv7.2 regulates the function of peripheral sensory neurons. J Comp Neurol (United States) 522:3262-3280.

Klos A, Tenner AJ, Johswich KO, Ager RR, Reis ES, Kohl J (2009) The role of the anaphylatoxins in health and disease. Mol Immunol (England) 46:2753-2766.

Klugmann M, Schwab MH, Puhlhofer A, Schneider A, Zimmermann F, Griffiths IR, Nave KA (1997) Assembly of CNS myelin in the absence of proteolipid protein. Neuron (UNITED STATES) 18:59-70.

Kole MH, Letzkus JJ, Stuart GJ (2007) Axon initial segment Kv1 channels control axonal action potential waveform and synaptic efficacy. Neuron (United States) 55:633-647.

Kordeli E, Lambert S, Bennett V (1995) AnkyrinG. A new ankyrin gene with neural-specific isoforms localized at the axonal initial segment and node of ranvier. J Biol Chem (UNITED STATES) 270:2352-2359.

Kornek B, Storch MK, Weissert R, Wallstroem E, Stefferl A, Olsson T, Linington C, Schmidbauer M, Lassmann H (2000) Multiple sclerosis and chronic autoimmune encephalomyelitis: A comparative quantitative study of axonal injury in active, inactive, and remyelinated lesions. Am J Pathol (UNITED STATES) 157:267-276.

Kuba H, Oichi Y, Ohmori H (2010) Presynaptic activity regulates na(+) channel distribution at the axon initial segment. Nature (England) 465:1075-1078.

Kuba H, Ishii TM, Ohmori H (2006) Axonal site of spike initiation enhances auditory coincidence detection. Nature (England) 444:1069-1072.

Kutzelnigg A, Lassmann H (2014) Pathology of multiple sclerosis and related inflammatory demyelinating diseases. Handb Clin Neurol (Netherlands) 122:15-58.

Kutzelnigg A, Lassmann H (2006) Cortical demyelination in multiple sclerosis: A substrate for cognitive deficits? J Neurol Sci (Netherlands) 245:123-126.

Kutzelnigg A, Lucchinetti CF, Stadelmann C, Bruck W, Rauschka H, Bergmann M, Schmidbauer M, Parisi JE, Lassmann H (2005) Cortical demyelination and diffuse white matter injury in multiple sclerosis. Brain (England) 128:2705-2712.

Lambert S, Davis JQ, Bennett V (1997) Morphogenesis of the node of ranvier: Co-clusters of ankyrin and ankyrin-binding integral proteins define early developmental intermediates. J Neurosci (UNITED STATES) 17:7025-7036.

Lappe-Siefke C, Goebbels S, Gravel M, Nicksch E, Lee J, Braun PE, Griffiths IR, Nave KA (2003) Disruption of Cnp1 uncouples oligodendroglial functions in axonal support and myelination. Nat Genet (United States) 33:366-374.

Leterrier C, Dargent B (2014) No pasaran! role of the axon initial segment in the regulation of protein transport and the maintenance of axonal identity. Semin Cell Dev Biol (England) 27:44-51.

Lubetzki C, Stankoff B (2014) Demyelination in multiple sclerosis. Handb Clin Neurol (Netherlands) 122:89-99.

Mainen ZF, Joerges J, Huguenard JR, Sejnowski TJ (1995) A model of spike initiation in neocortical pyramidal neurons. Neuron (UNITED STATES) 15:1427-1439.

Marcus J, Popko B (2002) Galactolipids are molecular determinants of myelin development and axo-glial organization. Biochim Biophys Acta (Netherlands) 1573:406-413.

Marcus J, Honigbaum S, Shroff S, Honke K, Rosenbluth J, Dupree JL (2006) Sulfatide is essential for the maintenance of CNS myelin and axon structure. Glia (United States) 53:372-381.

Marik C, Felts PA, Bauer J, Lassmann H, Smith KJ (2007) Lesion genesis in a subset of patients with multiple sclerosis: A role for innate immunity? Brain (England) 130:2800-2815.

Martinez FO, Gordon S (2014) The M1 and M2 paradigm of macrophage activation: Time for reassessment. F1000Prime Rep (England) 6:13-13. eCollection 2014.

Martini R, Schachner M (1986) Immunoelectron microscopic localization of neural cell adhesion molecules (L1, N-CAM, and MAG) and their shared carbohydrate epitope and myelin basic protein in developing sciatic nerve. J Cell Biol (UNITED STATES) 103:2439-2448.

Mastellos D, Prechl J, Laszlo G, Papp K, Olah E, Argyropoulos E, Franchini S, Tudoran R, Markiewski M, Lambris JD, Erdei A (2004) Novel monoclonal antibodies against mouse C3 interfering with complement activation: Description of fine specificity and applications to various immunoassays. Mol Immunol (England) 40:1213-1221.

Mathey EK, Derfuss T, Storch MK, Williams KR, Hales K, Woolley DR, Al-Hayani A, Davies SN, Rasband MN, Olsson T, Moldenhauer A, Velhin S, Hohlfeld R, Meinl E, Linington C (2007) Neurofascin as a novel target for autoantibody-mediated axonal injury. J Exp Med (United States) 204:2363-2372.

Matsebatlela TM, Anderson AL, Gallicchio VS, Elford H, Rice CD (2015) 3,4-dihydroxy-benzohydroxamic acid (didox) suppresses pro-inflammatory profiles and oxidative stress in TLR4-activated RAW264.7 murine macrophages. Chem Biol Interact (Ireland) 233:95-105.

Menon KK, Piddlesden SJ, Bernard CC (1997) Demyelinating antibodies to myelin oligodendrocyte glycoprotein and galactocerebroside induce degradation of myelin basic protein in isolated human myelin. J Neurochem (UNITED STATES) 69:214-222.

Merle NS, Church SE, Fremeaux-Bacchi V, Roumenina LT (2015a) Complement system part I - molecular mechanisms of activation and regulation. Front Immunol (Switzerland) 6:262.

Merle NS, Noe R, Halbwachs-Mecarelli L, Fremeaux-Bacchi V, Roumenina LT (2015b) Complement system part II: Role in immunity. Front Immunol (Switzerland) 6:257.

Mews I, Bergmann M, Bunkowski S, Gullotta F, Bruck W (1998) Oligodendrocyte and axon pathology in clinically silent multiple sclerosis lesions. Mult Scler (ENGLAND) 4:55-62.

Mikita J, Dubourdieu-Cassagno N, Deloire MS, Vekris A, Biran M, Raffard G, Brochet B, Canron MH, Franconi JM, Boiziau C, Petry KG (2011) Altered M1/M2 activation patterns of monocytes in severe relapsing experimental rat model of multiple sclerosis. amelioration of clinical status by M2 activated monocyte administration. Mult Scler (England) 17:2-15.

Mills CD, Kincaid K, Alt JM, Heilman MJ, Hill AM (2000) M-1/M-2 macrophages and the Th1/Th2 paradigm. J Immunol (UNITED STATES) 164:6166-6173.

Mistry N, Tallantyre EC, Dixon JE, Galazis N, Jaspan T, Morgan PS, Morris P, Evangelou N (2011) Focal multiple sclerosis lesions abound in 'normal appearing white matter'. Mult Scler (England) 17:1313-1323.

Morell P, Radin NS (1969) Synthesis of cerebroside by brain from uridine diphosphate galactose and ceramide containing hydroxy fatty acid. Biochemistry (UNITED STATES) 8:506-512.

Mortensen S, Kidmose RT, Petersen SV, Szilagyi A, Prohaszka Z, Andersen GR (2015) Structural basis for the function of complement component C4 within the classical and lectin pathways of complement. J Immunol (United States) 194:5488-5496.

Nikic I, Merkler D, Sorbara C, Brinkoetter M, Kreutzfeldt M, Bareyre FM, Bruck W, Bishop D, Misgeld T, Kerschensteiner M (2011) A reversible form of axon damage in experimental autoimmune encephalomyelitis and multiple sclerosis. Nat Med (United States) 17:495-499.

Orsini F, De Blasio D, Zangari R, Zanier ER, De Simoni MG (2014) Versatility of the complement system in neuroinflammation, neurodegeneration and brain homeostasis. Front Cell Neurosci (Switzerland) 8:380.

Palmer LM, Stuart GJ (2006) Site of action potential initiation in layer 5 pyramidal neurons. J Neurosci (United States) 26:1854-1863.

Pan Z, Kao T, Horvath Z, Lemos J, Sul JY, Cranstoun SD, Bennett V, Scherer SS, Cooper EC (2006) A common ankyrin-G-based mechanism retains KCNQ and NaV channels at electrically active domains of the axon. J Neurosci (United States) 26:2599-2613.

Pangburn MK, Schreiber RD, Muller-Eberhard HJ (1977) Human complement C3b inactivator: Isolation, characterization, and demonstration of an absolute requirement for the serum protein beta1H for cleavage of C3b and C4b in solution. J Exp Med (UNITED STATES) 146:257-270.

Peferoen LA, Vogel DY, Ummenthum K, Breur M, Heijnen PD, Gerritsen WH, Peferoen-Baert RM, van der Valk P, Dijkstra CD, Amor S (2015) Activation status of human microglia is dependent on lesion formation stage and remyelination in multiple sclerosis. J Neuropathol Exp Neurol (United States) 74:48-63.

Pillai AM, Thaxton C, Pribisko AL, Cheng JG, Dupree JL, Bhat MA (2009) Spatiotemporal ablation of myelinating glia-specific neurofascin (nfasc NF155) in mice reveals gradual loss of paranodal axoglial junctions and concomitant disorganization of axonal domains. J Neurosci Res (United States) 87:1773-1793.

Pirko I, Lucchinetti CF, Sriram S, Bakshi R (2007) Gray matter involvement in multiple sclerosis. Neurology (United States) 68:634-642.

Poliak S, Gollan L, Martinez R, Custer A, Einheber S, Salzer JL, Trimmer JS, Shrager P, Peles E (1999) Caspr2, a new member of the neurexin superfamily, is localized at the juxtaparanodes of myelinated axons and associates with K+ channels. Neuron (UNITED STATES) 24:1037-1047.

Poliak S, Salomon D, Elhanany H, Sabanay H, Kiernan B, Pevny L, Stewart CL, Xu X, Chiu SY, Shrager P, Furley AJ, Peles E (2003) Juxtaparanodal clustering of shaker-like K+ channels in myelinated axons depends on Caspr2 and TAG-1. J Cell Biol (United States) 162:1149-1160.

Polman CH, Reingold SC, Banwell B, Clanet M, Cohen JA, Filippi M, Fujihara K, Havrdova E, Hutchinson M, Kappos L, Lublin FD, Montalban X, O'Connor P, Sandberg-Wollheim M, Thompson AJ, Waubant E, Weinshenker B, Wolinsky JS (2011) Diagnostic criteria for multiple sclerosis: 2010 revisions to the McDonald criteria. Ann Neurol (United States) 69:292-302.

Pomicter AD, Shroff SM, Fuss B, Sato-Bigbee C, Brophy PJ, Rasband MN, Bhat MA, Dupree JL (2010) Novel forms of neurofascin 155 in the central nervous system: Alterations in paranodal disruption models and multiple sclerosis. Brain (England) 133:389-405.

Popescu BF, Pirko I, Lucchinetti CF (2013) Pathology of multiple sclerosis: Where do we stand? Continuum (Minneap Minn) (United States) 19:901-921.

Quarles RH, Macklin WB, Morell P (2006) Myelin formation, structure, and biochemistry. In: Basic neurochemistry: Molecular, cellular, and medical aspects (Brady S, Siegel G, Albers RW, Price D, eds), pp51. New York: Elsevier Academic Press.

Raine C, S. (1984) Morphology of myelin and myelination. In: Myelin (Morrell P, ed), pp1. New York: Plenum Press.

Ramaglia V, Hughes TR, Donev RM, Ruseva MM, Wu X, Huitinga I, Baas F, Neal JW, Morgan BP (2012) C3-dependent mechanism of microglial priming relevant to multiple sclerosis. Proc Natl Acad Sci U S A (United States) 109:965-970.

Ramagopalan SV, Sadovnick AD (2011) Epidemiology of multiple sclerosis. Neurol Clin 29:207-217.

Ramio-Torrenta L, Sastre-Garriga J, Ingle GT, Davies GR, Ameen V, Miller DH, Thompson AJ (2006) Abnormalities in normal appearing tissues in early primary progressive multiple sclerosis and their relation to disability: A tissue specific magnetisation transfer study. J Neurol Neurosurg Psychiatry (England) 77:40-45.

Ransohoff RM, Engelhardt B (2012) The anatomical and cellular basis of immune surveillance in the central nervous system. Nat Rev Immunol (England) 12:623-635.

Rasband MN, Peles E (2015) The nodes of ranvier: Molecular assembly and maintenance. Cold Spring Harb Perspect Biol (United States) 8:10.1101/cshperspect.a020495.

Rasband MN, Peles E, Trimmer JS, Levinson SR, Lux SE, Shrager P (1999) Dependence of nodal sodium channel clustering on paranodal axoglial contact in the developing CNS. J Neurosci (UNITED STATES) 19:7516-7528.

Rasband MN, Park EW, Zhen D, Arbuckle MI, Poliak S, Peles E, Grant SG, Trimmer JS (2002) Clustering of neuronal potassium channels is independent of their interaction with PSD-95. J Cell Biol (United States) 159:663-672.

Rawji KS, Yong VW (2013) The benefits and detriments of macrophages/microglia in models of multiple sclerosis. Clin Dev Immunol (Egypt) 2013:948976.

Rhodes KJ, Strassle BW, Monaghan MM, Bekele-Arcuri Z, Matos MF, Trimmer JS (1997) Association and colocalization of the Kvbeta1 and Kvbeta2 beta-subunits with Kv1 alpha-subunits in mammalian brain K+ channel complexes. J Neurosci (UNITED STATES) 17:8246-8258.

Rios JC, Melendez-Vasquez CV, Einheber S, Lustig M, Grumet M, Hemperly J, Peles E, Salzer JL (2000) Contactin-associated protein (caspr) and contactin form a complex that is targeted to the paranodal junctions during myelination. J Neurosci (UNITED STATES) 20:8354-8364.

Rudick RA, Lee JC, Simon J, Fisher E (2006) Significance of T2 lesions in multiple sclerosis: A 13-year longitudinal study. Ann Neurol (United States) 60:236-242.

Schachner M, Bartsch U (2000) Multiple functions of the myelin-associated glycoprotein MAG (siglec-4a) in formation and maintenance of myelin. Glia (UNITED STATES) 29:154-165.

Schafer DP, Lehrman EK, Kautzman AG, Koyama R, Mardinly AR, Yamasaki R, Ransohoff RM, Greenberg ME, Barres BA, Stevens B (2012) Microglia sculpt postnatal neural circuits in an activity and complement-dependent manner. Neuron (United States) 74:691-705.

Scherer SS, Braun PE, Grinspan J, Collarini E, Wang DY, Kamholz J (1994) Differential regulation of the 2',3'-cyclic nucleotide 3'-phosphodiesterase gene during oligodendrocyte development. Neuron (UNITED STATES) 12:1363-1375.

Secor McVoy JR, Oughli HA, Oh U (2015) Liver X receptor-dependent inhibition of microglial nitric oxide synthase 2. J Neuroinflammation (England) 12:27-015-0247-2.

Siffrin V, Vogt J, Radbruch H, Nitsch R, Zipp F (2010) Multiple sclerosis - candidate mechanisms underlying CNS atrophy. Trends Neurosci (England) 33:202-210.

Sobotzik JM, Sie JM, Politi C, Del Turco D, Bennett V, Deller T, Schultz C (2009) AnkyrinG is required to maintain axo-dendritic polarity in vivo. Proc Natl Acad Sci U S A (United States) 106:17564-17569.

Song AH, Wang D, Chen G, Li Y, Luo J, Duan S, Poo MM (2009) A selective filter for cytoplasmic transport at the axon initial segment. Cell (United States) 136:1148-1160.

Sospedra M, Martin R (2005) Immunology of multiple sclerosis. Annu Rev Immunol (United States) 23:683-747.

Stanley ER, Berg KL, Einstein DB, Lee PS, Pixley FJ, Wang Y, Yeung YG (1997) Biology and action of colony--stimulating factor-1. Mol Reprod Dev (UNITED STATES) 46:4-10.

Stecca B, Southwood CM, Gragerov A, Kelley KA, Friedrich VL,Jr, Gow A (2000) The evolution of lipophilin genes from invertebrates to tetrapods: DM-20 cannot replace proteolipid protein in CNS myelin. J Neurosci (UNITED STATES) 20:4002-4010.

Stein M, Keshav S, Harris N, Gordon S (1992) Interleukin 4 potently enhances murine macrophage mannose receptor activity: A marker of alternative immunologic macrophage activation. J Exp Med (UNITED STATES) 176:287-292.

Stephan AH, Barres BA, Stevens B (2012) The complement system: An unexpected role in synaptic pruning during development and disease. Annu Rev Neurosci (United States) 35:369-389.

Stevens B, Allen NJ, Vazquez LE, Howell GR, Christopherson KS, Nouri N, Micheva KD, Mehalow AK, Huberman AD, Stafford B, Sher A, Litke AM, Lambris JD, Smith SJ, John SW, Barres BA (2007) The classical complement cascade mediates CNS synapse elimination. Cell (United States) 131:1164-1178.

Stuart GJ, Sakmann B (1994) Active propagation of somatic action potentials into neocortical pyramidal cell dendrites. Nature (ENGLAND) 367:69-72.

Susuki K (2013) Node of ranvier disruption as a cause of neurological diseases. ASN Neuro (England) 5:209-219.

Susuki K, Chang KJ, Zollinger DR, Liu Y, Ogawa Y, Eshed-Eisenbach Y, Dours-Zimmermann MT, Oses-Prieto JA, Burlingame AL, Seidenbecher CI, Zimmermann DR, Oohashi T, Peles E, Rasband MN (2013) Three mechanisms assemble central nervous system nodes of ranvier. Neuron (United States) 78:469-482.

Tang Y, Le W (2016) Differential roles of M1 and M2 microglia in neurodegenerative diseases. Mol Neurobiol (United States) 53:1181-1194.

Traka M, Goutebroze L, Denisenko N, Bessa M, Nifli A, Havaki S, Iwakura Y, Fukamauchi F, Watanabe K, Soliven B, Girault JA, Karagogeos D (2003) Association of TAG-1 with Caspr2 is essential for the

molecular organization of juxtaparanodal regions of myelinated fibers. J Cell Biol (United States) 162:1161-1172.

Trapp BD, Nave KA (2008) Multiple sclerosis: An immune or neurodegenerative disorder? Annu Rev Neurosci (United States) 31:247-269.

Trapp BD, Peterson J, Ransohoff RM, Rudick R, Mork S, Bo L (1998) Axonal transection in the lesions of multiple sclerosis. N Engl J Med (UNITED STATES) 338:278-285.

Tremblay ME, Majewska AK (2011) A role for microglia in synaptic plasticity? Commun Integr Biol (United States) 4:220-222.

Tsuruta T, Yamamoto T, Matsubara S, Nagasawa S, Tanase S, Tanaka J, Takagi K, Kambara T (1993) Novel function of C4a anaphylatoxin. release from monocytes of protein which inhibits monocyte chemotaxis. Am J Pathol (UNITED STATES) 142:1848-1857.

Turchan J, Pocernich CB, Gairola C, Chauhan A, Schifitto G, Butterfield DA, Buch S, Narayan O, Sinai A, Geiger J, Berger JR, Elford H, Nath A (2003) Oxidative stress in HIV demented patients and protection ex vivo with novel antioxidants. Neurology (United States) 60:307-314.

Vabnick I, Shrager P (1998) Ion channel redistribution and function during development of the myelinated axon. J Neurobiol (UNITED STATES) 37:80-96.

Wang H, Kunkel DD, Martin TM, Schwartzkroin PA, Tempel BL (1993) Heteromultimeric K+ channels in terminal and juxtaparanodal regions of neurons. Nature (ENGLAND) 365:75-79.

Winckler B, Forscher P, Mellman I (1999) A diffusion barrier maintains distribution of membrane proteins in polarized neurons. Nature (ENGLAND) 397:698-701.

Woyciechowska JL, Brzosko WJ (1977) Immunofluorescence study of brain plaques from two patients with multiple sclerosis. Neurology (UNITED STATES) 27:620-622.

Wraith DC, Nicholson LB (2012) The adaptive immune system in diseases of the central nervous system. J Clin Invest (United States) 122:1172-1179.

Wu G, Morris SM,Jr (1998) Arginine metabolism: Nitric oxide and beyond. Biochem J (ENGLAND) 336 (Pt 1):1-17.

Wucherpfennig KW, Strominger JL (1995) Molecular mimicry in T cell-mediated autoimmunity: Viral peptides activate human T cell clones specific for myelin basic protein. Cell (UNITED STATES) 80:695-705.

Wunsch M, Rovituso DM, Kuerten S (2014) KIR4.1 antibodies as biomarkers in multiple sclerosis. Front Neurol (Switzerland) 5:62.

Xie L, Kang H, Xu Q, Chen MJ, Liao Y, Thiyagarajan M, O'Donnell J, Christensen DJ, Nicholson C, Iliff JJ, Takano T, Deane R, Nedergaard M (2013) Sleep drives metabolite clearance from the adult brain. Science (United States) 342:373-377.

Xu L, Hilliard B, Carmody RJ, Tsabary G, Shin H, Christianson DW, Chen YH (2003) Arginase and autoimmune inflammation in the central nervous system. Immunology (England) 110:141-148.

Yang Y, Ogawa Y, Hedstrom KL, Rasband MN (2007) betaIV spectrin is recruited to axon initial segments and nodes of ranvier by ankyrinG. J Cell Biol (United States) 176:509-519.

Yoshimura T, Rasband MN (2014) Axon initial segments: Diverse and dynamic neuronal compartments. Curr Opin Neurobiol (England) 27:96-102.

Zhou D, Lambert S, Malen PL, Carpenter S, Boland LM, Bennett V (1998) AnkyrinG is required for clustering of voltage-gated na channels at axon initial segments and for normal action potential firing. J Cell Biol (UNITED STATES) 143:1295-1304.

Zonta B, Desmazieres A, Rinaldi A, Tait S, Sherman DL, Nolan MF, Brophy PJ (2011) A critical role for neurofascin in regulating action potential initiation through maintenance of the axon initial segment. Neuron (United States) 69:945-956.

Zonta B, Tait S, Melrose S, Anderson H, Harroch S, Higginson J, Sherman DL, Brophy PJ (2008) Glial and neuronal isoforms of neurofascin have distinct roles in the assembly of nodes of ranvier in the central nervous system. J Cell Biol (United States) 181:1169-1177.

Vitae

Rebecca Kathleen Hartley was born in Nashville, Tennessee on March 3rd, 1991. She grew up in Clifton, Virginia and graduated from Centreville High School in 2009. She received her Bachelor of Science degree in Biochemistry, with a minor in Anthropology, from Indiana University of Pennsylvania in 2013. She currently resides in Richmond, Virginia.